Mass Spectroscopy Using Single Ion Cyclotron Resonance

by

Eric Allin Cornell

B.S. Stanford University (1985)

Submitted to the Department of Physics
in partial fulfillment of the requirements for the degree of

Doctor of Philosophy

at the

MASSACHUSETTS INSTITUTE OF TECHNOLOGY

May 1990

Signature of the Author . . . . . .
Department of Physics
May, 1990

Certified by . . . . . .
David E. Pritchard
Professor, Department of Physics
Thesis Supervisor

Accepted by . . . . . .
George Koster
Chairman,
Departmental Committee
on Graduate Students

MASS SPECTROSCOPY USING SINGLE ION CYCLOTRON RESONANCE

by

ERIC ALLIN CORNELL

Submitted to the Department of Physics on
May 11, 1990 in partial fulfillment of the requirements
for the Degree of Doctor of Philosophy in Physics

ABSTRACT

Using single ions in Penning trap, we determine the mass ratio of carbon monoxide to molecular nitrogen to be 0.9995988876(4), an accuracy of 4 parts in 10^{10}. The major source of error is temporal instabilities in the magnetic field. All other sources of error, including special relativistic effects and spatial inhomogeneity in the trapping fields, are believed to contribute an error of less than a part in 10^{10} to the measured ratio.

Cyclotron frequency measurements are made using a novel, phase-sensitive, twin-pulse technique which makes use of a classical "pi-pulse" to move the phase and action from one normal mode into another.

We discuss the possibility of simultaneously trapping two ions, one of each species, thereby circumventing the problem of magnetic field drift. Our calculations and some preliminary experiments indicate that this technique should permit mass comparisons with accuracies at a part in 10^{11} or better.

Thesis Supervisor: Dr. David E. Pritchard
Title: Professor of Physics

To my parents

Table of Contents

Chapter 1 Introduction

1A. My Theses:

That, with cyclotron resonance measurements on a single ion in a Penning trap, we can determine ion mass ratios to better than a part in 10^9;

that, in particular, the ratio of the mass of CO^+ to the mass of N_2^+ is 0.9995988876, to an accuracy of four parts in 10^{10};

and that, with two ion techniques, determining ion mass ratios to better than a part in 10^{11} is ultimately feasible.

1B. Motivation and a Little History

> [I]f one is being iconoclastic about precise measurement, the power of a measurement to generate other measurements is hardly compelling justification.
>
> --- Ian Hacking [HAC83]

The relative masses of the stable ions are already known to better than a part in 10^7. Many are known to parts in 10^9. [WAA85] Why on earth should we want to do orders of magnitude better? The short answer, in defiance of Hacking, is that we measure masses more precisely because it gives us the power to generate other more precise measurements. Three such measurements bear mentioning.

The first is the electron neutrino rest mass. Does it have any at all? Currently experiments [BGL85] and observations [ARR87]

put an upper bound around 20 eV. At least one group [BGL85] reports a non-zero result around 17 eV. About a dozen groups are performing experimental studies of the high energy tail of the tritium beta decay spectrum in an effort to measure the m_ν. These efforts would greatly benefit from an independent measurement of the total energy available to the decay, the mass difference between tritium and helium-3. A part in 10^9 measurement of the mass ratio determines the mass difference to 3 eV.

A second more precise measurement we could generate with better mass spectroscopy is the combination of fundamental constants $N_A h$. Better knowledge of the product of Avogadro's number and Planck's constant would in turn help determine a better value for the fine structure constant [JOH84]. Mass difference measurements, combined with gamma-ray wavelength measurements, can determine the energy of a gamma ray both in amu and in inverse centimeters. The conversion factor between the units is $N_A h$. One implementation [JOH84] of this scheme requires measuring the mass ratio of an ammonia isomeric doublet to better that a part in 10^{11}, in order to contribute to a part in 10^7 determination of α^2.

Finally, improvements in mass spectroscopy will bring enough precision to weigh the binding energy of molecules, atoms and clusters. For certain classes of molecules, calorimetric and spectroscopic measurements of energies don't work. To weigh molecular bonds at a generally useful level, mass spectroscopy has to reach accuracies of parts in 10^{12}.

The mass comparison techniques described in this thesis involve single ion cyclotron resonance in a Penning trap. The Penning trap was originally developed into a precision instrument originally at the University of Washington by Hans Dehmelt and his colleagues, including Gabrielse, Schwinberg, Van Dyck, Wells and Wineland. It was at the University of Washington that the first precision trap was machined, the first single particles detected, almost all the single ion theory worked out, sideband cooling developed, etc. The most renowned Penning trap experiments performed there are the parts in 10^{12} measurements of the electron and positron magnetic moments [VSD87]. For a summary of these developments see for instance Brown and Gabrielse's comprehensive review article [BRG86] or Weisskoff's very readable thesis [WEI88]. Current high precision ion mass comparison efforts of which I am aware are by Dunn's group in Boulder, van Dyck's in Seattle [VMF85, MOO89], and G. Werth's in Mainz, Germany.

1C The Basic Idea

Here, in essence, is how we compare the masses of ions: We load the trap with ions of one species, ejecting all accidentally trapped impurity ions and all but one ion of the desired species, and measure the normal mode trap frequencies. Then we dump the ion out and repeat the procedure with the second species. From the trap frequencies of each ion we reconstruct the free-space cyclotron frequency, that is, the cyclotron frequency we would have

measured had there been no electric fields. Assuming the magnetic field remains constant while we exchange ions, the ratio of the ion masses is just the inverse of the ratio of the cyclotron frequencies.

As it turns out, the magnetic field does *not* remain constant, at least not at the part in 10^{10} level, and that is why we are developing techniques to measure the cyclotron resonance of two trapped ions simultaneously.

1D Penning Trap Primer

The ideal Penning trap consists of a strong, uniform magnetic field, and a quadrupole electric field, usually established by 3 electrodes, hyperbolae of rotation. (Fig. 1.1) We write the electric and magnetic fields respectively as

$$\vec{E}(\rho,z) = (V_t/d^2)(\rho\hat{\rho}/2 - z\hat{z}) \qquad (1.1a)$$

$$\vec{B} = B\hat{z} \qquad (1.1b)$$

where V_t is the potential between the ring electrode and the endcap electrodes, and d is the characteristic trap size, defined in fig 1.1.† For a single ion of mass m and charge e, the equation of motion is:

---

† Here, and throughout the thesis, boldface type denotes vectors and normal weight type denotes the scalar length of the corresponding vector. For example, r = |r|. For typographical reasons, vectors labeled with Greek letters have to be indicated with arrow superscripts rather than bold type. The Greek letter ρ is always a component of a vector given in cylindrical coordinates, $\mathbf{r} = (\rho,\theta,z)$; the right-handed set of orthogonal unit vectors is $(\hat{\rho},\hat{\theta},\hat{z})$. The vector $\vec{\rho} = \rho\hat{\rho}$ is always used to refer to a vector with no axial

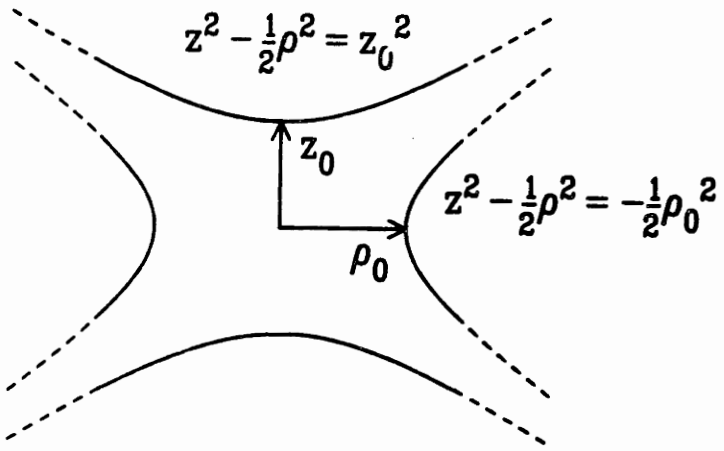

Fig. 1.1 The geometry of the Penning trap. The electrodes are hyperbolic surfaces of rotation. In our trap, ρ_o = 0.696 cm and z_o = .600 cm, giving an effective trap size d = $(\rho_o^2/4 + z_o^2/2)^{1/2}$ = 0.549 cm.

$$m\ddot{\mathbf{r}} = e\mathbf{E}(\mathbf{r}) + (e/c)\,\dot{\mathbf{r}} \times \mathbf{B}\,(\mathbf{r}) \qquad (1.2)$$

In the ideal fields, the equation of motion is linear and is readily solved to yield three normal modes, known as the axial, the magnetron and the trap cyclotron modes. The frequencies are, respectively,

$$\omega_z = [eV_t/(md^2)]^{1/2}$$
$$\omega_m = [\omega_c - (\omega_c^2 - 2\omega_z^2)^{1/2}]/2$$
$$\omega_c = [\omega_c + (\omega_c^2 - 2\omega_z^2)^{1/2}]/2 \qquad (1.3)$$

where ω_c is the free-space cyclotron frequency, $\omega_c = eB/(mc)$. The ion motion will be some linear superposition of the three normal modes, which are as follows:

$$\text{Axial:} \quad z(t) = \mathrm{Re}\left(Z \exp(i\omega_z t)\,\hat{z}\right)$$
$$\text{Magnetron:} \quad \vec{\rho}_m(t) = \mathrm{Re}\left(M \exp(i\omega_m t)(\hat{x} + i\,\hat{y})\right)$$
$$\text{Trap Cyclotron:} \quad \vec{\rho}_c(t) = \mathrm{Re}\left(C \exp(i\omega_c t)(\hat{x} + i\,\hat{y})\right) \qquad (1.4)$$

Z, M, and C are the complex amplitudes of the axial, magnetron and trap cyclotron modes. The magnitude of the normal mode motions, referred to as the mode radii, are also written $a_z = |Z|$, $\rho_m = |M|$, and $\rho_c = |C|$. The trap cyclotron mode is so named because

---

component. When convenient, I also use right-handed rectangular coordinates (x,y,z). The two systems are aligned conventionally: $\hat{z} = \hat{z}$, and $\hat{x} = \hat{\rho}(\theta=0)$. One final convention: V_t and B are positive; we trap an ion with positive charge e.

in the limit of vanishing electric fields the trap cyclotron frequency approaches the free-space cyclotron frequency. For precision mass spectroscopy in a Penning trap, the electric field is always weak enough that $\omega_c' >> \omega_z >> \omega_m$. (For instance, for our measurements on N_2^+, $\omega_c' = 2\pi$ x 4.5MHz, $\omega_z = 2\pi$ x 160 kHz, and $\omega_m = 2\pi$ x 2.8 kHz.) For the actual determination of precision mass ratios, we need to correct the trap cyclotron frequency for the effects of the electric field, but when it is clear from context that I'm discussing motion in the trap, I will sometimes drop the "trap" from "trap cyclotron mode."

1E. Summary of Contents

If you set about reading this thesis cover-to-cover, here is what to expect.

In Chapter 2, I discuss the improvements we have made to the apparatus since Weisskoff and Flanagan wrote their theses. The term "apparatus" is used inclusively; the chapter includes techniques in data analysis as well as physical modifications to the trap.

Chapter 3 is a summary of the factors determining the accuracy of single particle measurements, including field imperfections, impurity ions, special relativity and a host of smaller effects. The gist is that for single ion comparisons, all these effects are small compared to errors arising from the magnetic field drift.

Chapter 4 is the real experimenter's chapter. I include all the major techniques and results obtained with single ions over the last

two years. Trapping and purifying individual ions of various species, measuring and shimming the field imperfections, and mode coupling and resonance techniques are all covered. The chapter culminates with an account of our measuring the CO^+/N_2^+ mass ratio to four parts in 10^{10}.

The forward-looking Chapter 5 deals with the proposed techniques for working with two ions simultaneously and thus beating the field drift problem. Some preliminary experimental results are presented, but most of the chapter is a theoretical discussion of the motion of two, interacting trapped ions, with emphasis on the implications for precision mass spectroscopy. The overall results: the dominant errors, from ion-ion perturbation and special relativity, can be held below a part in 10^{11}.

Chapter 2 Apparatus and Analysis Technology

The apparatus used in our experiment has not changed very much since Robert Weisskoff wrote his thesis two years ago. Accordingly, this chapter will include only a brief overview of the basic machinery, with particular emphasis on modifications made since the spring of 1988. For further details see the theses of Weisskoff [WEI88] and of Flanagan [FLA87].

Our trap hangs vertically in the bore of an 8.5T superconducting Oxford magnet (Fig. 2.1). The magnet is fitted with superconducting shims and a custom Dewar in the bore which allows us to cycle the trap from room temperature to 4.2K while keeping the magnet itself cold. The main electrodes of the trap are precision-machined oxygen-free high-conductivity copper, plated with gold and coated with a layer of graphite particles (Aquadag) to minimize patch effects. The three main electrodes are spaced by machinable ceramic (MACOR) rings on which are painted guard ring electrodes, used to shim out higher-order electric field components. The lower guard ring is split into halves to permit both driving the radial modes of the trapped ion and also coupling the three modes one to the other (Fig. 2.2). The trap has a minimum endcap-to-endcap spacing of 1.2 cm, and a minimum radius of 0.696 cm, giving and effective trap size $d = (z_0^2/2 + \rho_0^2/4)^{1/2} = 0.549$ cm. Guard rings are of the orthogonal design invented by Gabrielse [GAB83]. The trap is inside a copper vacuum can, which cryoadsorbs to ultrahigh vacuum, but there is a line-of-

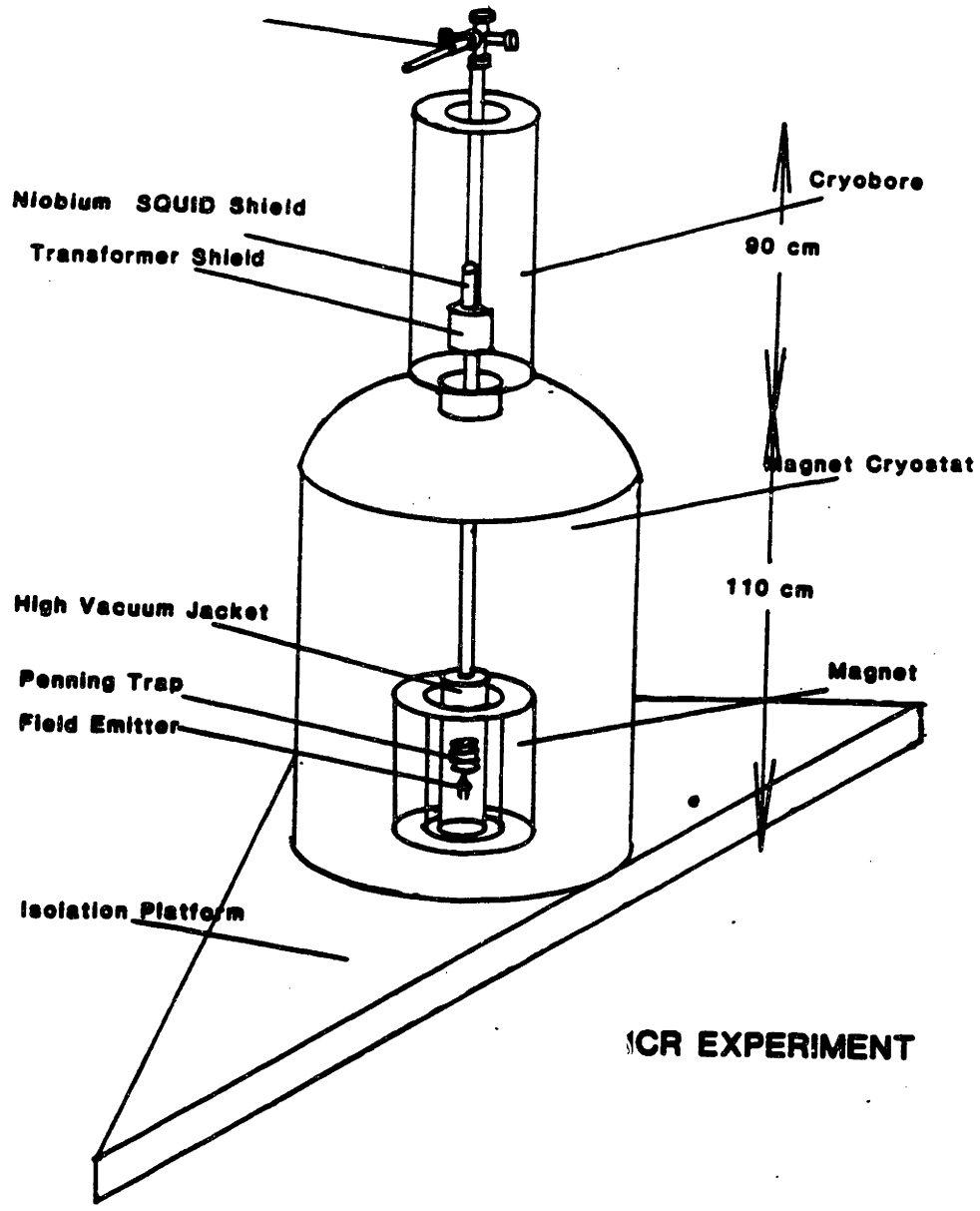

Fig. 2.1 The overall physical arrangement of the trap, the magnet, and the SQUID detector circuit.

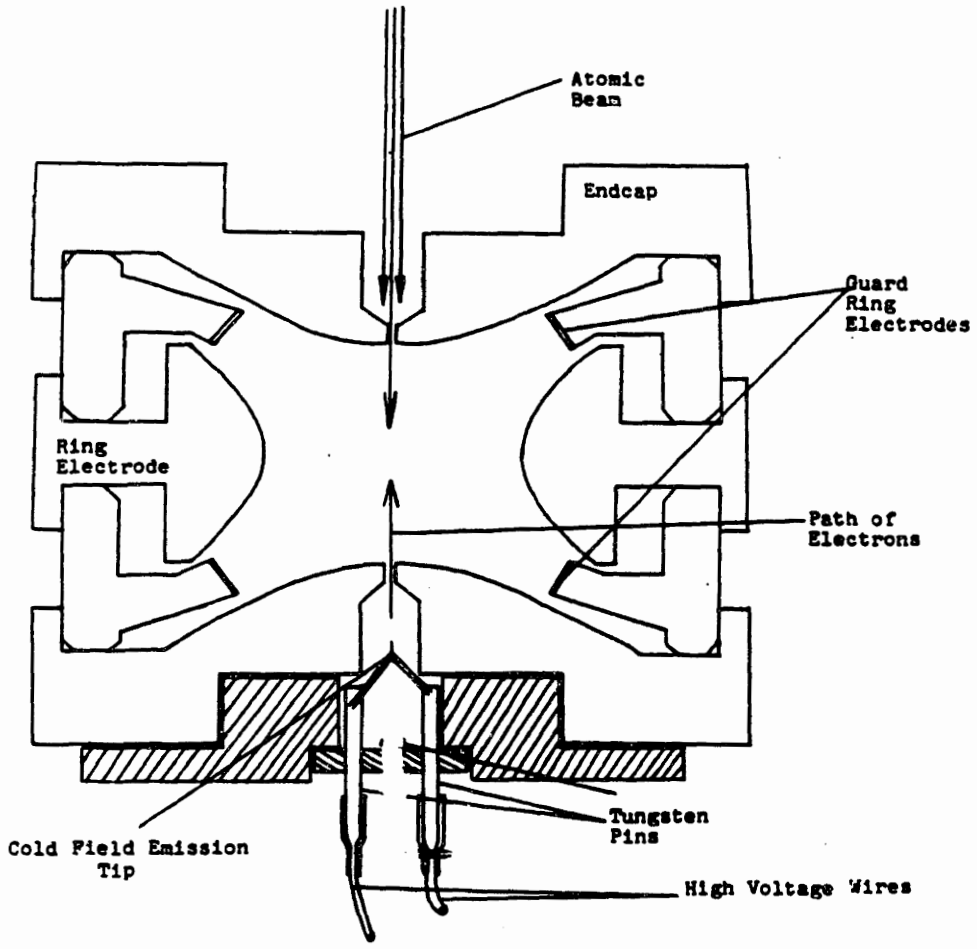

Fig. 2.2 The Penning trap, with field emitter mounted. The trap is axially symmetric, except that the lower guard ring electrode is split into halves to permit driving the radial modes.

sight path through a hole in the center of the upper endcap up the pumpout tube to a room-temperature gas-handling manifold. The vacuum can and pump-out tube are immersed in liquid helium. Ions are created *in situ* from neutral gas admitted from above colliding with electrons which enter the trap from a field-emission point just below.

The ion's motion is detected via the image current induced in the upper endcap. The detection circuit, described in detail in [WLB88 and WEI88], includes a superconducting tank circuit (Q=25,000) and an rf SQUID. When the axial motion of a single ion is in resonance with the detector, the real part of the impedance damps the ion's motion with a 1/e amplitude time constant that scales with the ion mass: $\tau_{1/e}$ = (0.21 sec)(M), where M is the ion mass in amu. A single N_2^+ ion, for example, damps in 6 seconds. The ion sees an effective noise temperature from the detector of about 15K, which is then the cooling limit for the axial motion. Detector signal-to-noise is adequate to detect a single ion driven to 1/4 of the trap size with less than one half second of averaging.

Pulse Sequencing and Data Acquisition: Wares both Hard and Soft

Our more intricate measuring schemes involve driving the ions with several pulses, at different frequencies, administered with precise timing, followed by recording of the ion's response in a way which is sensitive to the phase relations between the pulses and the resulting ion motion. Small wonder a computer figures prominently in the requisite electronics.

The excellent data acquisition software left to us by Robert Weisskoff [WEI88] has been augmented in several ways. First, the programs have themselves been made programmable, in the sense that whole series of little experiments can be performed while the graduate student is asleep, at play, or (more typically) trying to figure out what to do next. More important, Weisskoff's "Transient" program has been generalized to permit any number of driving pulses to be applied to the ions, at various frequencies, in a completely flexible way, before the resulting transient in the ion signal is recorded.

Fig. 2.3 shows a schematic of the ion driving and detecting electronics. Note that the frequency synthesizers, the analog-to-digital converter and the pulse controller are all phase-locked to the same 10 MHz stable clock. The frequency synthesizers are always set to generate integer frequencies. This means that once one has arbitrarily picked a point in time, one second later and every integer number of seconds thereafter the synthesizers will all have the same phase as they had at initial arbitrary point. When we do phase sensitive measurements, the beginning of each pulse-and-detect sequence is triggered by a 1 Hz square wave, thus ensuring the reproducibility of the initial phase of each synthesizer.

Fitting Routine for the Phase and Frequency

Most of the data we take is in a pulsed mode -- we have driven the ion's axial motion suddenly, either directly or via a pulse of energy coupled from a radial mode, and we take data during the few seconds it takes for the motion to damp. The signal (Fig 2.4a),

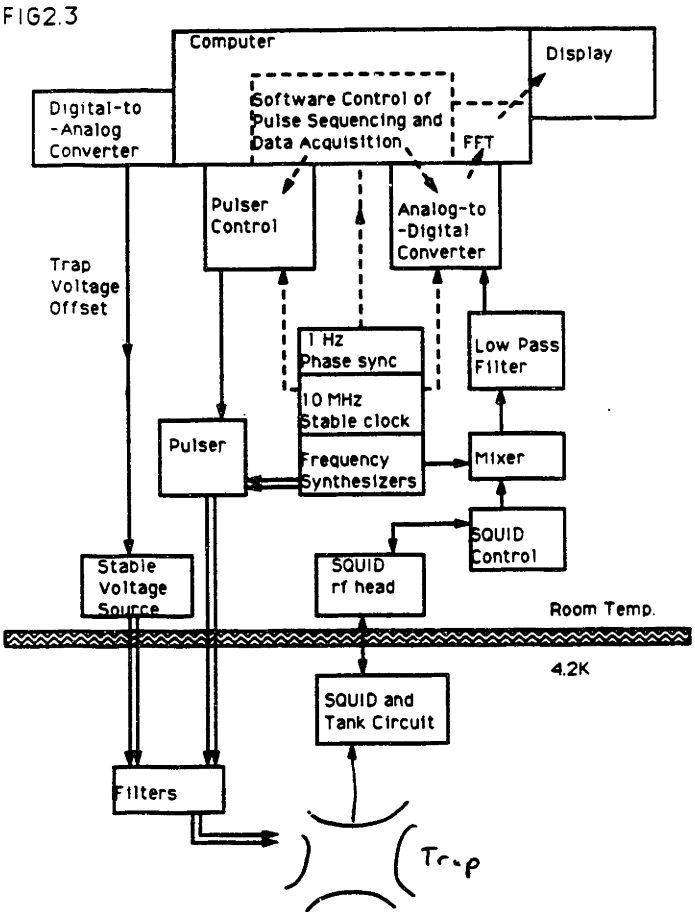

Fig. 2.3 A schematic of some of the electronics for driving and detecting ions. Not shown: electronics for "killing" bad ions.

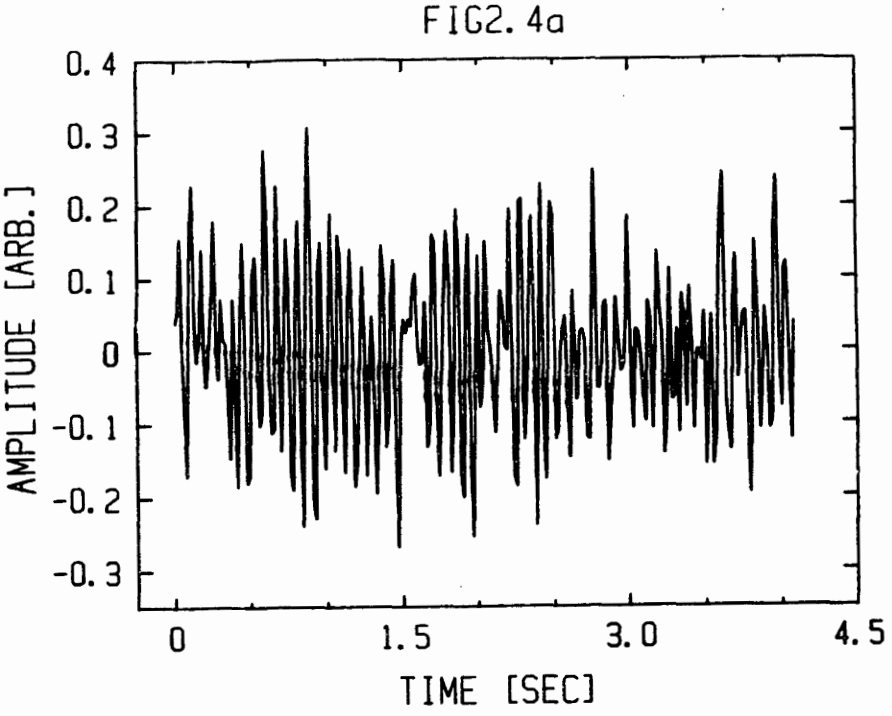

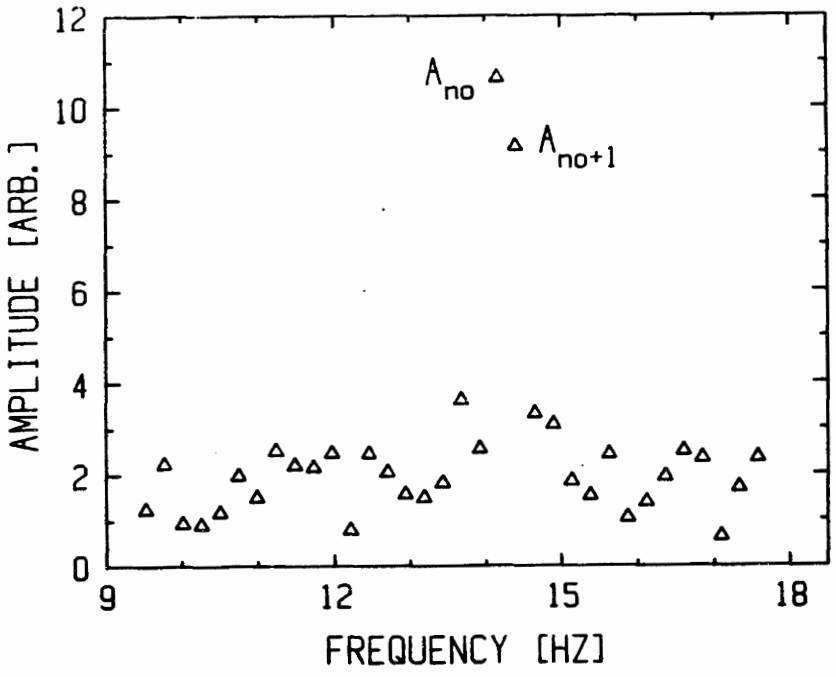

Fig. 2.4 (a) The signal from a single ion that has been excited into an axial orbit of initially 1/5 the trap size. (b) A portion of the discrete Fourier Transform of the signal. The two peak bins, A_{no} and A_{no+1}, are used to determine the central frequency and initial phase and amplitude of the ion signal.

an exponentially damped sinusoid, is always buried in a lot of noise, from which we want to extract three values: the initial amplitude, the initial phase, and the central frequency. A fourth parameter, the damping constant, is necessary to describe a damped sinusoid, but the damping may be independently determined and does not vary much from shot to shot.

One approach to reducing the data would be to use a nonlinear fitting routine, adjusting initial phase, amplitude and central frequency to determine a damped sinusoid shape which best fits the data. Although conceptually simple, this approach is computationally disastrous.

It turns out to be far better for us to use a discrete fourier transform (DFT) to separate the wheat from the chaff. A typical transform of four seconds of signal from a single ion ringing down contains only two or at most three bins of information distinguishable from the noise (Fig. 2.4b). If we include both the real and the imaginary part of the transform, the values in the two highest bins include four real numbers worth of information. If the original input has adequate signal-to-noise, we can use these four numbers to determine the central frequency to better than a bin width and to extract the initial phase and amplitude with a technique free from DFT "windowing" errors. For a very clear explanation of the pitfalls inherent in DFT data analysis, see for instance [WEI88].

The input signal has the form

$$z(t) = \mathrm{Re}\ (B\ e^{i2\pi\nu t - \gamma t}) + \mathrm{noise}\ (t)$$

from which we wish to determine the phase and magnitude of the complex amplitude B and the central frequency ν, given that we already know the damping γ. We will ignore the noise in this treatment, although of course it causes scatter in our final results. The initial data set is a series of N voltage measurements, recorded over time with a sampling rate f_{samp}:

$$z(t_m) = z_m = (B\, e^{(i2\pi mk - 2\pi\beta m)/N} + c.c)/2 \qquad 0 <= m < N-1$$

where N is the number of data points, $t_m = m/f_{samp}$, $k=N\nu/f_{samp}$, and $\beta=N\gamma/(2\pi f_{samp})$

The DFT converts the N initial real values to N/2 complex amplitudes as shown:

$$A_n = \frac{2}{N} \sum_{m=0}^{N-1} z_m\, e^{-2\pi inm/N} \qquad (2.1)$$

Plug in z_m and carry out the summation:

$$A_n = \frac{1}{N}\left[B\left(\frac{1-e^{2\pi i(k-n)-2\pi\beta}}{1-e^{2\pi i(k-n)/N-2\pi\beta/N}}\right)+B^*\left(\frac{1-e^{2\pi i(-k-n)-2\pi\beta}}{1-e^{2\pi i(-k-n)/N-2\pi\beta/N}}\right)\right] \qquad (2.2)$$

Since we are only interested in the peak value of A_n, which we will call A_{no}, and in the neighboring bins, which we will call A_{n-1} and A_{n+1}, we write the frequency $k = k_o + \varepsilon$, with $|\varepsilon| < 1/2$ and k_o an integer. We expand the exponential in the denominator and

ignore the B* term, a good approximation as long as N >>2π and the peak bin n_o is not too near either side of the spectrum, i.e. $(N/2-n_o)$ >> 1, and n_o >>1.

$$A_{no} = B\left[\frac{1-e^{2\pi(i\varepsilon-\beta)}}{2\pi(-i\varepsilon+\beta)}\right] \qquad (2.3a)$$

$$A_{n\pm1} = B\left[\frac{1-e^{2\pi(i\varepsilon-\beta)}}{2\pi(-i\varepsilon+\beta\pm i)}\right] \qquad (2.3b)$$

Now to determine ε from the peak bin and the larger of the A_{n+1} and A_{n-1}, take the ratio $\alpha = (|A_{no}|^2/|An_{+/-1}|^2)$ and solve:

$$\varepsilon = \left[-(\pm1) \pm \left(1-(\alpha-1)^2\beta^2+(\alpha-1)\right)\right]^{1/2} /(\alpha-1) \qquad (2.4)$$

Where the upper (lower) sign corresponds to the case that A_{n+1} (A_{n-1}) is larger. Once we know ε, it is easy to solve equation 2.3 for the initial complex amplitude of the sinusoid:

$$B = A_{no}\left[\frac{2\pi(-i\varepsilon+\beta)}{1-e^{2\pi(i\varepsilon-\beta)}}\right] \qquad (2.6)$$

Of course, B can be expressed as an initial phase and amplitude, and the central frequency is just $\nu = f_{samp}\ (n_o + \varepsilon)/N$. Since B and ν together are only three real numbers, and since real and imaginary parts of the two peak bins are four real numbers, there is some redundancy, which can be useful. If there were no noise, and if the signal were purely a damped sinusoid, certain relations would hold

among the real and imaginary parts of the four peak bins. Assume for definiteness that the upper sidebin is the larger. We use B and ε, which we determine using the magnitude but not the phase of A_{n+1}, to predict a value for Re (A_{n+1}) (Eqn. 2.6). We compare the predicted value with the actual value and use the normalized difference, $(\delta \text{ Re } (A_{n+1}))^2/|B|^2$, as a measure of the "goodness of fit."

Routine to Fit the Two-Ion Difference Frequency

Another analysis trick worth describing here is a technique to extract the difference frequency from two simultaneously recorded signals such as we detect when we have two simultaneously trapped ions. As explained in chapter V below, when two ions are trapped simultaneously, their interaction is nonlinear and thus their frequencies will be amplitude dependent, but under certain conditions the difference frequency will not. The input voltage might look like $z_T = z_1 + z_2$, where the two components are:

$$z_1 = \text{Re } A_1 \exp(2\pi i(\nu_1+f(t))t - \gamma t)$$
$$z_2 = \text{Re } A_2 \exp(2\pi i(\nu_2+f(t))t - \gamma t) \qquad (7)$$

where f(t) represents a frequency shift over time that both ions undergo. Thus at any moment the instantaneous difference frequency, $\nu_1 - \nu_2$, is a constant.

The simplest way to recover $\nu_1 - \nu_2$ from the signal is to square the data in the time domain:

$$(z_T)^2 = \ldots + B_1 B_2^* \exp\{ 2\pi i(\nu_1-\nu_2)t - 2\gamma t \} + c.c + \ldots$$

so that when we take the DFT of z_T^2, there will be a clean, single frequency peak in the spectrum at $\nu_{z1}-\nu_{z2}$. The central frequency and even the difference in the initial *phase* $(B_1B_2^*)/|B_1B_2|$ may be extracted using the debinning technique outlined in the section just above. The problem is that squaring data wastes information -- decreases the signal-to-noise, and in practice the difference frequency peak will not emerge above the noise in the DFT of z_T. We get around this problem as follows: First, we use the DFT of z_T to compute the DFT of z_T^2. If we write

$$Z_{Tm} = \frac{1}{2} \sum_{n=0}^{N/2\ -1} \left[A_n\, e^{2\pi inm/N} + \text{c.c.}\right] \quad \text{, then}$$

$$Z_{Tm}^{\,2} = \frac{1}{2} \sum_{k=0}^{N/2\ -1} \left[C_k\ e^{2\pi ikm/N} + \text{c.c.}\right] \quad \text{, where}$$

$$C_k = \frac{1}{2} \sum_{n'=0}^{N/2\ -1} \sum_{n=0}^{N/2\ -1} \left[\cdots + A_n\, A_{n'}{}^{*}\, \delta_{k,n-n'} + \cdots\right] \qquad (2.8)$$

We see here the "physical" origin of the increased noise after squaring the data: For most values of n, A_n is just noise, but the squaring operation folds this noise into the bins of C_k that contain the desired signal. In our application, the amount the frequency of each ion shifts as it damps is equivalent to only six or seven binwidths in A_n, depending on the size of the initial excitation and the time span of data recorded. The signal for the two ions, then, appears in two sets of seven contiguous bins each in A_n, and nowhere else (Fig. 5.5a). The computer is trained, when performing

the summation (Eqn 8), to include only the bins of A_n that contain signal. This minimizes the noise in the final result. (Fig 5.5b).

Shielding

The SQUID detector is an extremely sensitive nonlinear device, and external electromagnetic noise at any frequency can manifest as noise at the signal detection frequency. To attain the very low noise level necessary to see a single ion, shielding out noise across a broad spectrum is necessary. Any of the half dozen cables attached to the apparatus is potentially an antenna, and higher frequency noise can penetrate the poorly conducting stainless steel Dewar walls and enter the detector directly.

Working to understand the sources of noise and to shield systematically and rationally has been very frustrating. Since the level of noise in our lab varies from minute to minute and from day to day, it is really hard to convince oneself that a particular component of the shielding is doing any good, or even that it is not doing harm. However, two recent modifications to the shielding seem to be big improvements (Fig. 2.5). First, a superconducting lead foil bag now completely surrounds the boxes that hold the tank circuit and the SQUID sensor. Soldered around the end of the SQUID probe tube at top, and around the tube shielding the twisted pair leading to the trap below, the foil bag is very nearly water tight. All seams are soldered shut (the solder should form a superconducting joint) and any holes are meticulously patched with additional foil and solder. Only two holes breech the bag, small pinholes at the top and bottom of the bag to allow liquid helium to

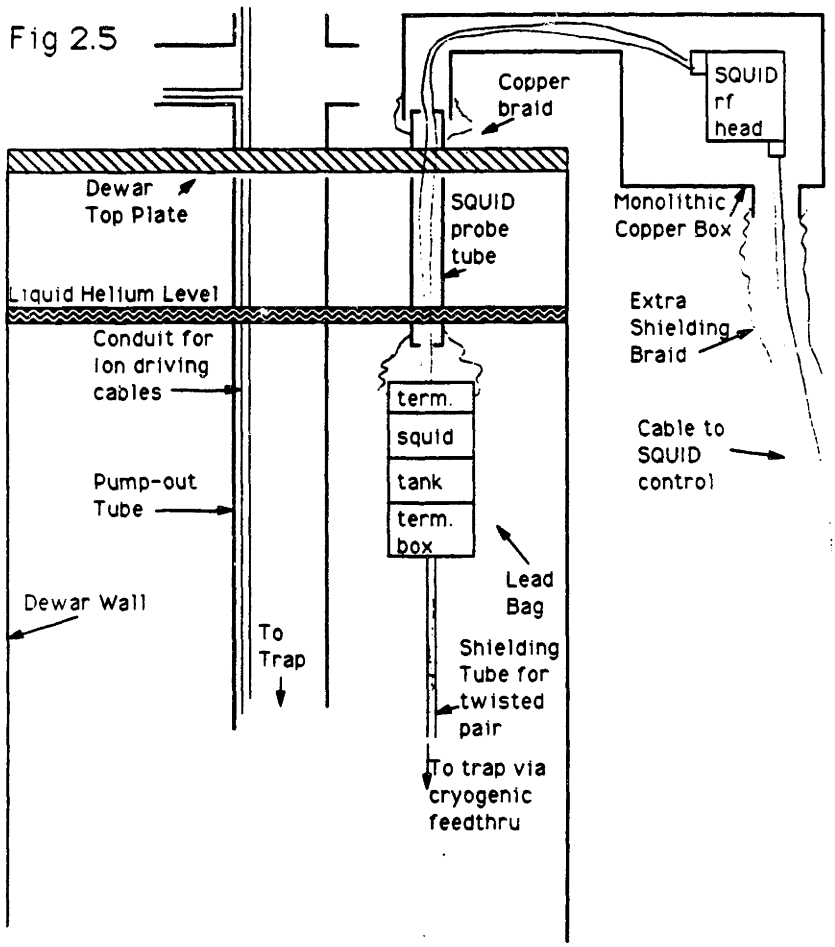

Fig. 2.5 A sketch of additional noise shielding added to the SQUID detector circuit.

flow in and out freely. The pinholes are tucked back into folds in the foil, which should serve to cut off any radiation trying to propagate through the holes. The lead bag itself is wrapped in a layer of aluminum foil, but we have come to mistrust the shielding properties of aluminum foil, and we think of the foil as a sheathing to protect the lead from tears, and not as additional electrical shielding.

A second helpful modification is a large copper box which surrounds the SQUID rf head and its cabling. We now distrust the noise seals on the rf head and on the jacks used to connect the rf head to the cables leading to the SQUID sensor and to the control electronics. Additional copper braid augments the shielding on the SQUID cabling.

Where we think it might be helpful, cables leading to the apparatus are wrapped through a torrus of highly permeable material (Fair-rite) to suppress common mode rf noise.

All in all, the current version of the shielding looks like a desperate overdesign, but it works. Often noise levels on the SQUID are acceptable for weeks or months on end.

External Magnetic Field Monitoring Station

Fluctuations in the external magnetic field cause error in our measurements (see sections 3D and 4C, below) and will continue to be a big problem until we install self-shielding coils [GAT88, and VMF86] or get the two-ion techniques working. Until then, we want to monitor the vertical component of the magnetic field as reliably as possible. The current situation, with a flux-gate

magnetometer probe mounted on a partition wall about three meters from the magnet, is not very satisfactory. For one thing, fluctuations from sources within the lab building may well vary considerable across the several meters from probe to trap. For another, the partition is made of soft steel, and its magnetic permeability may affect the field seen by the probe.

Both problems would be solved if we could mount the magnetometer on a stand near the experiment's Dewar. Unfortunately, the fringe fields from the superconducting solenoid are large enough to drive the magnetometer reading off scale if the probe is any closer than about three meters to the magnet. We are currently building an apparatus to overcome this problem. A solid, mechanically stable stand will incorporate a smaller solenoid coil of its own to null out the fringe fields immediately around the magnetometer probe. The stand and the stable current source for the solenoid are completed, and the solenoid itself is under construction.

Gas Handling System

The room temperature gas handling manifold, used to prepare and dispense the small puffs of neutral gas from which we make ions, has been completely overhauled. Up to five different species of gas may now be stored in various bottles plumbed directly into the manifold. In anticipation of our tritium experiment, much of the plumbing is stainless steel. In addition to a conventional oil-sealed mechanical pump, there is also an oil-free pump to allow us

to flush the tritium out of the system without permanently contaminating a pump.

Magnetic Field Homogeneity

As soon as we had progressed in our technique far enough to be able to use the ion itself to probe the spatial inhomogeneity of the Oxford magnet's field, (section IV, below) we immediately noticed that the field gradients were much larger than we had anticipated, larger, in fact, than could be compensated for using the superconducting shim coils built into our magnet. The main problem turned out to be the field emission point, which was mounted on posts constructed not only of tungsten, as we had thought [WEI88], but of ferromagnetic nickel. Moreover, earlier calculations [FLA87] had suggested that the MACOR guard rings, which are both paramagnetic and near the trap center, were responsible for some portion of the gradients. We replaced the field emission point and also installed a thin nickel ring around the outer circumference of the central electrode, a ring of size and location calculated to compensate for the bulk of the MACOR effect (Fig. 2.6). We constructed a current source to charge the Oxford magnet shim coils. The shimming procedure is described in section 4C, below.

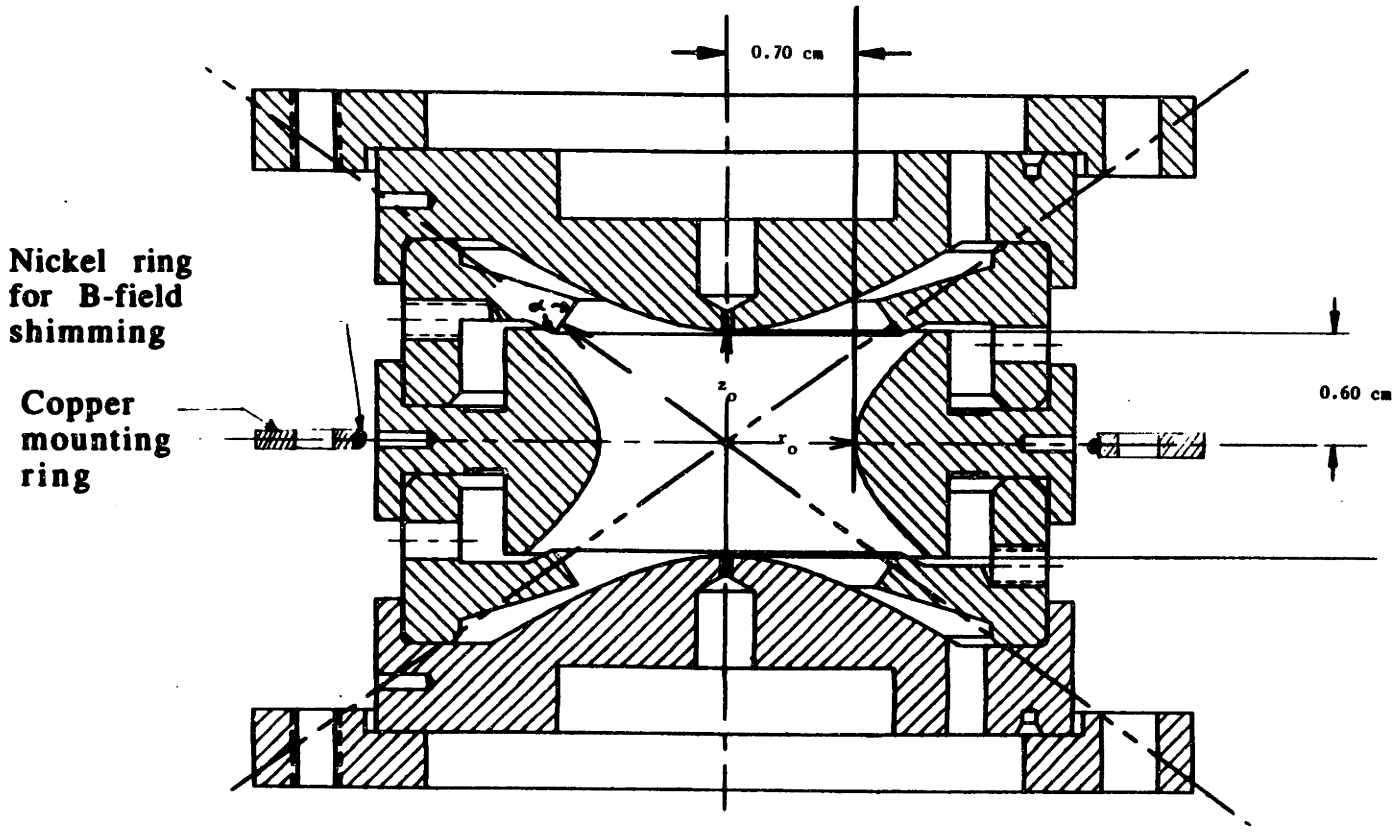

Fig. 2.6 Drawing shows the location of a thin, ferromagnetic nickel ring added to compensate for some of the magnetic distortions caused by the MACOR guard rings.

Chapter 3 Sources of Error in Single Ion Mass Spectroscopy

This chapter discusses the sources of error in single ion cyclotron resonance mass comparisons. In section 3A I review how to correct the trap cyclotron frequency for the effects of the electric field in order to determine the free-space cyclotron frequency. Although this correction is a large one, it can in principle be done exactly and thus is not strictly speaking a source of error in and of itself. Section 3B covers the effects of electric and magnetic field imperfections and of special relativity. The magnitudes of these effects are about a part in 10^9, but they will typically be the same for both species to within a few percent and thus, for a mass doublet,† will affect the measured mass ratio hardly at all. Section 3C covers several miscellaneous sources of error. These effects are all small but potentially treacherous because they may vary systematically with ion species. Section 3D assesses the errors due to the temporal drift in the magnetic field. For single ion measurements on mass doublets, drift in the magnetic field is much the largest source of error.

---

† The mass ratios we are most interested in determining are those between two molecules that each have the same total number of protons and neutrons, so-called "mass doublets." The two molecules in a mass doublet will differ in mass by less than a part in 10^3.

3A. Correcting for the Electric Field

The presence of the electric field in our Penning trap perturbs the cyclotron frequency by almost a part in 10^3 -- for part in 10^9 mass spectroscopy, the electric field is no small correction! Fortunately, there is a theorem, due to Brown and Gabrielse [BRG82], relating the free space cyclotron frequency to the three measured trap frequencies.

$$\omega_c^2 = (\omega_c')^2 + \omega_z^2 + \omega_m^2 \qquad (3.1)$$

Here ω_c', ω_z, and ω_m are the frequencies measured in the (possibly) imperfect trap. This relationship is exactly correct as long as the magnetic field is uniform and the electric field is purely quadrupole. The magnetic field need not be aligned with the axis of the electric field, nor need the electric quadrupole field be axially symmetric.

Because of the inequality $\omega_c' >> \omega_z >> \omega_m$, we see from Eqn. 3.1 that only ω_c' need be measured to the final accuracy desired, $\delta\omega_c/\omega_c$. An error in measuring the axial frequency $\delta\omega_z$ contributes a relative error of $(\omega_z^2/\omega_c^2)\delta\omega_z/\omega_z$ to the determination of ω_c. An error in measuring the magnetron frequency contributes only $(\omega_m^2/\omega_c^2)\delta\omega_m/\omega_m$.

If the trap is neither out-of-round nor tilted, we can determine† the magnetron frequency from the other two measured

---

† None of the equations in section 3A and 3B is my work. Anything not specifically attributed in the text is derived, or at least reviewed, in [BRG86] or [WEI88] . I recommend both works; the material is summarized here only as a convenience to the reader.

frequencies: $\omega_m = \omega_z^2/(2\omega_c')$. For a small tilt θ between the magnetic field and the electric quadrupole axis, the magnetron frequency is

$$\omega_m = \omega_z^2/(2\omega_c')[1 + (9/4)\sin^2\theta + O(\theta^4)]. \qquad (3.2)$$

If all three trap frequencies are measured, Eqn. 3.2 may be used to estimate the trap tilt angle θ. It is frequently the case that θ and ω_m^2/ω_c^2 are sufficiently small that ω_m need not be separately measured, and Eqn 3.1 may be approximated as follows:

$$\omega_c^2 = (\omega_c')^2 + \omega_z^2 + (\omega_z^2/(2\omega_c'))^2 \qquad (3.3)$$

The relation (Eqn 3.1) does not include the effects of a nonuniform magnetic field, nor of a nonquadrupole electric field, nor of special relativity. In a physically realizable trap, the effects of field flaws and special relativity are always present, and they are discussed in the next section.

3B. Field Flaws and Special Relativity

If the ion were confined to a infinitesimally small region around the center of the trap -- that is, if its cyclotron, magnetron and axial radii were all very small -- the ion would have no way of knowing that the magnetic field was nonuniform, or that the electric field had nonquadrupole components. Moreover, in this small-radii regime, the magnitude of the ion's velocity would vanish as well. Therefore, special relativity and field flaws would have no effect on the measured trap frequencies. In reality, the ion *does* have some finite motion about the trap center; the imperfect fields *are* sampled; the velocity does *not* vanish; and the measured

trap frequencies will be shifted from their ideal values, the perturbation proportional to even powers of the radii.

This section describes how flawed electric and magnetic fields can be characterized by polynomial expansions about the center of the trap, and how the frequency shifts resulting from these field flaws and from special relativity can be expressed in power series expansions of the cyclotron, axial and magnetron radii. Knowing the form of these shifts, one can extrapolate to vanishing radii to recover frequencies that would be measured in an ideal trap.

Electric Field Expansion

Assuming that the trap is axially symmetric,* we can write the electric potential in *spherical* † coordinates as follows:

$$V(r) = V_t \sum_{k=0}^{\infty} C_k \left(\frac{r}{d}\right)^k P_k(\cos\theta) \qquad (3.4)$$

where P_k are the Legendre polynomials. For the region of the trap in which the ion moves, r/d is a small number, perhaps 0.2 at most, so the expansion converges rapidly. C_0 is a uniform potential without physical significance. C_1 vanishes with appropriate choice of the origin. C_2 is just the desired quadrupole trapping potential. The lowest order field imperfections then are C_3 and C_4. The trap is

---

* The effect of small axial asymmetries will be thoroughly averaged away by the ion's magnetron motion over the course of a measurement. The exception is a tilt of the electric quadrupole axis with respect to the magnetic field (discussed in section 3A, above).

† Well, I lied. It turns out once in a while I need to use spherical instead of cylindrical coordinates.

constructed to be very symmetric with respect to reflection about the z = 0 plane, so the C_3 component of the electric field, odd with respect to reflection across the z = 0 plane, is small. For most purposes C_4 is the only component of the electric field imperfection we need to worry about. If the ion is excited to particularly large orbits, as when the axial frequency is being measured, the value of C_6 can become important. The principal function of the guard ring electrodes is to shim out the C_4 fields resulting from patches of surface charge and from imperfect trap construction. If C_4 has been very nearly nulled out, the effect of the asymmetric C_3 may become significant (see below in this section and also in Chapter 4C).

Magnetic Field Expansion, and Ion Velocity

The magnetic field, like the electric field, may be expanded in components about trap center. We consider only the three lowest order axially symmetric terms:

$$\mathbf{B} = B\hat{z} + B_1\left[z\hat{z} - \frac{\rho}{2}\hat{\rho}\right] + B_2\left[\left(z^2-\frac{\rho^2}{2}\right)\hat{z} - z\,\vec{\rho}\right] \qquad (3.5)$$

The coefficient B is just the uniform trapping field. B_1 is essentially a linear gradient field and B_2 is the second order gradient. B_1 and B_2 may be independently corrected for with superconducting shim coils in the Oxford magnet. (See chapter 4B below.)

The special relativistic frequency shift

$$\delta\omega_i/\omega_i = (1-\langle v^2/c^2\rangle)^{-1/2} - 1 \qquad (3.6)$$

is to lowest order proportional to the mean square velocity. Motion in all three normal modes contribute to the total mean square velocity

$$\langle v^2 \rangle = \omega_c^2 \rho_c^2 + (a_z^2/2)\, \omega_z^2 + \rho_m^2\, \omega_m^2 . \qquad (3.7)$$

The cyclotron frequency is so much the highest of the frequencies that for most purposes we need consider only the cyclotron contribution to the velocity: $\langle v^2 \rangle = \rho_c^2\, \omega_c^2$.

Effect on Normal Mode Frequencies of "The Big Three" -- B_2, C_4 and Special Relativity

In most situations, the three largest radius-dependent perturbations are the B_2 magnetic gradient, the C_4 electrostatic component, and special relativity. I recapitulate here the results from [BRG86] concerning the effects of these three perturbations, to second order in the mode radii. The results are readily expressed in matrix form:

$$\begin{bmatrix} \delta\omega_c'/\omega_c' \\ \delta\omega_z/\omega_z \\ \delta\omega_m/\omega_m \end{bmatrix} = D \begin{bmatrix} \rho_c^2 \\ a_z^2 \\ \rho_m^2 \end{bmatrix} \qquad (3.8)$$

where the matrix D is given by

$$D = \begin{bmatrix} \frac{-B_2}{2} - \frac{\omega_c^2}{2c^2} + \frac{3\omega_m C_4}{2\omega_c d^2} & \frac{+B_2}{2} - \frac{3\omega_m C_4}{\omega_c d^2} & \frac{-B_2}{2} - \frac{3\omega_m C_4}{\omega_c d^2} \\ \frac{-\omega_c B_2}{4\omega_m} - \frac{\omega_c^2}{2c^2} - \frac{3C_4}{2d^2} & \frac{3C_4}{4d^2} & \frac{B_2}{4} - \frac{3C_4}{2d^2} \\ \frac{\omega_c B_2}{2\omega_m} - \frac{\omega_c^2}{2c^2} - \frac{3C_4}{d^2} & \frac{-B_2}{2} + \frac{3C_4}{d^2} & \frac{B_2}{2} - \frac{3C_4}{2d^2} \end{bmatrix}$$

(Eqn. 3.9)

I have already simplified this matrix somewhat by not including the velocity associated with the axial and magnetron motion in the special relativistic shift (represented in Eqn 3.9 by the terms with c^2 in the denominator). Many of the other terms are also absolutely negligible. Since we are interested in the frequency shifts of the axial and the magnetron modes only in as much as they affect our final determination of the free space cyclotron frequency, let's look at another matrix:

$$\begin{bmatrix} \delta\omega_c/\omega_c[\omega_c'] \\ \delta\omega_c/\omega_c[\omega_z] \\ \delta\omega_c/\omega_c[\omega_m] \end{bmatrix} = D' \begin{bmatrix} |C|^2 \\ |Z|^2 \\ |M|^2 \end{bmatrix} \qquad (3.10)$$

here the notation $\delta\omega_c/\omega_c[\omega_i]$ refers to the portion of the error in determining ω_c contributed by the error in measuring the perturbed frequency of the i_{th} mode. As explained in section 3A above, the contribution to the final error from the measurement of the axial frequency is down by ω_z^2/ω_c^2 and from the magnetron frequency, by ω_m^2/ω_c^2. To get D' from D, multiply the first row of D by 1, the second row by ω_z^2/ω_c^2 and the third row by ω_m^2/ω_c^2.

This matrix notation is very compact, but potentially misleading, because it leads one to believe that there is a single vector, (ρ_c, a_z, ρ_m) that describes the mode radii during the frequency measurement of all three modes. Actually, for any given measurement, the two modes which aren't being measured have only thermal motion, while the measured mode's radius has been driven to a much larger value. (See section 4G). So we must use a different set of radii to calculate the error associated with each different mode. Because the measured mode's radius is always the largest, it is the diagonal elements of D' that contribute most of the error. In Tables 3.1 and 3.2, I evaluate some experimentally useful numerical examples of the matrix elements D'_{cc} and D'_{zz}.

In the particular case of our measurement of $M(CO^+)/M(N_2^+)$, only the elements D'_{cc} and D'_{zz} contribute errors larger than five parts in 10^{11}. But in writing out D' I preserve several smaller terms for illustrative purposes explained below.

$$D' = \begin{bmatrix} \frac{-B_2}{2} - \frac{\omega_c^2}{2c^2} + \frac{3\omega_m C_4}{2\omega_c d^2} & \frac{+B_2}{2} - \frac{3\omega_m C_4}{\omega_c d^2} & \frac{-B_2}{2} - \frac{3\omega_m C_4}{\omega_c d^2} \\ \frac{-B_2}{2} & \frac{3\omega_m C_4}{2\omega_c d^2} & 0 \\ 0 & 0 & 0 \end{bmatrix} \quad (3.11)$$

For determining the mass ratio of a doublet, (see the footnote on the first page of Chapter 3, above) the size of the average perturbations, given by the matrix D', is not the key issue. If a

perturbation is constant and identical for the two ions, it affects the ratio hardly at all. There are two important questions then: First, how much scatter do "thermal" fluctuations in ρ_c, a_c, and ρ_m, cause in a particular frequency from measurement to measurement. It is the size of this scatter that determines the number of times a frequency must be measured to reach a desired precision. Second, how does the average value of the radii vary systematically with ion species? Any systematic variation is obviously very worrisome.

Thermal Fluctuations in Radii

It is easy to predict the thermal fluctuations in the mode radii, although it is hard to verify them experimentally. In theory it should be like this: The axial motion is coupled to the tuned circuit, and it comes to equilibrium with the effective temperature of the circuit, T_z. Mode coupling pulses applied at the cyclotron and magnetron coupling frequencies will reduce their temperatures, T_c and T_m, to the pi-pulse cooling limit: $T_c = (\omega_c/\omega_z)T_z$, and $T_m = (\omega_m/\omega_z)T_z$ (see e.g. [CWB90], reprinted as section 4B, below) These temperatures correspond to the following thermal radii:

$\rho_{cth} = \langle\rho_c^2\rangle^{1/2} = [\ (2T_z)/(\omega_z\omega_c m)\ ]^{1/2} = 1.3\text{x}10^{-3}$ cm.

$\rho_{mth} = \langle\rho_m^2\rangle^{1/2} = [\ (2T_z)/(\omega_z\omega_c m)\ ]^{1/2} = 1.3\text{x}10^{-3}$ cm.

$\rho_{zth} = \langle\rho_z^2\rangle^{1/2} = [\ (2T_z)/(\omega_z\omega_z m)\ ]^{1/2} = 7\text{x}10^{-3}$ cm.

The quoted numerical values are for single mass 28 ions in our trap, in which T_z is about 15K. (Amplifier noise prevents the axial mode from coming into equilibrium with the 4.2K liquid helium bath).

The two modes whose frequencies are not being measured have thermal radii. The mode being measured has been driven by

a short pulse to some larger value, perhaps 20 times the thermal radius. The thermal radius that the driven mode has just before the driving pulse is applied adds vectorially to the effect of the drive pulse, so the variance in the square of the driven radius is just $2\rho_o \rho_{th}$, where ρ_o is radius the driven ion would have in the absence of initial thermal motion.

The measurement-to-measurement variation in the mean square radius depends on the mode due to the specific measurement procedure which we employ. When we measure for example the trap cyclotron frequency, we observe how much cyclotron phase evolves during a long period of time between two widely separated pulses (In the case of the $M(CO^+)/M(N_2^+)$ measurement, the pulses are separated by up to 65 seconds.) During the measurement, the axial motion remains coupled to a thermal bath via the tuned circuit. Thus although the scatter in the initial axial radius is the full thermal value, the axial radius reequilibrates with the thermal bath 22 times in the course of the measurement, so the scatter in the square of the axial radius, averaged over the whole measurement period, is not ρ_{zth}^2 but $\rho_{zth}^2/(22)^{1/2}$.

The magnetron radius, on the other hand, is not coupled to the thermal bath (except when we deliberately apply the mode coupling fields, as we do before each sequence of measurements). So no matter how long a cyclotron measurement takes, the scatter in the mean square magnetron radius is just the thermal value, ρ_{mth}. In fact, unless we deliberately cool the magnetron radius in

the middle of a series of cyclotron measurements (we don't, as a rule), the magnetron radius remains constant, and thus error proportional to ρ_m^2 will not average away over the series of measurements. The case of the cyclotron radius is intermediate between the case of the axial and of the magnetron radii. The cyclotron radius does not couple to the thermal bath during a particular measurement, but the process of reading out the cyclotron phase after each measurement reequilibrates the cyclotron motion with the thermal bath, so that the scatter in the ρ_c-dependent perturbation is reduced by the square root of the number of individual cyclotron measurements made.

Some numerical examples of the size of thermal effects are presented in Tables 3.1 and 3.2.

Systematic Dependence on Species

If we average away thermal effects, are the two ions always measured at exactly the same radii? A systematic difference could arise in several different ways -- frequency-dependent driving amplitudes, background-pressure effects (see section 3C, below), leakage drive from an a.m. radio station resonantly heating one species more than the other, etc. Experimentally, every phase or frequency measurement we make yields an amplitude measurement as well, and we can verify, by averaging many of these measurements, that any species-dependent amplitude change is less than 3% for N_2^+ and CO^+. This means that a systematic error

from perturbations proportional to the radius squared must be less than 6% of the the average value of the perturbation.

Numerical examples are presented in Tables 3.1 and 3.2.

Cancelling Relativistic Perturbation of the Cyclotron Frequency

There is no fundamental reason why we can't adjust C_4 and B_2 to be as small as we like, and thus minimize the effects of field flaws. But we have no knob we can turn to eliminate special relativity. We have, however, considered a scheme to cancel out the effects of relativity by intentionally leaving residual field gradients. Notice the first row of the matrix D. (Eqn. 3.3) If we adjust $C_4=0$ and $B_2 = -\omega_c^2/c^2$, the cyclotron frequency becomes independent to second order of ρ_c.

Further, with the appropriate choice of B_2 and C_4, it is possible to make ω_c independent, to second order, of both the cyclotron and the magnetron radii. Such a configuration may be particularly useful for two-ion cyclotron resonance, during which the magnetron orbits are quite large, and the average relativistic shift is a hundred times larger than the desired final accuracy. This will be discussed in Chapter 5, below.

Frequency Shifts from Potentials with Odd Symmetry

The B_1 and the C_3 field components, because of their odd parity, contribute to frequency perturbations in second order, i.e. as B_1^2, C_3^2, or B_1C_3. For instance, the ρ_c^2-dependent effect of B_1 on the trap cyclotron frequency is $\delta\omega_c'/\omega_c' = (\omega_c^2/\omega_z^2)(B_1^2/2)\rho_c^2$.

The a_z^2-dependent effect of C_3 on the axial frequency is $\delta\omega_z/\omega_z = (-15/16)(C_3^2/d^2)a_z^2$.

B_1 can be accurately measured and shimmed (See Chapter 4) to a point where its effect is negligible. Unfortunately, it is difficult to measure C_3^2 independently from C_4, which may make it difficult to perform the delicate adjustment of C_4 necessary to implement the relativity-cancelling scheme suggested above.

Effects Proportional to Higher Powers of the Mode Radii -- And Summary of Radius-Dependent Effects

The field components of higher order than C_4 and B_2 give rise to frequency shifts in most combinations of even powers of the mode radii -- a_z^4, $a_z^2\rho_c^2$, ρ_m^6, whatever. A thorough analysis of all these dependencies becomes very tedious, but we are saved by the simple fact the expansion parameters $(\rho_i/d)^2$ are very small, and thus the fourth and higher order perturbations are correspondingly much smaller than the quadratic perturbations.

The one exception to this rule is the quartic dependence of ω_z on a_z, which we will discuss in Chapter 4C.

I will conclude this section by emphasizing two crucial points: First, all the perturbations due to field imperfections and special relativity vanish quadratically in the limit of very small mode radii. Thus if we extrapolate frequency measurements made at various-sized radii down to vanishing radii, we recover the ideal frequency values. Second, for the purpose of determining the mass ratio of a doublet, there is no need to explicitly perform the extrapolation, as

long as we are convinced the frequencies of the two different ion species are measured at nearly identical radii.

Section 3C. Miscellaneous Little Effects

Unseen Impurity Ions

The effects of impurity ions trapped along with a single ion are usually quite obvious. The axial frequency is anharmonic and unstable, and magnetron cooling seems ineffectual. We go to great lengths to eject the impurity ions, and we are confident that we usually succeed. After performing the ion purification routine (see Chapter 4), we are rewarded with a stable and well-behaved ion that shows no sign of being affected by impurity ions. Sometimes, however, the bad ion seems to "reappear", in the form of observable instability in the good ion, perhaps some 10 to 15 minutes after completion of the purification routine. The timing of the bad ion's return leads us to believe that the bad ion was never completely ejected from the trap, but rather inserted into a very large orbit, where it did not significantly perturb the good ion. Over the course of ten minutes the bad ion cooled, (perhaps via collisions with neutral gas or via weak interactions with the resistively cooled good ion,) until its orbit was small enough to allow it once again to manifest its presence by perturbing the good ion.

It is very rare for a bad ion to resurrect itself after more than about 15 minute's absence from view. A series of precision

cyclotron measurements takes 30 minutes, and we habitually assume that if no instability disturbs the good ion over these 30 minutes, then measurements made on that ion are free from bad ion perturbations.

Our assumption that absence of instability implies absence of perturbations carries a risk. The possibility exists that the purification process drives bad ions into some very large orbit, a sort of Oort cloud if you will, out of which the bad ions do not cool in the course of 30 minutes, and that the separation is such that although the trap frequencies do not exhibit instability, they are unacceptably perturbed from their single ion values.

This is a rather conspiratorial scenario and although we can not discard it out of hand, we *can* say that the effect of the Oort cloud ions is not very large, or not very large very often, or it would have appeared as scatter in our ion mass comparisons.

Residual Neutral Gas Atoms

During the course of several days measurements, we load new ions into the trap a dozen or more times, injecting perhaps 10^2 torr-cc into the high vacuum system. Most species of atoms and molecules have completely negligible vapor pressure at 4.2K, and thus the residual pressure in the trap remains below 10^{-12} torr. At this pressure, interactions between trapped ions and background neutral gas will affect the measured frequencies not at all. But in the particular case of measurements on hydrogen and helium atoms there is some cause for concern. The bulk vapor pressure of helium

(760 torr) and hydrogen (approximately 10^{-7} torr) at 4.2 K are far too high to permit precision trap measurements. We rely on the fact that the vapor pressure of thin films of molecules adsorbed on surfaces is usually much lower than for the same molecules in bulk. As long as we admit only small quantities of gas, the gas should distribute itself thinly over the available cold surfaces, and the residual vapor pressure should be acceptable.

How low must the vapor pressure be to be acceptable? One major concern is that there be no hard, cyclotron-dephasing collisions occurring between the pulses of the separated oscillatory fields measurement of the cyclotron frequency. If the ion has a cross section σ for a hard collision with the dominant species of background gas, then during a s.o.f. measurement of duration T the ion sweeps out a volume $\sigma\rho_c\omega_c T$, where ρ_c is radius of the initial cyclotron excitation. We require that there usually be no neutral atom in this volume. For a precision measurement on a mass 3 amu ion, with an approximate cross-section $\sigma = 10^{-14}\ cm^2$, this requirement is met if the density is lower than 10^7 neutral molecules/cc, which is to say, if the pressure at 4.2K is lower than 3×10^{-12} torr.

Less obvious (and more insidious) are the effects of grazing collisions. It takes some time for the pressure to reequilibrate after each burst of atoms is admitted into the vacuum system, time for the neutral atoms "find their niche". The pressure in the system during the equilibration period will most likely differ depending on whether, say, helium-3 or tritium has just been loaded. If the

pressure is low enough that there are seldom hard, dephasing collisions, but high enough to slightly damp the amplitude of the cyclotron motion, cyclotron frequencies for the two species will be measured at different average radii. This raises the specter of a measurement error with systematic dependence on species. If we do wind up making a mass 3 measurement, some thought should be put into ruling out pressure-dependent frequency shifts.

Tuned Circuit Pulling

The tuned circuit coupled to the ion's axial motion not only damps the axial motion but also shifts its frequency slightly. Since the ion's coupling to the detector is weak, (the damping time for the ion τ_z is much greater that the damping time for the detector τ_{coil}) the magnitude of the ion's frequency shift is small and proportional to the imaginary component of the circuit's impedance. If the ion's detuning from the circuit's resonance is small, $(\omega_{coil} - \omega_z) << 1/\tau_{coil}$, the resulting shift in the axial frequency is given by [WEI88]

$\delta\omega_z = - (\omega_z - \omega_{coil}) (\tau_{coil} / \tau_z)$.

For example, an N_2^+ ion has a damping time of $\tau_z = 6$ seconds, while our resonant detection circuit damps in $\tau_{coil} = 43$ msec. If we were particularly sloppy in tuning the axial frequency to the circuit frequency, we might have $(\omega_z - \omega_{coil})/2\pi = 1.5$ Hz. The resulting shift in the axial frequency is then on the order of a few mHz, which contributes a relative error to the free space cyclotron frequency of less than a part in 10^{10}.

Patch-Effect Shifts

Please see section 4F for a description of this source of error. Though only a problem at the part in 10^{11} level for mass doublets, it can cause significant error in measurements on non-doublets.

III.D Temporal Changes in the Magnetic Field

Our approach to comparing masses by comparing cyclotron frequency measurements rests on the assumption that the magnetic field remains constant. The field at the center of our trap is *not* constant, and it is the uncertainty in the field change that is the dominant source of error in our experiment. Specific details of the causes and consequences of the field drift are presented in Chapter 4E, but a few general comments are appropriate here.

If the field variations were very smooth, if they could be represented by say a linear or a quadratic in time, we could readily remove the field variations from the data; the variations would be no limit on our overall accuracy. If, on the other hand, the field variations were totally uncorrelated, just normally distributed scatter about an average field value, we could make N measurements on one ion and N measurements on the other, and be able to determine -- in a completely orthodox way -- the error in our average difference frequency.

When we fit the cyclotron frequency data to two offset smooth curves, (Chapter 4F, 4G) our initial estimate of the error is based on the assumption that the field variations are accounted for by a "linear combination" of these two extremes: uncorrelated

scatter on a smooth underlying drift. If the actual field behavior is more complicated -- in the conspiratorial worst case the field varies in a square wave with phase and frequency commensurate with our ion swaps -- our naive initial estimate may understate the error.

I emphasize that temporal variations in the magnetic field have several causes, and that it is difficult even to *a priori* estimate their relative contributions, let alone compensate for them. We are confident, however, that the magnetic field variation is in no way a *systematic* effect. We take great care to avoid doing anything that might change the magnetic field in a way which is correlated to ion species. On the other hand, to the extent that the field changes have a *random* effect, the obvious way to estimate their magnitude is to use the scatter in our data. Our approach has been to collect several sessions of data, average the results using our preliminary error estimate as a weighting function, and then set conservative error bars based on the scatter.

For example, in section 4G (the CO^+/N_2^+ comparison) our error bars encompass the values from all three runs, whether the magnetic field drift is fit by a linear, quadratic or cubic polynomial (the one exception being the results of the linear fit to run #1, a fit whose poorness is manifest in the large error bars assigned by the fitting routine). See Table 1 at the end of section 4G. See chapter 4E for further discussion.

3E Single Ion Error -- Conclusion

The main result of this chapter is that, for the time being, magnetic field temporal instability is the major source of error in comparing the masses of doublets. We have considered a large variety of other frequency perturbations, and found them all to have an insignificant affect on mass doublet ratios. To review:

The presence of the electrostatic quadrupole field perturbs the cyclotron frequency in a very well understood way, which can be corrected for to very high accuracy. [BRG83]

Frequency shifts having to do with spatial inhomogeneity of the fields and special relativity are small, less than a part in 10^9, and moreover are the same to much higher accuracy for both members of the doublet. This conclusion has been subjected to a number of experimental tests, the most crucial of which I cover in section 4C.

A variety of smaller effects, some quite exotic, have been analyzed, and in some cases investigated experimentally, and are shown to cause insignificant error.

Not covered so far in this chapter, but worthy of dispatching here, are several possible objections which are not a source of concern at all:

Although the cyclotron frequency is measured by a phase-sensitive technique, (see Section 4B) the measurement is not sensitive to accumulated phase shifts, whether in the driving

electronics, the detection electronics, or in the phase read-out routine. This is because we measure the frequency from the *change* in measured phase with respect to the length of a time delay.

Another potential concern is that the physical process of changing from one ion species to another induces some systematic change in the trapping fields. We go to great lengths to avoid any such shift and are quite confident that none occur. Any *random* change in trapping fields with the injection of a new ion, while undesirable, manifests itself as increased scatter in the measurements and is duly incorporated into the error estimate. Incidentally, in our earlier experiments we did see large (perhaps part in 10^8) and unpredictable cyclotron frequency jumps when we switched from one ion to another. But we were able to reduce the size of these jumps to the point of undetectability (parts in 10^{10}) by reducing the residual magnetic field gradients and by modifying our procedure for loading ions in such a way as to avoid physically bumping the apparatus during the ion interchange procedure. See Section 4F, and Fig. 4.9 for some data taken with this particular concern in mind.

Thus it is really only unpredictable changes in the magnetic field that contribute significantly to the overall comparison error. But we expect that two ion cyclotron resonance techniques will reduce the effect of field jitter to the point where we will once again have to worry about field inhomogeneity, special relativity, the "pulling" effect of the tuned circuit, and so on.

An overall accuracy of 4 parts in 10^{10} is not necessarily the limit for single ion cyclotron resonance with our apparatus. There is always the possibility of simply taking more data. With perhaps a week of nighttime runs, it should be possible to reduce the field jitter noise to perhaps 2 parts in 10^{10}. We considered a project like that for our carbon monoxide-nitrogen measurement but decided against it because half a part per billion seemed good enough, for the time being, and because we anticipated advances in field stabilization and two-ion resonance techniques.

	$\delta\omega_c'/\omega_c'$ Analytic Form	Corresponding $\delta\omega_c/\omega_c$					
		Mass 3		Mass 28		Mass 18	
		now	soon	now	soon	soon	cancelling
Size of Effect	$\rho_c^2\{-\omega_c^2/2c^2-B_2/2 +(3C_4\omega_m)/(2d^2\omega_c)\}$	2×10^{-9}	2×10^{-9}	8×10^{-10}	3×10^{-10}	4×10^{-10}	4×10^{-11}
Thermal Fluctuation	$2\rho_c\rho_{cth}\{$ " " $\}$	3×10^{-10}	3×10^{-10}	1×10^{-10}	1×10^{-11}	2×10^{-11}	3×10^{-12}
Systematic Difference	$2\rho_c\delta\rho_c\{$ " " $\}$	1×10^{-10}	1×10^{-10}	4×10^{-11}	6×10^{-12}	8×10^{-12}	1×10^{-12}

Table 3.1. Effect, to second order, of cyclotron radius on cyclotron frequency. The thermal fluctuation is the shot-to-shot variation in the measured frequency. The systematic difference refers to possible ion species-dependent frequency shifts. The numerical values are evaluated for three different sets of parameters, "now", corresponding to typical current trap tuning, "soon", reflecting feasible improvements, and "cancelling", a scenario in which the trap is shimmed to cancel the effect of special relativity. Common to all three situations in the assumption that the cyclotron radius is large enough so that, after a pi-pulse, the resulting axial amplitude is a_z = 0.13 cm, thus initial $\rho_c = (\omega_z/\omega_c)^{1/2}(.13\text{cm})$. The thermal cyclotron motion, $\rho_{cth} = [2kT_c/(m\omega_c^2)]^{1/2}$. The errors quoted are "worst case" in the sense that I assume that relativity and the maximum absolute values of C_4 and B_2 quoted below all contribute with the same sign to the total error.

The values "now" are $|C_4| < 5\times10^{-5}$, $|B_2| < 1.5\times10^{-6}$, T_z = 15K, $T_c = (\omega_c/\omega_z)T_z$, and the maximum systematic difference in cyclotron radius sizes for the two species is $\delta\rho_c/\rho_c < 3\%$.

The values "soon" are $|C_4| < 1.5\times10^{-5}$, $|B_2| < 1\times10^{-7}$, T_z = 5K, $T_c = (\omega_c/4\omega_z)T_z$, and $\delta\rho_c/\rho_c < 1\%$.

The values "cancelling" involve arranging B_2 so as to cancel the relativistic perturbation and make ω_c' independent of ρ_c to second order. $|C_4| < 1.5\times10^{-5}$, $B_2 = -\omega_c^2/c^2$, T_z = 5K, $T_c = (\omega_c/\omega_z)T_z$, and $\delta\rho_c/\rho_c < 1\%$ The quoted errors assume B_2 has been incorrectly adjusted by 10% ($\delta B_2 = 1 \times 10^{-7}$).

	$\delta\omega_z/\omega_z$ Analytic Form	Corresponding $\delta\omega_c/\omega_c$ (D'_{zz}) Mass 3 now	Mass 3 soon	Mass 28 now	Mass 28 soon	Mass 18 soon
)f Effect	a_z^2 $\{(3C_4/(4d^2)\}$	$2x10^{-11}$	$7x10^{-12}$	$2x10^{-9}$	$6x10^{-10}$	$3x10^{-10}$
mal uation	$2a_z a_{zth}$ $\{(3C_4/(4d^2)\}$	$3x10^{-12}$	$6x10^{-13}$	$3x10^{-10}$	$5x10^{-11}$	$2x10^{-11}$
matic rence	$2a_z\delta a_z$ $\{(3C_4/(4d^2)\}$	$2x10^{-12}$	$2x10^{-13}$	$1x10^{-10}$	$1x10^{-11}$	$6x10^{-12}$

3.2. Effect, to second order, of axial amplitude on axial frequency, and the sponding error introduced into the determination of the cyclotron frequency (by 3.11). The axial amplitude a_z = 0.13 cm. The thermal axial motion, a_{zth} = $/(m\omega_z^2)]^{1/2}$.

The values "now" are $|C_4| < 5x10^{-5}$, T_z = 15K, and the maximum systematic ence in axial amplitudes for the two species is $\delta a_z/a_z < 3\%$.

The values "soon" are $|C_4| < 1.5x10^{-5}$, T_z = 5K, and $\delta a_z/a_z < 1\%$.

Chapter 4 Techniques and Results

Section 4A Catching a Single Ion

Catching an Ion, Tuning the Trap

When the ring and guard-ring voltages are correctly set, when the protocol for getting rid of impurity ions is in order, and when all the electronics are all working well -- in short, when everything is tuned up -- trapping a single ion is the work of less than half an hour. But getting to that well-tuned state may take weeks or months, even understanding the apparatus as well as we do now.

On a typical well-tuned day, the procedure for trapping a single ion is as follows: Briefly reverse the voltage on the trap to remove any ions left-over from previous experiments. Fill the gas-handling manifold with the appropriate pressure of the desired species of gas. Turn on the electron gun and leave it on a few seconds while admitting the neutral gas into the cryogenic region of the apparatus. Reduce the voltage on the lower endcap for 1 second, "dip" the ions, as we say, to allow most of the newly created ions to escape. Verify, by pulsing the axial motion and seeing how large a transient signal results, that of the desired species only a single ion remains. Run an automated purification routine which excites the axial motion of impurity ions with white noise (band-limited, so that the axial motion of the good ion is not excited) and then dips the ions, so that only the good ion remains in the trap. Finally, apply a coupling drive at the axial-magnetron cooling

frequency to remove the magnetron excitation that often results from the purification routine. The whole procedure should take only 20 minutes, 45 minutes at the outside.

Unfortunately, when the trap is reinserted in the magnet after a round of repairs or modifications, it is not in a well-tuned state. The ring voltage, the guard-ring voltage, the correct endcap voltage for "dipping" the ions very close to the lower endcap, and even sometimes the efficiency of the cryogenic electronics all change from cool-down to cool-down. It is hard to adjust the guard-ring voltage when there are impurity ions present, and it is hard to eject the impurity ions when the guard-rings are mistuned. Tuning up the trap is a process of inspired guessing which may take dozens of working sessions.†

Other Ion Species -- the Patch Effect

Once we have managed to tune the trap for one species, usually N_2^+, tuning the trap up for other ion species is much easier. We find that for a well-tuned trap, the voltages for the ring and the guard ring electrodes are given by

$$V_{ring} = m(\omega_z^2 d^2/e) + V_{ringpatch} \qquad (4.1)$$

$$V_{guardring} = m(\omega_z^2 d_{gr}^2/e) + V_{guardringpatch} \qquad (4.2)$$

---

† We are considering a modification to the apparatus which will allow externally produced, mass-selected ions to be injected into the trap. This might greatly simplify the tuning problem by insuring that there are no bad ions in the trap from the start.

where d_{gr} is a constant with dimensions of length that sets the slope of the guard-ring potential with respect to ion mass, and d becomes the measured trap size (as opposed to the machined trap size, defined in Fig. 1.1). $V_{ringpatch}$ and $V_{guardringpatch}$ are voltage offsets which vary from month to month. In the absence of any better understanding, we call these offsets "the patch effect". $|V_{ringpatch}|$ is usually on the order of 30 or 40 mV, and changes discontinuously when the trap is warmed to room temperature and recooled. $|V_{guardingpatch}|$ can be as large as 200 mV and is also "reset" every time the trap is cycled. The trap dimensions d and d_{gr} are much more stable. We measure

d = 0.5479(1) cm. and d_{gr}= 0.3973(8) cm. The measured value of d agrees well with the value specified for machining, d = 0.5487(10) cm. The experimentally determined value of d has remained constant to a part in a thousand, and of d_{gr} to a two parts in a thousand, over several years of trapping experiments. (However, if the trap is tilted, both d and d_{gr} must be multiplied by a factor of $(1 + 3/2\sin^2\theta)$ in order to correctly predict the tuned trap voltages.)

Other Ion Species -- Signal-to-Noise, Bad Ions, Background Pressure

Working with each species of ion has its own particular challenges. For instance, the lighter the ion we are working with, the less energy there is in an axial excitation of given amplitude. (Recall that the axial frequency is always tuned to be resonant with our detector at 160 kHz.) Less energy in turn means smaller

signal-to-noise ratios in our measurements of transient excitations. While the signal-to-noise detected from a single pulsed N_2^+ ion is adequate and from a single N^+ ion is marginal, there is no hope of being able to detect the axial signal from a single $^3He^+$ ion in the time it takes to damp (about 0.5 seconds). Precision work with very low mass ions will require us to use different (non-pulsed) techniques or else improve our detector.

Another species-dependent experimental difficulty is impurity ion expulsion. Let us imagine, for instance, that the dominant impurity species is tungsten ions that have been sputtered out of the field emission point. When we are working with N_2^+ ions, the trap voltage is such that the axial frequency of W^+ is about 62 kHz. When we work with N^+ ions, the voltage on the trap is lower, and the W^+ axial frequency is only 44 kHz. It may be that a impurity ion ejection protocol we developed while experimenting with N_2^+ is adequate to eject ions at 62 kHz but inadequate to eject ions at 44 kHz. (The efficiency of the ion driving electronics starts to fall off quite rapidly around 60 kHz.) With each new ion species, we have been obliged to reoptimize our impurity ion ejection protocol, a trial-and-error process that establishes ejection drives strong enough to get rid of the bad ions while gentle enough to preserve the desired species.

The least tractable problem we have encountered with novel ion species concerns background neutral gas. Tuning up the trap for mass 3 amu ions, (so that we can measure the helium-3/tritium mass ratio) has been a priority with us for over 18 months. Our

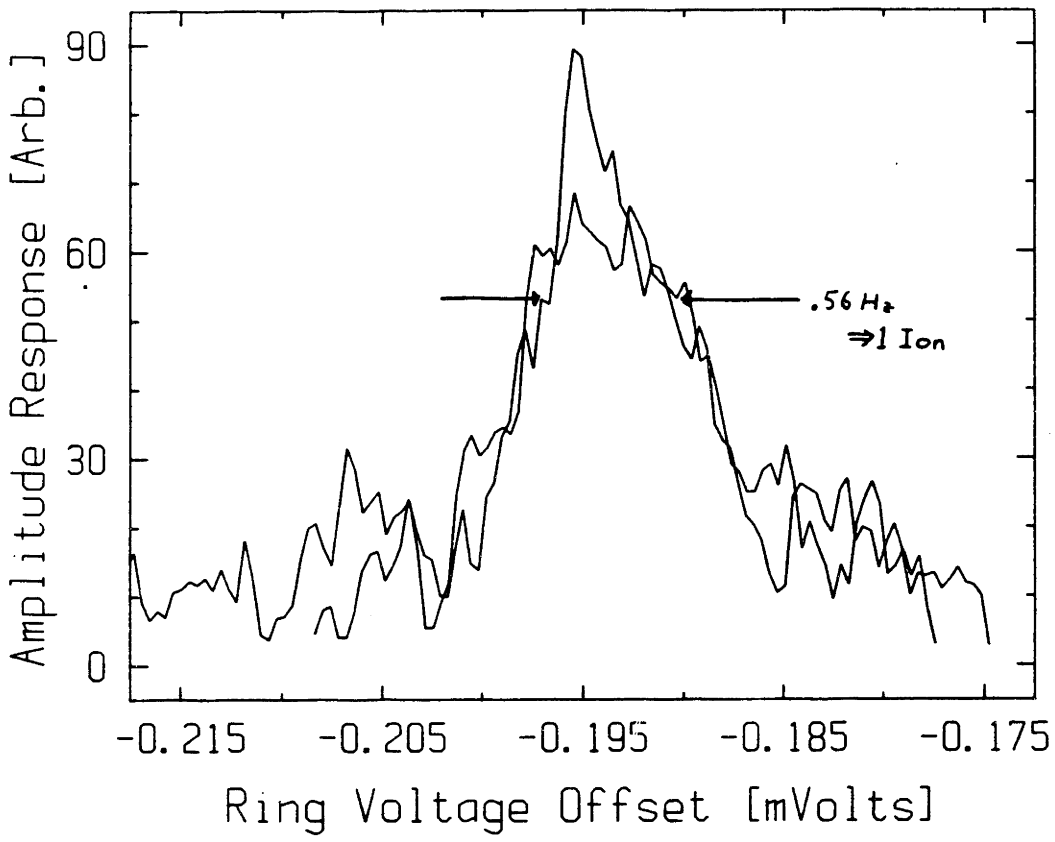

Fig. 4.1 The signal from a single HD^+ ion, detected by ramping the trap voltage so as to sweep the ion's resonant frequency across the two-frequency drive. The homogeneous width of the resonance is proportional to the number of trapped ions. The FWHM calculated for a single ion is .48 Hz.

approach has been to load the trap with HD^+ molecular hydrogen ions, a species which is very close in mass to helium-3 and tritium. (Fig. 4.1) Unfortunately, every time we begin work with the hydrogen gas, we always find experimental conditions deteriorating after a only a very few days of tests. Our suspicion is that the hydrogen gas in not cryopumping efficiently, and that background neutral gas pressure is building up in the apparatus. However, we can't rule out other possible explanations -- for instance, that for some reason an unusually large number of impurity ions are made after the trap has been contaminated with hydrogen.

Section 4B Mode Coupling Techniques

In our trap, only the axial mode couples directly to the detector. As a consequence, the cyclotron and magnetron modes are normally undamped and undetectable. In order to cool these motions, and in order to measure their frequencies, we need to temporarily couple the two radial modes to the axial mode. We accomplish this with an inhomogeneous rf electric field applied via oscillating potentials [WID74, VSD78] on the split guard rings. Such coupling fields have typically been used in a continuous wave fashion for damping the magnetron motion, so-called sideband cooling. We have developed a pulsed technique, which enables us to swap the action of one mode with the action of another, in a phase-coherent way, using a single pulse. We use this "pi-pulse" technique for measuring frequencies and also for cooling the

cyclotron motion. Typically we use the more conventional sideband cooling for damping the magnetron motion.

Section 4B was originally published [CWB90] in *Physical Review A* in January of 1990, with three coauthors listed on the title page below:*

* There is a notation change in section 4B. Note that the complex mode amplitudes, C, M and Z, have dimensions of [(action)$^{1/2}$] in section 4B, whereas elsewhere in this thesis they have dimensions of [length].

Mode Coupling in a Penning Trap: π-pulses and a Classical Avoided Crossing

Eric A. Cornell, Robert M. Weisskoff*,
Kevin R. Boyce and David E. Pritchard

Research Laboratory of Electronics
Department of Physics
Massachusetts Institute of Technology
Cambridge, MA 02139

Abstract:

An inhomogeneous radio frequency electric field can couple the cyclotron and axial modes of a single ion in a Penning trap. The classical equations of motion are the same as those of a driven quantum mechanical two-level system. We discuss an analog of the π-pulse, which can exchange mode actions, and an analog of avoided crossing. Experimental illustrations are presented.

PACS: 07.75.+h, 46.10.+z, 41.70.+t, 32.90.+a

Submitted to Phys. Rev. A

In experiments to perform precise resonance measurements on single charged particles in a Penning trap[VSD87,VMF88,CWB89], only one of the particle's normal mode motions is typically detected directly. For example, in our recent single ion cyclotron resonance experiment[CWB89,WLB88], only the axial mode couples to our detector. The cyclotron and the magnetron modes are undetected and essentially undamped. Cooling, driving and measuring the frequency of the undetected modes require techniques for coupling them to the detected mode.

Wineland and Dehmelt[WID75] suggested that an inhomogeneous rf electric field at the sum or difference frequency of two modes will couple those modes, and that in particular the magnetron mode can be cooled by coupling it to the damped axial mode. The technique was demonstrated experimentally by Van Dyck, Schwinberg, and Dehmelt[VSD78], Cohen-Tannoudji[COH84] and Brown and Gabrielse[86] discuss rf coupling fields in some generality and rigor. In this paper we develop two particular effects of such coupling fields, using an analogy with a two-state quantum mechanical system to motivate our purely classical results.

The data which we present here were taken on an apparatus designed to compare the cyclotron frequencies of single ions with the eventual goal of measuring ion mass ratios to parts in 10^{12}. The apparatus, an orthogonally compersated [GAB85], hyperbolic Penning trap in a cryogenic environment is described in references [CWB89 and WLB88].

For work with a single particle of mass m and charge e it is convenient to write the

electric and magnetic fields in an ideal Penning trap as

$$\vec{E} = \frac{-\omega_z^2 m}{e} z\hat{z} + \frac{1}{2}\frac{\omega_z^2 m}{e}(x\hat{x} + y\hat{y})$$

$$\vec{B} = \frac{c\,\omega_c m}{e}\hat{z}$$

where $\omega_z^2 \equiv e V_{trap}/(md^2)$, $\omega_c \equiv eB_o/(mc)$, d is the characteristic trap size, and e is the charge on the ion. The motion of the ion in these fields is a linear superposition of the three normal modes,

$$\vec{r} = \mathrm{Re}\left(a_c e^{i\omega_c' t}(\hat{x} + i\hat{y}) + a_z e^{i\omega_z t}\hat{z} + a_m e^{i\omega_m t}(\hat{x} + i\hat{y})\right)$$

where

$$\omega_c' = \tfrac{1}{2}\left[\omega_c + \sqrt{\omega_c^2 - 2\omega_z^2}\right]$$

$$\omega_m = \tfrac{1}{2}\left[\omega_c - \sqrt{\omega_c^2 - 2\omega_z^2}\right]$$

and a_c, a_z, and a_m are the complex amplitudes of the cyclotron, axial, and magnetron motions, respectively[BRG86]. We will work in the approximation $\omega_c \gg \omega_z \gg \omega_m$. For most of this paper, we study the example of cyclotron-axial coupling, although, as explained below, this approach can be adapted to magnetron-axial coupling. For cyclotron-axial coupling, the perturbation frequency ω_p must be near the difference frequency, with a small detuning δ: $\delta \equiv \omega_p - \omega_c' + \omega_z$. In our experiment, the fields are produced by applying voltages to segments of the guard rings. Near the center of the trap, the coupling field to lowest order is an oscillating quadrupole field tilted with respect to the static electric field:

$$\vec{E}_p = \mathrm{Re}(\mathcal{E}_p e^{i\omega_p t})(x\hat{z} + z\hat{x})$$

where $\mathcal{E}_p$ is the complex amplitude of the coupling field gradients.

For simplicity, we assume that the cyclotron mode may be treated as if it were a one dimensional harmonic oscillator, with spring constant $k = \omega_c'^2 m$. In the presence of a driving force in the $\hat{x}$ direction, we ignore the $\hat{y}$ motion and write the equation of motion:

$$\ddot{x} + \omega_c'^2 x = \frac{F_x}{m}$$

A Green function treatment of the ion's motion in the $x-y$ plane shows that this assumption is good for $\omega_c' \gg \omega_m$ when F_x is nearly resonant with the undriven cyclotron motion, at ω_c' [BRG86,WEI88]. Then the forces from the coupling field give two parametrically coupled simple harmonic oscillators.

$$\ddot{z} + \omega_z^2 z = \mathrm{Re}\left[\frac{e\mathcal{E}_p}{m} e^{i\omega_p t} x\right] \tag{1a}$$

$$\ddot{x} + \omega_c'^2 x = \mathrm{Re}\left[\frac{e\mathcal{E}_p}{m} e^{i\omega_p t} z\right] \tag{1b}$$

We guess solutions

$$z = \mathrm{Re}\left[\frac{Z(t)}{\sqrt{\pi m \omega_z}} e^{i\omega_z t}\right]$$

$$x = \mathrm{Re}\left[\frac{C(t)}{\sqrt{\pi m \omega_c'}} e^{i\omega_c' t}\right]$$

and define the coupling strength in units of frequency:

$$V \equiv \frac{ie\mathcal{E}_p}{2m\sqrt{\omega_z \omega_c'}}$$

Z and C are slowly varying functions of t, such that $|Z|^2$ and $|C|^2$ equal the classical action (i.e. $|\oint p_{canon.} \cdot dq|$, see Table 1) in each mode. Making the adiabatic approximation, and keeping only secular terms, Equation 1 becomes

$$\dot{Z} = \frac{+V^*}{2} e^{-i\delta t} C \tag{2a}$$

$$\dot{C} = \frac{-V}{2} e^{+i\delta t} Z \tag{2b}$$

We recognize the standard equations for a driven two-level system[CDL77]. Two particular properties of these equations are of experimental importance to us.

Action Exchanging Pulses

The first property concerns the special case $\delta = 0$. Imagine that the coupling drive is on between $t = 0$ and $t = \tau$. Before the pulse, the initial conditions are:

$$Z(t) = Z_o \qquad t \leq 0 \tag{3a}$$

$$C(t) = C_o \tag{3b}$$

where C_o (Z_o) is a complex number proportional to the initial phase and action of the cyclotron (axial) motion.

During the pulse, the solution to Equation 2 satisfying Equation 3 is

$$C(t) = C_o \cos\frac{|V|t}{2} - \frac{V}{|V|} Z_o \sin\frac{|V|t}{2} \qquad 0 < t \leq \tau$$

$$Z(t) = \frac{V^*}{|V|} C_o \sin\frac{|V|t}{2} + Z_o \cos\frac{|V|t}{2}$$

If the strength and duration of the pulse is such that $|V|\tau = \pi$, then after the pulse:

$$C(t) = \frac{-V}{|V|} Z_o \qquad t > \tau$$

$$Z(t) = \frac{V^*}{|V|} C_o$$

Note that the action and phase information of the cyclotron motion is preserved now in the axial motion (but shifted by the phase of the perturbing field). Similarly, the π-pulse has put the initial phase and action of the axial mode into the cyclotron mode. The total action, $|Z|^2+|C|^2$, is a constant of the motion. Figure 1 illustrates the effect of mode-coupling pulses of varying strengths.

This π-pulse is used in a novel technique for measuring the cyclotron frequency ω_c'. We begin the measurement by driving the (initially cold) ion into a cyclotron orbit of known phase with a pulse of rf electric field directly at the cyclotron frequency. The cyclotron motion evolves in the dark, unperturbed by coupling fields, for a precise length of time T, and then, with a π-pulse, the cyclotron motion is swapped into the axial mode. We then detect the current induced on the endcaps and determine the phase. The procedure is repeated with a variety of lengths of time between pulses T, to determine the cyclotron phase as a function of T. The cyclotron frequency is simply the time derivative of the cyclotron phase. Reference [CWB89] describes a precision mass comparison made using this technique. The procedure is essentially a variant of Ramsey's method of separated oscillatory fields[RAM56], except that it is the final *phase,* rather than the transition probability, that is measured after the two pulses.

The π-pulse may be used to cool rapidly the cyclotron mode by exchanging its action with that of the resistively cooled axial mode. The cooling limit for this scheme

(Table 1) is the same as the limit for cw sideband cooling[BRG86], but the π-pulse cooling *rate* is higher.

Avoided Crossing

The second interesting property, which we call a "classical avoided crossing" is again easily understood in analogy with a near-resonantly driven two-level system. In this case, the analogy is to the dressed atom formalism[DAC85]. Instead of thinking of the motion of the perturbed ion as swinging back and forth between the axial and cyclotron modes, we can find time-independent linear superpositions of cyclotron and axial motions, the normal modes of an ion "dressed" by the oscillatory perturbative field.

By analogy with driven systems generally, we expect that the two components will oscillate with frequencies which differ by the driving frequency, ω_p. We guess that the dressed modes consist of the ion moving in the axial direction with a frequency ω near ω_z, with $\varepsilon \equiv \omega - \omega_z$, and at the same time moving in the cyclotron direction with frequency $\omega + \omega_p$, so that $(\omega + \omega_p) - \omega_c' = +\delta + \varepsilon$.

Then solutions to Equations 2 will have the form

$$Z(t) = D_z e^{i\varepsilon t}, \; C(t) = D_c e^{i(\varepsilon+\delta)t}$$

where (D_z, D_c) describes the eigenvector of the dressed mode. Plugging these solutions into Equation 2, and solving the characteristic equation for ε, we get two solutions:

$$\varepsilon = \frac{-\delta}{2} \pm \tfrac{1}{2}\sqrt{\delta^2 + |V|^2} \qquad (4)$$

We can observe the dressed modes directly by exciting the axial motion of an ion with a short pulse and then detecting the axial component of its ring-down signal in the presence of a coupling drive. As the coupling drive approaches resonance, the observed axial frequency shifts from its unperturbed frequency. For small detunings both modes have significant axial components and it is possible to detect the axial component of both modes simultaneously (Fig. 2). By fitting the observed frequency shifts to the avoided crossing line shape (Eq. 4), one obtains a value for the cyclotron frequency and a calibration for the strength of the coupling drive, $|V|$, a quantity which is difficult to calculate from electrode geometry a priori.

Magnetron Motion

Extending the preceding results to magnetron/axial couplings involves a few subtleties. To begin with, the magnetron motion, driven near resonance in the $\hat{x}$ direction, does *not* act like a simple harmonic oscillation with spring constant $k = \omega_m^2 m$. But again using a Green function approach, we find that by rescaling the applied force

$$F_x' = -F_x \frac{\omega_m}{\omega_c'}$$

we can write the equation for the near resonantly driven magnetron motion in the familiar form

$$\ddot{x} + \omega_m^2 x = \frac{F_x'}{m}$$

In order to get coupled equations of motion in the form of Equation 2, it is necessary for the coupling frequency to be near the *sum*, rather than the difference frequency, so we define the detuning $\eta \equiv \omega_p - \omega_z - \omega_m$

Guessing solutions

$$z = \mathrm{Re}\left[\frac{Z(t)}{\sqrt{\pi m \omega_z}} e^{i\omega_z t}\right]$$

$$x = \mathrm{Re}\left[\frac{M(t)}{\sqrt{\pi m \omega_c'}} e^{i\omega_m t}\right]$$

and defining V exactly as before, we get the equations

$$\dot{Z} = \frac{-V}{2} e^{+i\eta t} M^*$$

$$\dot{M}^* = \frac{+V^*}{2} e^{-i\eta t} Z$$

The π-pulse and the avoided crossing results follow from here.

Acknowledgements

We are grateful for helpful discussions and advice from G. Gabrielse, R. Van Dyck, and D. Wineland. This work was supported by the National Science Foundation (grant #PHY86-05893) and by the Joint Services Electronics Program (DAAG-29-83-K-0003). E.A.C. acknowledges support from an NSF graduate fellowship.

*present address: Advanced NMR Systems, 30 Sonar Drive, Woburn, MA 01801

Figure Captions

Fig. 1 For each plotted point, the following experiment is performed: An N_2^+ ion is excited into a 0.2 mm radius cyclotron orbit, a 40 msec coupling pulse (of indicated strength) is applied, and the resulting axial amplitude measured. The solid curve, the absolute value of a sine wave, is fit to the points. The peak at pulse strength 11 mV-sec corresponds to a π-pulse, the zero at 22 mV-sec, a "2π-pulse", and so on.

Fig. 2 An experimental illustration of the avoided crossing effect, using a single N_2^+ ion. We adjust the coupling frequency in 1 Hz increments, then excite the axial motion by pulsing. Each trace is the fast fourier transform (fft) of the detected signal from the axial motion after the excitation. The dotted lines are a fit of the peak centers to the avoided crossing line shape (Eqn. 4) . The fit yields $|V|=1.5(1)$ Hz and $\nu_c'-\nu_z=4{,}467{,}761.36(15)$ Hz.

Table 1. A summary of mode properties and cooling limits. The action of the cyclotron or magnetron mode is just 2π times the magnitude of the canonical angular momentum, (note that the magnetron canonical angular momentum is dominated by the field term, $\vec{r}\times e\vec{A}/c$). The cooling limits given for the cyclotron and magnetron modes are reached after a single π-pulse exchanges the action in the mode to be cooled with the action in the axial mode, which is assumed to have been cooled resistively to an rms radius r_{zth}, corresponding to a temperature T_z. The cyclotron or magnetron motion is then cooled by a single π-pulse at the appropriate frequency.

Figures for Section 4B

TABLE I. Summary of mode properties and cooling limits. The action of the cyclotron or magnetron mode is just 2π times the magnitude of the canonical angular momentum [note that the magnetron canonical angular momentum is dominated by the field term, $\mathbf{r}\times e\mathbf{A}/c$ (Ref. 14)] The cooling limits given for the cyclotron and magnetron modes are reached after a single π pulse exchanges the action in the mode to be cooled with the action in the axial mode, which is assumed to have been cooled resistively to a rms radius r_{zth}, corresponding to a temperature T_z.

Mode	Angular momentum $\mathbf{r}\times(m\mathbf{v}+e\mathbf{A}/c)$	Action $\lvert\oint p\cdot dq\rvert$	Cooling limit for π pulses rms radius	T_{eff}
Axial		$\pi m\omega_z a_z^2$	a_{zth}	T_z
Cyclotron	$-\frac{1}{2}m\omega_c' a_c^2$	$\pi m\omega_c' a_c^2$	$(\omega_z/\omega_c')^{1/2}a_{zth}$	$(\omega_c'/\omega_z)T_z$
Magnetron	$\frac{1}{2}m\omega_c' a_m^2$	$\pi m\omega_c' a_m^2$	$(\omega_z/\omega_c')^{1/2}a_{zth}$	$(\omega_m/\omega_z)T_z$

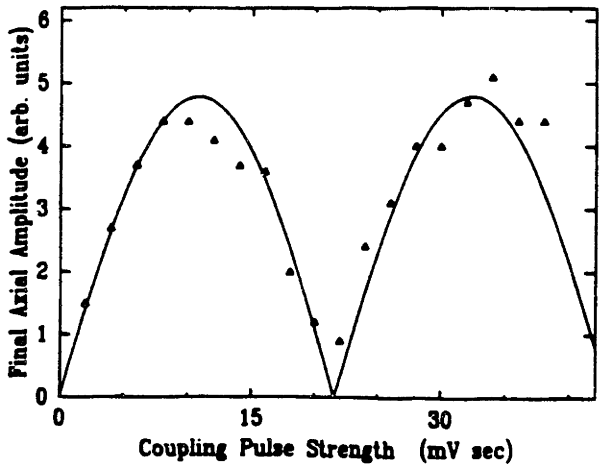

FIG. 1. For each plotted point, the following experiment is performed: An N_2^+ ion is excited into a 0.2-mm-radius cyclotron orbit, a 40-msec coupling pulse (of indicated strength) is applied, and the resulting axial amplitude measured. The solid curve, the absolute value of a sine wave, is fit to the points. The peak at pulse strength 11 mV sec corresponds to a π pulse, the zero at 22 mV sec to a 2π pulse, and so on.

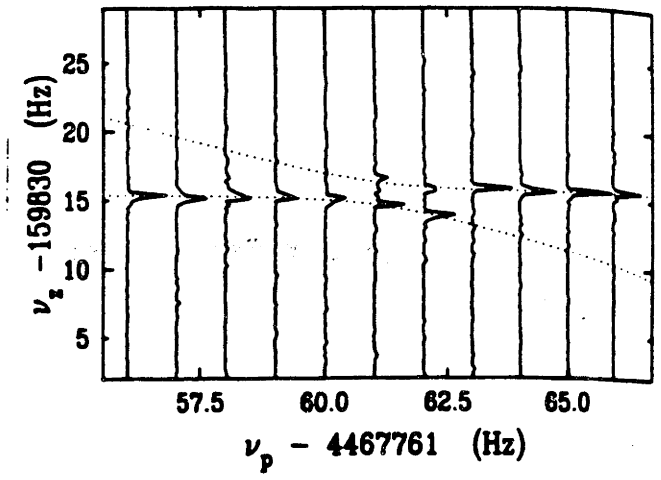

FIG. 2. Experimental illustration of the avoided crossing effect, using a single N_2^+ ion. We adjust the coupling frequency in 1-Hz increments and then excite the axial motion by pulsing. Each trace is the fast Fourier transform of the detected signal from the axial motion after the excitation. The dotted lines are a fit of the peak centers to the avoided-crossing line shape [Eq. (4)]. The fit yields $|V|=1.5(1)$ Hz and $\nu_c'-\nu_z = 4\,467\,761.36(15)$ Hz.

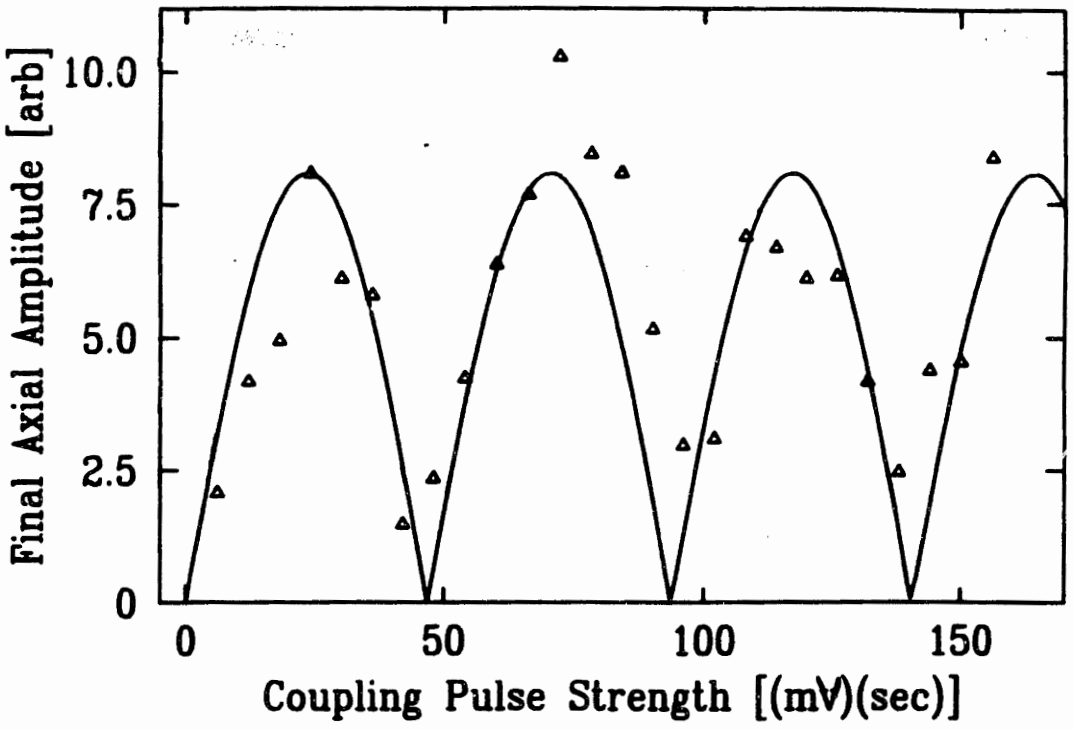

Fig. 4.2 The results of a magnetron pi-pulse experiment, similar to the cyclotron pi-pulse experiment described in Fig. 2 of the mode-coupling paper [CWB90], reprinted on the preceeding page. Note that the voltages in both figures refer to signal generator outputs; delivered voltages on the electrodes are not directly comparable because of frequency dependence in transfer efficiency.

Addendum to Section 4B. Although we don't often need to measure the magnetron motion to great accuracy, the pi-pulsed frequency measurement technique described above works well for the magnetron motion. In Fig. 4.2 I present some coupling pulse data taken on the magnetron motion. The experiment is a little harder than with the cyclotron motion because a short pulse with central frequency $\omega_z + \omega_m$ will have significant energy at ω_z, which excites the axial motion directly in an undesirable way. To assure ourselves that we have attained maximum cooling, we usually do not use the pi-pulse technique for cooling the magnetron motion, but instead apply the coupling drive at very low amplitude for several minutes.

4C Measuring and Shimming Field Imperfections

In this section I discuss our efforts to characterize, and to minimize, amplitude-dependent frequency shifts caused by imperfect electric and magnetic fields.†

Electrostatic Anharmonicity -- Dependence of ω_z on a_z

Imperfections in the electric field are revealed by anharmonic behavior of the the axial motion, that is, by ω_z having a dependence on the axial amplitude, a_z. We expand this dependence

† This section is the experimental companion to section 3B. Make sure you are familiar with that material before plunging on.

in powers of a_z (for symmetry reasons, we can exclude odd powers of a_z):

$$(\omega_z/\omega_{zo}) = 1 + \alpha_2(a_z/z_o)^2 + \alpha_4(a_z/z_o)^4 + \alpha_6(a_z/z_o)^6 + \ldots \quad (4.3)$$

For small a_z, the quadratic term α_2 is sufficient to describe the amplitude-dependent frequency shift. In this regime, we can measure α_2 with two different techniques -- pulsing or sweeping. With the sweeping technique, we drive the ions at a fixed frequency, while sweeping the trap voltage to bring the ion's axial frequency into resonance with the applied drive. The shape of the resulting resonance curve, which depends on the value of α_2, is in general asymmetric and hysteretic with respect to sweep direction. See Weisskoff's thesis [WEI88] for data taken in our trap with the sweep technique.

If the drive amplitude is sufficient to excite the axial motion into the regime where the frequency shifts quartic (and higher) in a_z become significant, the swept lineshapes become very difficult to interpret. For quantifying the higher-order frequency shifts, the pulsed technique is useful. The ion is driven into an axial orbit with a single pulse, and the discrete fourier transform of the resulting axial signal is analyzed to determine the central frequency. By using pulses of varied amplitude, ω_z as a function of a_z can be mapped out. (Fig 4.3)

The main limit to the pulsed technique is that as the ion signal is detected, the axial motion is damping, and as a_z decreases the axial frequency shifts; the detected signal is "chirped". However, the routine for extracting the average frequency and

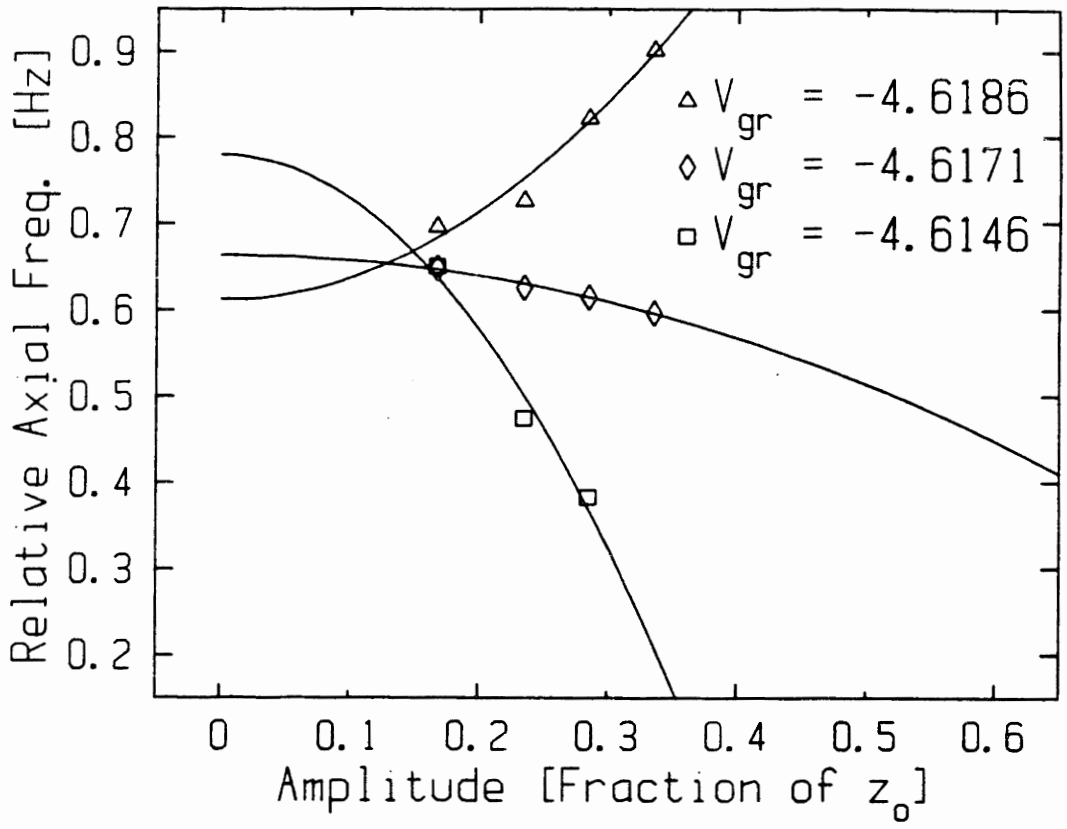

Fig. 4.3 The axial frequency as a function of axial amplitude, for different values of V_{gr}. The ion is pulsed to a certain axial amplitude, and as it damps the axial signal is recorded. The central frequency is extracted from the fourier transformed signal. The indicated axial amplitude is not the peak amplitude (that is, not the amplitude immediately after the excitation pulse) but the amplitude-weighted time-average amplitude. Note that V_{gr} affects not only the dependence on amplitude but also the extrapolated zero-amplitude frequency. The near orthogonality of the guard-ring design minimizes this inconvenient effect.

initial phase of the signal (See Ch. 2, above) performs adequately as long as the chirp, or frequency shift during the data-taking interval, is less than about 40% of the fft bin width -- that is, as long as the chirp in Hertz is less than 40% of the inverse of the data-taking time. In practice, as we drive the ion to larger pulses, we take data for shorter periods, which minimizes "chirping" artifacts but which reduces signal-to-noise and frequency resolution. As a consequence, the electrostatics in the trap volume beyond the central two or three millimeters can not be characterized.

By tuning the guard ring voltage, we can make α_2 very small, less than 3×10^{-6} (Fig. 4.4). The coefficient α_2 is related to the coefficients of the Legendre polynomial expansion of the electric field [GAB83]

$$\alpha_2 = (3C_4/4 - 15\ C_3^2/16)(z_0^2/d^2). \qquad (4.4)$$

The symmetry of the guard rings is such that change in the voltage of the guard rings can not effect C_3. Thus the change we observe in α_2 due to a change in the guard ring voltage must be due to a change in C_4 with respect to the guard ring voltage. Using the pulsed technique, we measure $(dC_4/dV_{gr})V_t = .09(2)$. See Fig. 4.4.

There are several sources of error in our measurement of C_4. One problem is that C_3 can mimic the effect of C_4 (Eqn. 4.4). The trap is constructed such that asymmetries with respect to reflection in the x-y plane should be small, but patch effects may contribute to a non-zero value of C_3. Based on the magnitude of observable patch effects, we crudely estimate C_3 to be less than about 3×10^{-3}, which means that there is possibly an error in our measurement of

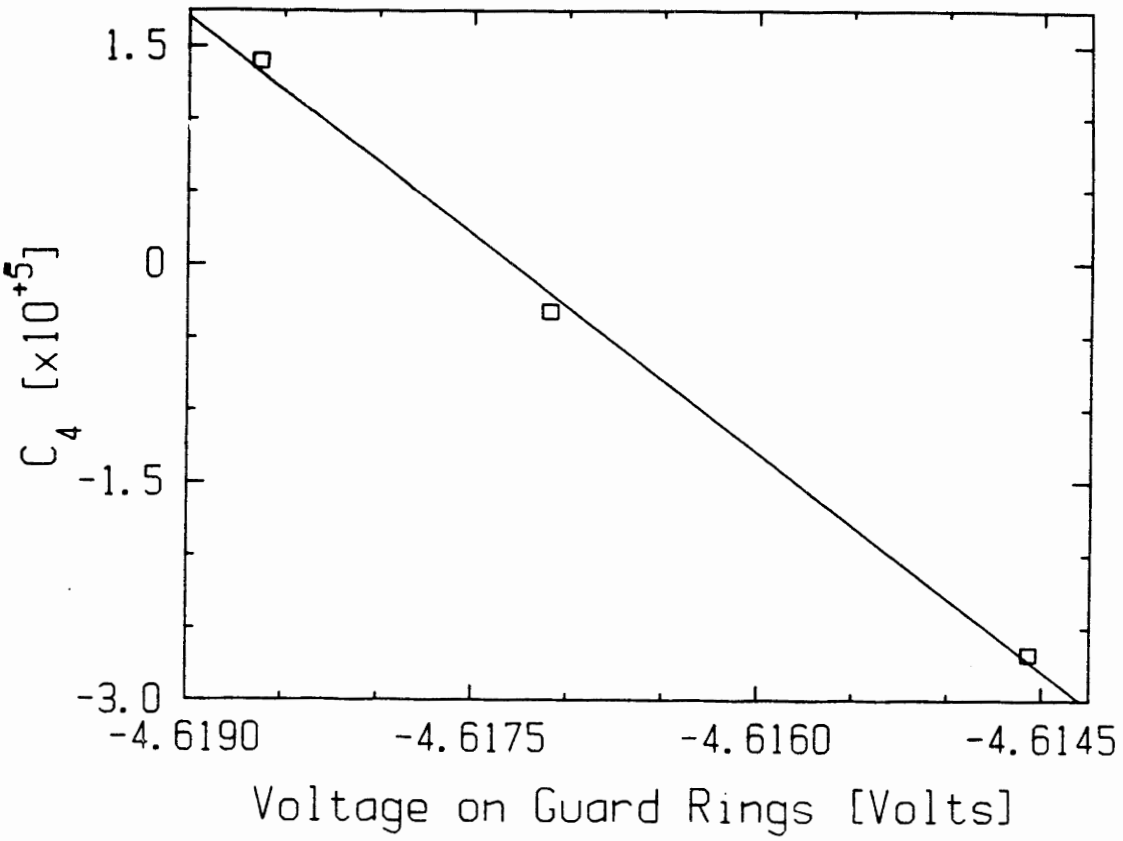

Fig. 4.4 A quadratic dependence of frequency on amplitude is extracted from the data in Fig. 4.3 and used to determine (from Eqn 3.9) C_4 as a function of V_{gr}. Strictly speaking, the zero crossing at V_{gr} =-4.6174 is not the guard-ring setting which nulls C_4, but it does indicate the zero of $\alpha_2 = (3C_4/4 - 4C_3^2/5)(z_o/d)^2$.

C_4 of about 1 x 10^{-5}. Until we better understand asymmetric patch effects, we cannot confidently reduce C_4 below about 1×10^{-5}, the value we use in our future error predictions in Tables 3.1 and 3.2. Another cause of error in our determination of C_4 stems from lingering uncertainty in our absolute amplitude calibration -- a 20% error in amplitude calibration (about what we estimate) corresponds to a 40% error in the C_4 measurement. This is not really a fundamental limitation. The frequency perturbation in the i_{th} mode is proportional to $\rho_i^2 C_4$, so the effect of an error in the absolute calibration cancels out. Finally, since C_4 is determined by fitting a quadratic curve to the ω_z vs a_z data, the presence of a quartic component (due to a C_6 component in the electric potential, for instance) can cause an error in the fit. This effect can be minimized by fitting only to the lower amplitude points.

Our measurement of the effectiveness of the guard-rings, $(dC_4/dV_{gr})V_t$ = .09(2), should be compared to that obtained by Weisskoff [WEI88] with the sweeping technique, 0.074(4). The difference can readily be accounted for by a change in our estimate of the overall absolute calibration of orbit sizes, a measurement which has had some inconsistencies that were only resolved in the spring of 1989.

Our trap was designed to have "orthogonal" compensation rings [GAB83], which is to say, designed so that changes in the guard ring voltage did not change the zero-amplitude ω_{zo}. (Earlier Penning trap workers found that the absence of this feature made guard ring tuning more tedious.) From the frequency vs. amplitude

data in Fig. 4.3, we can extrapolate to determine ω_{zo} as a function of guard-ring voltage. Time dependent drifts in ω_{zo} confound the results somewhat, but we estimate $(d\omega_{zo}/dV_{gr})/(d\omega_{zo}/dV_t) = -0.0055(8)$ from the data in Fig. 4.3. Gabrielse points out that what really matters is the ratio of the undesired guard-ring effect $(d\omega_{zo}/dV_{gr})$ to the desired guard-ring effect, (dC_4/dV_{gr}). Gabrielse defines the figure-of-merit $\gamma=[(d\omega_{zo}/dV_{gr})/(d\omega_{zo}/dV_t)] / [(dC_4/dV_{gr})V_t]$. From the data in Fig. 4.3, we measure $\gamma = -0.061$. It has been pointed out that for negative γ, there must be some finite value of a_z for which the trap is perfectly compensated -- the nearly triple crossing that occurs in Fig. 4.3 suggests that in our trap is "perfectly compensated" for an excitation of $a_z/z_o = 0.15$. But in any case, we are not inconvenienced by the residual non-orthogonality of the trap.

Fig. 4.5 presents evidence for shifts in ω_z that are quartic or higher-order in a_z. Although the data are not very good, we can use it to estimate $\alpha_4 = -1.0(5)\times10^{-4}$. Several terms in the electrostatic expansion contribute to the quartic dependence, but the most likely culprit in our case is C_6. Interpreting the quartic shift we see as a C_6 effect, gives $C_6 = 16\alpha_4/15 = -1 \times 10^{-4}$ [GAB83].

With the trap configured as it is now, we can not tune out the shifts in ω_z proportional to quartic and higher powers of a_z. Since we can not fit initial frequencies and phases to signals whose chirp is comparable to the fft bin-width, the quartic shifts constitute an absolute ceiling on useful axial pulse size. (At present, the maximum useable a_z/z_o is about 0.25). Additional sets of guard

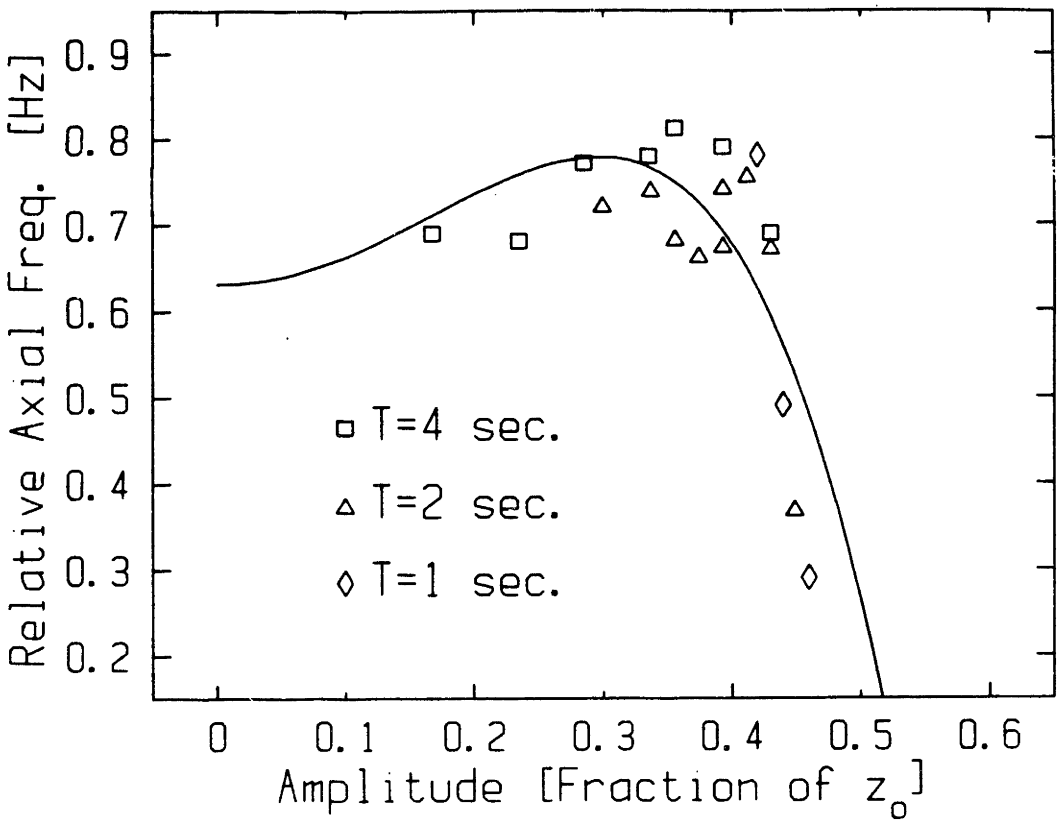

Fig 4.5 When the ions are driven to only slightly larger orbits, the frequency's amplitude dependence is clearly no longer simply quadratic. The solid line is a fit to a quartic polynomial (even powers only). The data may indicate that still higher powers of amplitude are involved, but more likely it simply indicates the limitations of our fourier transform-based analysis technique, which was never meant to handle time-varying frequencies.

rings might improve the situation, but it is not clear they would be worth the trouble.

Measuring the Magnetic Field Nonuniformity - B_2

A glance at the perturbation matrix (Eqn 3.9) is enough to convince one that the most apparent signature of the second-order magnetic field gradient (B_2) is the quadratic dependence of ω_z on ρ_c:

$$\delta\omega_z/\omega_z = [-\omega_c B_2/(4\omega_m) - (3/2)C_4/d^2]\rho_c^2. \qquad \text{(Eqn 4.5)}$$

Determining B_2 then becomes particularly easy. The procedure is as follows: The axial and cyclotron motions are cooled to their thermal values. Then the cyclotron motion is excited with a single rf pulse, so that ρ_c is driven to a preselected value. Then the axial motion is excited, and the axial frequency is extracted from the resulting axial signal. This procedure is repeated for a range of values for the driven ρ_c, and a plot is made of ω_z vs ρ_c. Finally, a polynomial is fit to the data; B_2 is proportional to the coefficient of the quadratic term. A measurement of B_2 with a precision of $5\times10^{-8}/cm^2$ can be completed in about 15 minutes. See Fig. 4.6.

There are two main sources of error in our B_2 measurements. The first is the confounding effect of C_4. As is apparent from Eqn 4.5, the presence of a residual C_4 term in the electrostatic potential mimics the effect of B_2 in this measurement. For the case of our N_2^+ measurements, as long as $|C_4| < 2 \times 10^{-5}$, the error in our determination of B_2 is less than about 2×10^{-7}. The second source of error is the same problem with the overall amplitude calibration

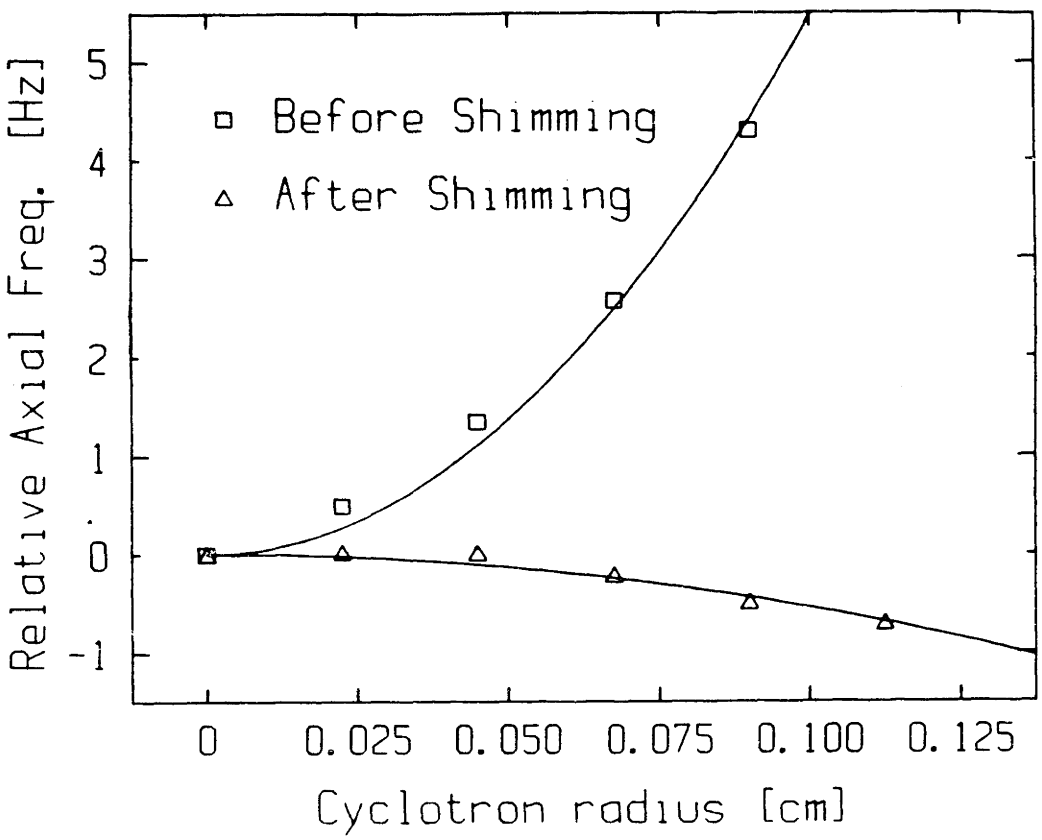

Fig 4.6 The B_2 second-order magnetic field gradient is measured by determining the axial frequency dependence on the cyclotron radius. Before we adjusted the current through the shim coils (square points) $B_2 = 9 \times 10^{-7}/cm^2$. After two cycles of adjusting the current and measuring the gradients, $B_2 = -8 \times 10^{-8}/cm^2$.

that caused uncertainty in the C_4 measurement. Again, this is not a real problem: if the orbits are larger than we believe them to be, then B_2 is smaller than we think it is, and our estimates for the frequency perturbations, which go as $\rho_i^2 B_2$, remain accurate.

Measuring the Magnetic Nonuniformity, Continued -- B_1

The first order gradient in the magnetic field, B_1, can not be unambiguously determined from amplitude-dependent frequency shifts. We measure B_1 by shifting the effective trap center vertically through the field gradient, and measuring the cyclotron frequency as a function of vertical position. We shift the vertical position of the ion with two different techniques, which produce slightly different effects. The simpler technique involves simply loosening the screws that clamp the top-plate of the dewar onto the O-ring seal. The resiliency of the O-ring lifts the top-plate, and with it the entire trap probe which hangs down into the center of the magnetic field. Knowing the number of threads per centimeter on the clamping screws, we can shift the vertical position with some accuracy -- perhaps to 0.003 cm accuracy across a useful range of 0.015 cm. This technique is not sensitive to gradients caused by magnetic materials attached to the trap or to its support structure. As we move the trap up and down, all of the associated paraphernalia move up and down with it, although the trap does move with respect to the coils of the magnet.

A second approach to moving the trap center is to apply a small d.c. offset voltage to the lower endcap, which moves the

equilibrium axial position of the ion [WEI88]. The effective trap center is then shifted with respect to the trap electrodes and support structure and so on, as well as with respect to the magnet.

The first time we compared the results of these two different techniques for determining B_1, we were astonished to find radically different numbers. See Fig. 4.7. When the whole apparatus was shifted up and down relative to the magnet, we saw relatively small changes in the cyclotron frequency. But when the ion was shifted with respect to the trap, we saw large shifts in the cyclotron frequency (corresponding to a gradient of 13 gauss/cm). This was the first evidence we encountered for the presence of strongly magnetic materials attached to the trap. Later we confirmed that the support posts of the field emitter point were made of ferromagnetic material. After the point was replaced, shifts in the cyclotron frequency associated with moving the ion up and down in the trap were much smaller (corresponding to a gradient of 0.6 gauss/cm.)

Shimming the Magnetic Fields

Our Oxford superconducting magnet has built-in superconducting shim-coils. The various coils were designed to be orthogonal, i.e. so that current flowing through each coil would affect only a particular component of the magnetic field. The currents in these coils may be adjusted by opening the appropriate superconducting switches and injecting the desired current into the desired coil. In principle, the procedure for shimming the field is

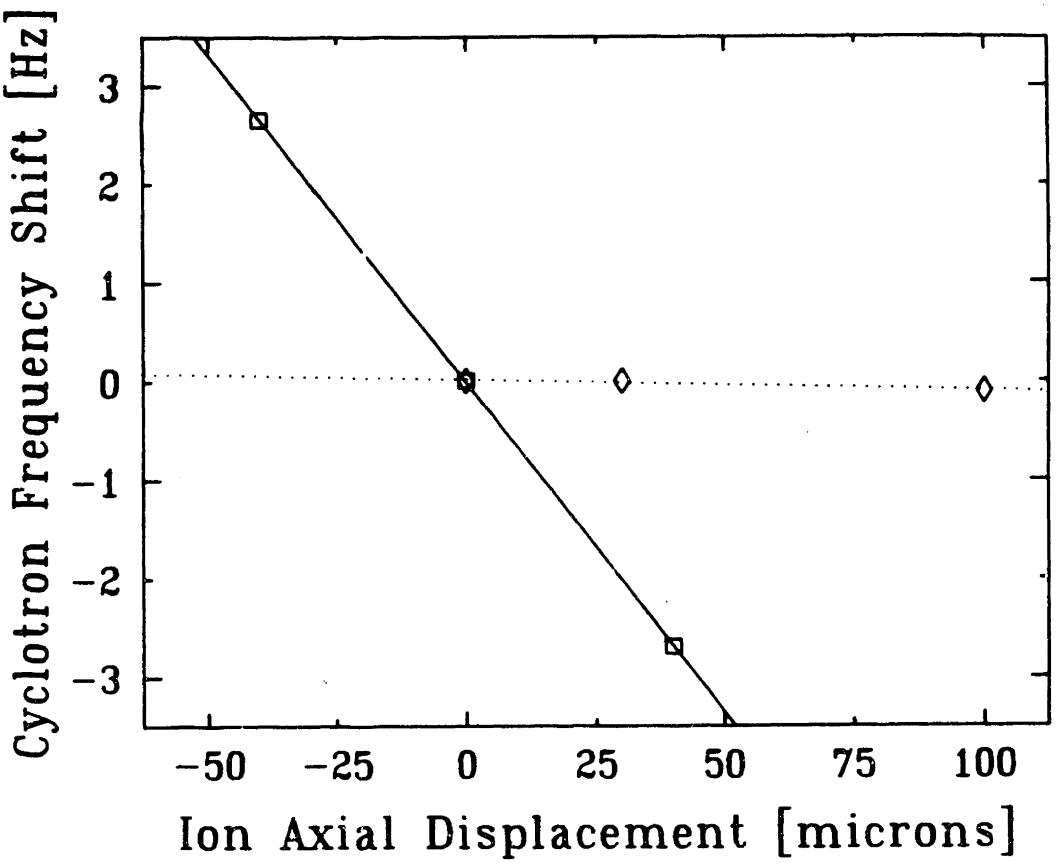

Fig. 4.7 Evidence for the existence of a magnetic field-distorting object attached to the trap-supporting structure. The square data points were recorded by moving the equilibrium position of the ion up and down in the trap using asymmetric d.c. voltages on the endcaps. The solid line fit to these data indicates a B_1 field gradient of 13 gauss/cm. The diamond points were recorded by moving the entire trap (and its support structure) with respect to the magnet coils, and show very little field change. Since these data were recorded, the offending field distorter has been removed and the gradient has since been shimmed to less than .25 gauss/cm, or $B_1=3\times10^{-6}$.

completely straightforward. We measure B_1 and B_2, adjust the currents in the coils, measure B_1 and B_2 again, and repeat until we have reduced the gradients to acceptable values. In practice, there are several complications.

During the adjustment, the leads to the shim coils carry several amps of current. Leads capable of carrying adequate current to the coils will of necessity carry heat to the helium bath--heat that increases the rate of liquid helium boil-off to unacceptable levels. The leads are therefore designed to be demountable. The leads are packaged in a long stainless steel tube which can be inserted down into the helium bath and then removed after shimming. At the end of the leads-containing tube is a plug which mates with a socket, located near the level of liquid helium, wired to the coils themselves. In our experience, connecting and disconnecting the plug and socket is a tricky business, with some risk of breaking pins off in the socket and even of freezing the two connectors together with inadvertently introduced frozen air. The prospect of having to warm up the experiment to repair the shim coils so frightened us that we were inclined to do as little shimming as possible, although the shimming procedure itself was not particularly tedious.

Another complication we had to confront is that the coils are not in fact perfectly orthogonal. Changes in the B_2 coil affect the first-order gradient as well as the second-order gradient, changes in the B_1 coil affect the second-order gradient, and a change in either coil affects the field at the center of the trap, the B_0 field.

Shimming Results

The following equations summarize the results of several days of tinkering with the shimming current.

$$\Delta(BB_1)= \underset{[\text{gauss/cm}]}{} (\Delta Z1C)[.33(7)] \underset{[\text{amps}]}{} +(\Delta Z2C)[?] \underset{[\text{amps}]}{}$$

$$\Delta(B_2)= m \underset{[\text{Hz/mV}^2]}{} (\Delta Z1C)[-0.2\text{x}10^{-5}] \underset{[\text{amps}]}{} +(\Delta Z2C)[-1.1(1)\text{x}10^{-5}] \underset{[\text{amps}]}{}$$

$$\Delta(B)= \underset{[\text{gauss}]}{} (\Delta Z1C)[.38(5)] \underset{[\text{amps}]}{} +(\Delta Z2C)[.10(2)] \underset{[\text{amps}]}{} \qquad \text{(Eqns. 4.6)}$$

ΔZ1C and ΔZ2C refer to changes in the current flowing through the superconducting shim coils which are supposed to compensate for the first and the second order gradient, respectively. The "C" in Z1C and Z2C refers to "coarse"; the magnet also is equipped with fine shim coils, but it appears as though it will not be necessary to make use of them. We measure changes in BB_1 and B in units of gauss by converting changes in frequency into changes in field. We know BB_1 in $[\text{cm}]^{-1}$ from lifting the ion up by twisting the endplate bolts. We measure B_2 in units of the "bottle", the amount the axial frequency shifts as a function of ρ_c (Eqn. 3.9). We measure ρ_c operationally in mVolts, referring to the amplitude of the 20 mSec pulse required to excite the ion to the desired value of ρ_c, the voltage being measured at the output of the signal

generator. The question mark refers to a value which was not readily determinable from our data.

The effectiveness of the shimming currents could be determined with more accuracy that the errors quoted in Eqn. 4.6 indicate. For instance, while we were performing the shimming procedure, we did not imagine that the results would ever be a component of the most reliable absolute amplitude calibration. (See below in this section, and below in section 4E.) Accordingly, the care with which we proceeded, and the thoroughness of the notes we recorded, were appropriate for the "zeroing" operation we thought we were performing, but a little lax for an amplitude calibration. This work could be repeated to good effect.

Our shimming work reduced $|B_1|$ to less than 3×10^{-6}, and B_2 got as low as 2×10^{-7}, although the final value of B_2 was $-1.0(2)\times10^{-6}$. There appeared to be no reason why another round or two of adjustments couldn't reduce these gradients another factor of ten.

Our measured values for the effectiveness of the coils should be compared with those specified by Oxford, the magnet's manufacturer:

$\Delta(BB_1)=$ [gauss/cm]	$(\Delta Z1C)$[.25] [amps]	$+(\Delta Z2C)$[?] [amps]	
$\Delta(B_2)=$ [gauss/cm^2]	$(\Delta Z1C)$[?] [amps]	$+(\Delta Z2C)$[.15] [amps]	
$\Delta(B)=$ [gauss]	$(\Delta Z1C)$[?] [amps]	$+(\Delta Z2C)$[?)] [amps]	(Eqns 4.7)

Oxford does not quote values for the "non-orthogonal" or off-diagonal effects of its shim coils, (the question marks in Eqn. 4.7) but it does specify the diagonal terms: Z1C changing B_1, Z2C changing B_2. Being able to compare values turns out to be very important for us. We compare our value for $\delta B_2/\delta Z2C$, -1.1(2) x 10^{-5} (Hz/mV^2)/amp, to the specified value, -.15 $(gauss/cm^2)$/amp, and, using equation 3.9, we are immediately able to establish an absolute calibration for the radius of the cyclotron orbit, ρ_c: ρ_c(in cm) = $(3.0(6)x10^{-4})$(pulse amplitude)(in mV at the signal generator for a 20 mSec pulse). This calibration procedure is discussed further in section 4E.

D. Magnetic Field Drift

Changes in the magnetic field which are smooth on the scale of 5 to 200 minutes can be removed from our data and do not cause major error in our doublet measurements. But sudden changes in the field or in its first time derivative are our chief source of experimental error. It has even been suggested that, significant as we believe the problem to be, we may *still* be underestimating its size. Our publication of the CO^+/N_2^+ mass ratio stimulated a Comment in Physical Review Letters to this effect [GAB90, see also our Reply, CWB90b].

We have considered several causes of the temporal instability of the magnetic field, three internal to the magnet dewar and one external.

First, the superconducting coil may have some residual resistance which causes a gradual decrease in current and field strength. This effect, if it exists at all, is tiny compared to other problems.

Second, the size of the superconducting coil can change due to pressure and temperature fluctuations. Thus even though the flux linking the solenoid is conserved, the field strength changes. We are not sure what the size of this effect is, but are constructing a pressure regulator to stabilize the pressure and temperature of the magnet's helium bath.

Third, an increase in room temperature causes expansion of the magnet housing, which in turn lifts the trap with respect to the magnet's field center. The residual linear field gradient would then cause a change in field strength at trap center. Rough calculations show that this may well be the dominant source of gradual field change at trap center, (See Fig 4.9 for an illustration of the long term smooth change) and indeed that fluctuations in the rate of this process may contribute to the unsmooth field change.

Finally, changes in the ambient magnetic field in the lab are not perfectly shielded by our finite superconducting solenoid, and thus are felt at trap center. The shielding of external field by a superconducting magnet may be quantified by the field penetration factor, the ratio of $\Delta B_{internal}$ to $\Delta B_{external}$ We have measured this ratio by finding the correlation coefficient between internal magnetic variations (seen as shifts of the ion cyclotron resonance frequency) and external magnetic field variations measured with a

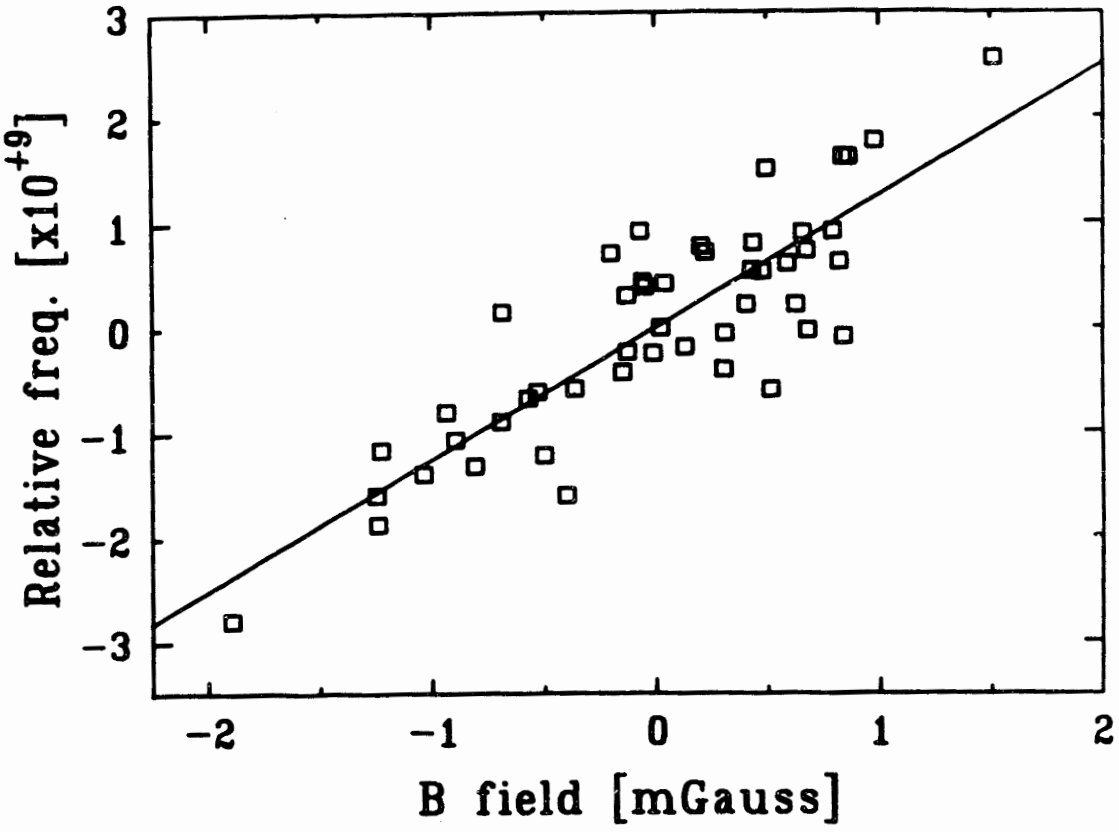

Fig. 4.8 A scatter plot of simultaneous cyclotron frequency and external magnetic field measurements. Before plotting, a quadratic time dependence was removed from the frequency data and, for consistency, from the field data as well. The remaining field dependence, 1.2(1) ppb/mGauss, indicated the field at trap center is 0.11(1) the field at the magnetometer probe. These data were taken during the day, with both subway and elevator running.

fluxgate magnetometer. We measured a field penetration factor of 0.03(2) when the subway was off and $\Delta B_{external}$ dominated by an elevator 12 m away, and of 0.11(1) when the subway dominated the magnetic field noise (though various apparatus within the building contributed as well). (Fig. 4.8) The large dependence of the observed penetration factor on the *source* of the external magnetic field suggests that magnetic materials in the building contribute to the *in situ* field penetration factor (and does not necessarily contradict Gabrielse's [GAB90] estimate of 0.3 for our solenoid in free space).

Between 1:30 a.m. and 4:30 a.m. the external field fluctuations are much lower (particularly if the elevator is disabled). It is not clear whether the remaining frequency jitter we see during this "quiet time" is due to processes external or internal to our magnet. During the day, however, external field noise is definitely the dominant problem. Daytime measurements of ambient (external) field fluctuation in our lab (using a fluxgate magnetometer), combined with our shielding estimate, suggest that we must expect an average error of around 8×10^{-10} for a daytime A-B-A measurement. (Measuring each ion about several times over the course of 40 minutes or so, and taking about 25 minutes to swap the ions).

Field stabilization techniques, such as those demonstrated by Gabrielse and Tan [GAT88] and Van Dyck et al [VMF86], may well be worth implementing. Myself, I'm more excited about developing the two-ion techniques suggested in Chapter 5, which should make

magnetic field jitter irrelevant for mass comparisons at parts in 10^{12}.

E. Absolute Amplitude Calibration, Absolute Error

Determining the absolute size of the ion's motion has proven to be harder than we anticipated. The overall sensitivity calibration of our detector suffers from our inability to inject a calibrated current into the extremely high impedance input circuit. On the other hand, our efforts to drive the ion to an orbit of known absolute size are frustrated by a change in the efficiency of the ion driving electronics that occurs as the apparatus is cooled to cryogenic temperatures. In the end, we turned to an indirect but robust calibration method (based on the effects of magnetic field gradients of known absolute magnitude) which continues to hold our confidence. These then are the three topics I'll discuss in section 4E: an *ab initio* calibration of the detector sensitivity, an attempt to calibrate the detector using the signal from an ion driven to a supposedly calibrated orbit size, and the field gradient calibration method currently in favor.

Ab Initio *Detector Calibration*

From the upper endcap electrode on which the ion's image current is first induced, through the SQUID which amplifies the current, to the software which puts the data in the format for storage and analysis, the detected signal must follow a technologically tortuous route. The most reliable way to calibrate

the entire system would be to inject a known current onto the upper endcap and compare it to the final value read in by the computer. Since this is not possible, we are left to combine the results of calibrations of the individual components of the system. The following data are relevant: the Q of the tank circuit, the tank circuit's primary-secondary mutual inductance, the SQUID input coil inductance, the SQUID open loop current sensitivity, the ratio of open-loop to closed-loop gain through our 160 kHz feedback amplifier, the combined transfer function of the mixer, lowpass filters, amplifier, and analogue-to-digital converter, and finally, for measurements made in transient mode, the numerical details of the discrete fourier transform routine.

We measure all of these quantities, except for the SQUID current sensitivity, which is specified by the manufacturer. The current induced in the endcap by a particular amplitude single ion motion is given by $i_{peak} = e\omega_z B_1 (a_z/z_o)$, where B_1 is constant determined by the trap geometry, calculated [BRG86] to be 0.8. Thus, if we believe our calibration, we readily relate the recorded ion signal to the absolute amplitude of the ion's motion.

Driven Ion Calibration

To increase our confidence in the above calibration, we decided to drive the ion to a known orbit size, and check that the signal we record corresponds with the anticipated current induced in the upper endcap. To make the ion dynamics as simple as possible to understand, we drive the ion 8 Hz off resonance (8 Hz is

160 damped linewidths) and detect the response at the driven frequency using a lock-in. With the ion driven so far off resonance, its response is not affected by anharmonicities or by damping. In practice we avoid capacitive feed-through of the driving signal onto the upper endcap by driving the ion with two different frequency fields (159 kHz and 1 kHz). The ion mixes these fields and feels a driving force at the sum frequency of the two drives, the force being proportional to the product of the amplitude of the two drives. The efficiency of the ion driving electronics from signal generators through to electrode surfaces is measured with the apparatus at room temperature.

When Robert Weisskoff first compared the results of these two independent calibration methods in the spring of 1988, he noted agreement at the 10% level [WEI88]. We attempted to repeat the double calibration, after making modifications to the detector and repairs to the trap, and concluded Weisskoff was either very talented or very lucky. No matter how many times we went over it, we were left with a discrepancy of nearly a factor of 2. Eventually, we found what we believe to be the source of the discrepancy: The efficiency of the electronics that filter the ion driving signal changes as the experiment is chilled to liquid helium temperature. We were able to detect this because of some redundancy built into the cabling that carries the driving signal to the trap, but the redundancy is inadequate to allow us to correct the calibration. We rely, therefore, on a third calibration:

Field Gradient Calibration

As described is section 4B, above, we can use the data from our magnetic field shimming work to absolutely calibrate the cyclotron drive in our trap. Once we are able to drive the ion to an absolutely known cyclotron radius, the remainder of the calibration is straightforward. To the ion with its known ρ_c we apply a pi-pulse, which swaps the action from the cyclotron motion into the axial mode. The ratio of ρ_c before the pi-pulse to a_z after the pi-pulse is readily calculated [CWB90] to be $(\omega_z/\omega_c)^{1/2}$, or 5.3, for a mass 28 amu ion. As the ion's axial motion damps we detect the signal from this now absolutely known axial motion and thus calibrate our detector. A similar pi-pulse experiment calibrates the magnetron drive.

The critical assumption in this calibration procedure is that Oxford gets right their specification of the Z2C shim coil efficiency. We have two assurances that they do. First, they quote two values for the effectiveness of each shim coil, a theoretical value (presumably calculated from shim coil geometry) and an experimental value. The two values agree within about 10%, suggesting they care about these things. Second, we are able to verify the specified Z1C shim coil efficiency ourselves: compare the values in equations 4.6 and 4.7: they are in marginal agreement, although our measurement is unfortunately only a 25% measurement. The fact that we predict the Z1C efficiency correctly indicates that we understand their specifications, and that there are no factors of two, for instance, that we interpret differently from Oxford.

There is further evidence that we are not making a large error (say, a factor of 1.5 or more) in our calibration: for one thing, the determination of the efficiency of guard-ring tuning scales quadratically with the amplitude calibration, and Weisskoff [WEI88] has found that our value for $(dC_4/dV_{gr})V_t$ agrees within 20% of Gabrielse's theoretical calculation for a trap of our design. Also scaling quadratically with calibration is our estimate for the effective noise temperature of the detection circuit -- our current estimate of 15K agrees with independent SQUID calibration measurements [WLB88]. All things considered, our calibration might be wrong by 20%, but not by 50%.

For predicting the size of errors proportional to the field flaws C_4 and B_2, errors in the absolute calibration are not important. In a calculation of the perturbation expected from a certain size excitation, the absolute calibration, which enters also into the determination of C_4 and B_2, cancels out. Special relativity is different. The factor which sets the scale of the special relativistic perturbation, (ω_c^2/c^2), does not depend on calibration considerations. Thus our prediction of the relativistic perturbation, which scales as $(\omega_c^2/c^2)\rho_c^2$, goes as the square of the absolute amplitude calibration.

Testing Special Relativity

During our N_2^+/CO^+ mass comparison experiments, we performed some tests designed explicitly to test the relativistic shift. Before the tests, we measured B_2 to be $-1.0(1)\times10^{-6}/cm^2$, and $|C_4| < 3\times10^{-5}$. Coincidentally, the value of B_2 was such as to almost

cancel the relativistic shift. We expected the cyclotron frequency to shift $\delta\omega_c/\omega_c = -2(1)\ x10^{-10}\ (\rho_c/0.024\ cm)^2$. Magnetic field fluctuations make it difficult for us to measure frequency shifts at the $2x10^{-10}$ level, but we performed a series of measurements alternating between $\rho_c = .021$ cm. and $\rho_c = .033$ cm., expecting to see a relative shift of $\delta\omega_c/\omega_c = -2(1)\ x10^{-10}$. We measured $\delta\omega_c/\omega_c = +1(3)\ x10^{-10}$, which is consistent if not informative.

The actual mass comparison experiments were performed at $\rho_c = .024$ cm. The important result here is that even if there is a factor of 2 error in our amplitude calibration (such that both our amplitude dependence tests and our mass comparisons were actually performed at radii twice as large as we imagined), we have shown that large variations in ρ_c (much larger than thermal or systematic effects could cause), cause frequency shifts smaller than our quoted error of 4 parts in 10^{10}.

F. Checks on the Overall Accuracy of Mass Comparisons

Unfortunately there are no "calibrated" mass doublets against which we can test our claims of unprecedented overall accuracy. However we can learn many of the things we would have learned from measuring a calibrated doublet simply by comparing the "identity doublet," that is, comparing N_2^+ to N_2^+. We followed exactly the same procedure described in for run #3 in section 4G, below, except instead of loading sequentially N_2^+ - CO^+ - N_2^+, we loaded N_2^+ - N_2^+ - N_2^+. When analyzing the data, we pretended that the second N_2^+ ion loaded was a different species, N_2^+.

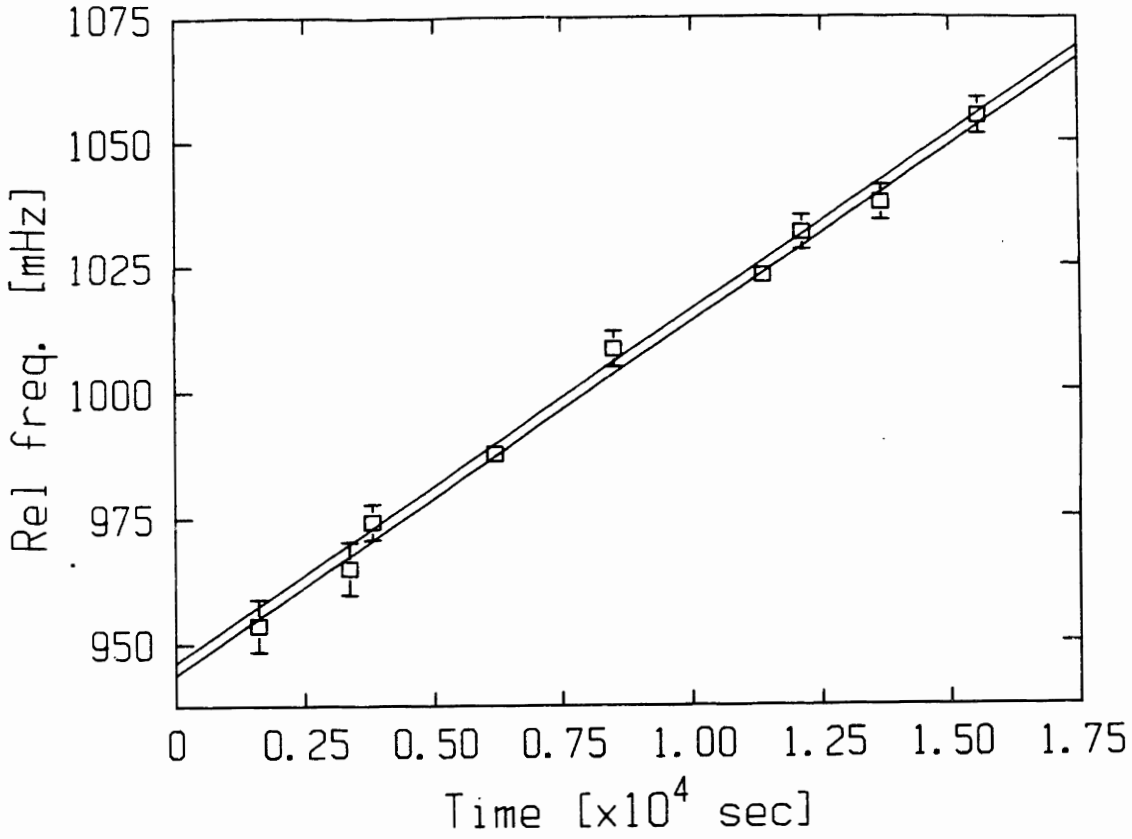

Fig. 4.9 The first four and the last two points plotted above correspond to, respectively, the first and the third of three N_2^+ ions trapped during an evening of cyclotron frequency comparisons. The lower solid line is fit to these data. The remaining points are from the second ion in the series. The upper line is fit to these data. The fit frequency difference is 2 mHz, with an estimated error of 2 mHz, which is an accuracy of about 5 parts in 10^{10}.

Compensating for the magnetic field drift exactly as in section 4G, we measured from a single evenings data $M(N_2^+)/M(N_2^+) = 1 + 4(4) \times 10^{-10}$ (Fig. 4.9). This measurement was a another confirmation that the process of loading and unloading ions does not cause discontinuous changes in the cyclotron frequency, and further evidence that night-time field instabilities are not a major concern at the 4 parts in 10^{10} level.

A second test of overall accuracy we performed was to compare the mass of N^+ to the mass of N_2^+. After correcting for binding energy and the mass of half an electron, the ratio $M(N^+)/M(N_2^+)$ is exactly 1/2. We performed the comparison and measured the significant discrepancy $2M(N^+)/M(N_2^+) = 1 + 3(1) \times 10^{-9}$. At first we believed that the discrepancy was due to the sort of amplitude-dependent errors described in 3B and 4C; since we were not measuring a mass doublet, we reasoned, we could not rely on frequency shifts cancelling out in a mass ratio determination. But we ruled out this scenario by measuring the dependence of the measured frequencies on mode radii for both N^+ and N_2^+, and extrapolating back to zero radius. This procedure puts a limit on the total radius-dependent frequency perturbation which is less than a part in 10^9.

The explanation we favor, although more experiments are required to verify it, is based on the "patch-effect" fields mentioned in section 4A, above. We have shown that there are fields (due to surface potential patches, we surmise) in the trapping volume which do not scale with applied bulk potential of the electrodes.

For instance the $V_{ringpatch}$ term defined in section 4A is the hypothetical d.c. surface potential on the central ring electrode which accounts for the observed offset in the strength of the quadrupole trapping fields. ("Offset" in the sense that it is the field that remains even with nominally zero volts applied to the ring.) Similarly, there is a $V_{guardringpatch}$ associated with the C_4 fields. It seems highly probable that this offset potential has an asymmetric component as well, corresponding to a non-vanishing axial component of the electric field at the trap's geometrical center. We define an effective potential $V_{endcappatch}$ which produces an axial field at trap center $V_{endcappatch}/(2d)$. This field shifts the effective trap center (the point where electric fields vanish) axially a distance $z_{patch}/d = V_{endcappatch}/(2V_t)$. This axial shift will couple with the residual linear magnetic field gradient, B_1, to cause a shift in the cyclotron frequency inversely proportional to the applied trapping voltage V_t. Since V_t is adjusted differently for different mass ions, this patch effect shift has a potentially very hazardous systematic dependence on ion species.

$\delta\omega_c/\omega_c = B_1 V_{endcappatch} d/(2V_t)$

How large is $V_{endcappatch}$? Well, the endcaps are made of the same material and are about the same size and distance from trap center as the ring, so an educated guess for the size of $V_{endcappatch}$ is on the order of $V_{ringpatch}$, that is, about 30 meV. In the case of our $M(N^+)/M(N_2^+)$ measurement, V_t is 9 volts for N_2^+ but only 4.5 volts for N^+. We determined that $|B_1|<3\times10^{-6}$. Thus we might expect a systematic error on the order of 8 parts in 10^9!

In light of these considerations, finding a final error as small as 3 parts in 10^9 in the $M(N^+)/M(N_2^+)$ measurement now seems rather fortuitous. If we wish to measure non-doublets to part in 10^9 accuracy we clearly must put more effort into understanding patch effect shifts. It is important to note that when measuring a mass doublet, the patch effect shift is tiny because V_t is so nearly the same for both ions. For instance, for our $M(CO^+)/M(N_2^+)$ doublet, using the same estimates for B_1 and $V_{endcappatch}$, we estimate a systematic error due to the patch effect shift of only 4 parts in 10^{12}.

G. CO^+/N_2^+ Mass Ratio Measurement

I conclude this chapter with an account of our best measurement to date, a 4 part in 10^{10} determination of the CO^+/N_2^+ mass ratio. Section 4G was originally published in October, 1989, in Physical Review Letters, with the five coauthors listed on the title page below.

A Single Ion Cyclotron Resonance Measurement of $M(CO^+)/M(N_2^+)$

Eric A. Cornell, Robert M. Weisskoff [a], Kevin R. Boyce, Robert W. Flanagan, Jr. [b], Gregory P. Lafyatis [c] and David E. Pritchard

Research Laboratory of Electronics
Department of Physics
Massachusetts Institute of Technology
Cambridge, Massachusetts 02139

Abstract

We have trapped single molecular ions in a precision Penning trap and, using cyclotron resonance techniques, have measured the mass ratio $M(CO^+)/M(N_2^+)$ to be 0.9995988876(4). Accuracy is limited at 4×10^{-10} predominantly by temporal instability in the magnetic field. All other systematic sources of error are $(\Delta M/M) \lesssim 10^{-10}$.

PACS: 35.10.Bg, 07.75+h

Submitted to Phys. Rev. Lett.

[a]Present address: Advanced NMR Systems, 30 Sonar Drive, Woburn, MA 01801

[b]Present address: Saunders Associates, Inc. 95 Canal St. Nashua, NH 03061

[c]Present address: Physics Dept., Ohio State Univ., Columbus, OH 43210

The Penning trap, with its strong uniform magnetic field and its much weaker electric field, has been used to perform a number of very accurate quantitative experiments.[VSD87, VMF85, WBI83, PBI85] We have used a Penning trap for mass spectroscopy using single ion cyclotron resonance (SICR). The absence of ion-ion interaction makes systematics easy to understand, hence SICR is the most accurate method of comparing mass. The $\Delta M/M = 4 \times 10^{-10}$ result reported here, limited predominantly by the temporal drift in the magnetic field, is a factor of six [actually, two] better than the value from current tables[WAA85], and may be the most accurate ion mass comparison to date.

A hyperbolic Penning trap[DEH67] consists of three main electrodes, all hyperbolic surfaces of rotation, which provide a restoring electric field which is linear with displacement along the axis of rotation. The much stronger axial magnetic field confines the particle radially. For a single charged particle there are three normal modes, one mode (the "axial" mode) which is aligned with the magnetic field, and two perpendicular to it. The perpendicular ("radial") modes are the electric field-modified cyclotron motion at frequency ν_c' and the slower magnetron orbit, due basically to $E \times B$ drift.

The ratio of the cyclotron frequencies for two different ion species, when corrected for electric field effects, is simply the inverse of their mass ratio. Our approach, then, is to compare the cyclotron frequencies of alternately loaded single ions. For an M = 28 a.m.u. ion, the cyclotron, axial and magnetron frequencies in our trap are respectively $\nu_c' \cong 4.5$ MHz, $\nu_z \cong 160$ kHz, and $\nu_m \cong 2.8$ kHz.

Our trap hangs vertically in the bore of an 8.5 Tesla superconducting Oxford magnet. The magnet has superconducting shims and a custom dewar in the bore which allows us to cycle the trap from room temperature to 4.2K while keeping the magnet itself cold. The main electrodes are precision-machined O.F.H.C. copper, plated with gold and coated with a layer of graphite particles (Aquadag) to minimize surface patch effects. The three main electrodes are spaced by machinable ceramic (MACOR) rings on which are painted guard ring electrodes, used to shim out higher-order electric field components. The lower guard ring is split into halves to permit driving of the radial modes of the trapped ion. The trap has a minimum endcap-to-endcap spacing 1.2 cm, and minimum radius .696 cm, giving an effective trap size d = .549 cm. The trap is inside a copper vacuum can, which cryo-adsorbs to ultra high vacuum, but there is a line-of-sight path through a hole in the center of the upper endcap up the pump-out tube to a room temperature gas-handling manifold. Ionizing electrons enter the trap from a field emission point just below.

The ion's axial motion is detected via the image current induced in the upper endcap. The detection circuit includes a superconducting tank circuit (Q = 25000) and an rf SQUID[WLB85]. The real part of the detector's impedance damps the axial motion with a damping time $\tau_z = 6$ seconds. For a single ion pulsed to 1/5 the trap size, detector signal/noise from 4 seconds of data is adequate to measure the axial frequency to 50 mHz and the phase to 15°.

The presence of even a single impurity ion has been observed perturb the trap frequencies of the desired ion unacceptably. Ejecting impurity ions is a surprisingly difficult task. Our approach has been to heat the axial motion of impurity ions with

band-limited white noise[MOO87] and then to lower ("dip") the voltage on the lower endcap, bringing the equilibrium position of the ion cloud very near the lower endcap. The more highly excited impurity ions are neutralized by striking the trap, leaving only the desired ion species in the trap. We use a similar dipping technique to thin the desired ions until only a single ion remains (Fig. 1).

The two radial ion modes do not couple to the detector and hence are undetected and undamped. In order both to cool these motions and to measure the all important cyclotron frequency, they must be coupled to the axial mode. We accomplish this with rf voltages applied across the halves of the lower guard ring at the sum or difference frequencies of the modes to be coupled[BRG86, WID75, WEI88]. To cool the magnetron motion we use the traditional sideband cooling scheme, a cw drive at $\nu_z+\nu_m$[WID75]. But for cooling the cyclotron motion, and for precision measurements of both the magnetron and cyclotron frequencies, we use a a short pulse at the coupling frequency of two modes. A pulse with the appropriate amplitude-duration product, (a "π-pulse"), will exchange the phase and action of one mode with those of the other[cwb90]. To cool the cyclotron motion, we cool the axial motion resistively, then use a π-pulse to swap the cooled axial motion into the cyclotron mode. The caption of Figure 2 describes how we use π-pulses to measure the trap cyclotron and magnetron frequency.

In order to measure the mass ratio of two ions, we alternate SICR measurements of the two ions under comparison — loading a CO^+, measuring its frequencies, then dumping it and loading an N_2^+ ion, measuring its frequencies, and so on. Figure 3 shows the results of an evening of such measurements. Preparing a new ion for precision measurement, that is, loading a cloud of ions, ejecting the impurity ions, reducing the

cloud to a single ion, and cooling the magnetron motion, requires at least 25 minutes. Any discontinuous field change, or even any dramatic change in the drift rate during this time will cause an error in the measured mass ratio.

Because our superconducting solenoid is only imperfectly self-shielding (85% efficient), changes in the ambient field are felt at trap center. The data from run 3 were taken early in the morning, when the ambient magnetic noise was very low, and the scatter correspondingly small.

We also observed frequency drifts over longer timescales that were evidently due to processes inside the apparatus. The drifts are affected by refilling the cryogenic fluids. We suspect they are caused at least in part by thermal expansion moving the trap center relative to the superconducting coils.

To extract a mass ratio from the data, we fit the magnetic field magnitude to a polynomial in time. The coefficients of that polynomial, and the CO^+/N_2^+ mass ratio, are the fit parameters. We fit the same data several times assuming, in turn, linear, quadratic and cubic magnetic field temporal profiles. The data seldom fit any better to a cubic shape than to a quadratic shape, whereas the linear shape seems overly restrictive. In any event, the difference in the final mass ratio results obtained from the different analyses is an informal measure of the price we pay for our ignorance of the temporal variation of the magnetic field. Combining the errors from the quadratic fits yields an overall error of .2 ppb (Table 1). Our judgement is that .2 ppb is insufficiently conservative and our best estimate for $M(CO^+)/M(N_2^+)$ is: 0.9995988876(4).

Although magnetic field uncertainties dominate our errors here, it is important to

consider other sources of error which arise in this experiment. Many of these (eg. effects which perturb the axial frequency) enter because the free space cyclotron frequency $\omega_c = eB/mc$, which must be used to determine the mass ratio, is[BRG86]

$$\nu_c^2 = \nu_c'^2 + \nu_z^2 + \nu_m^2 \qquad (1)$$

where ν_c',ν_z and ν_m are the measured trap frequencies. Eqn (1) is exact even when the axis of the electrostatic field is not aligned with the magnetic field provided that the magnetic is uniform and the electric field is a pure quadrupole. The hierarchy of frequencies, $\nu_c >> \nu_z >> \nu_m$, implies that for a desired final uncertainty ($\delta\nu_c/\nu_c$), we need measure ν_z to a much lower precision, and ν_m to a still lower precision. In practice, we do not worry about any corrections to the magnetron frequency.

The finite sensitivity and nonzero temperature of our detector require the use of finite ion orbit radii a_c, a_z, and a_m. For finite radii, the measured frequencies are perturbed by the gradients in the magnetic field, the nonquadrupole components in the electric field, and special relativistic effects. The effects of these errors, which depend on various powers of the orbit radii, are summarized in Table 2. The only systematic error which does not depend on the orbit radii is frequency pulling of ω_z due to coupling to the detector's tuned circuit, which causes a random error less than 4×10^{-11}.

Clearly, the first obstacle to higher accuracy is temporal instability. While better engineering can stabilize the field somewhat[MOO89,GAT88], a more elegant route to ultra-high precision would be trapping one ion of each species to be compared and measuring them simultaneously. Preliminary theoretical and experimental work on the two-ion problem encourages our belief that ion-ion perturbations are controllable[KUC89].

We estimate that the troublesome field inhomogenities B_2 and C_4 (which are higher-order spatial components of the magnetic and electric fields, defined in reference [BRG86]) can each be reduced by at least a factor of ten by more careful shimming techniques, but relativistic mass shifts will limit accuracy to the 10^{-11} level unless there are improvements in cooling the cyclotron motion. Feedback cooling with a subthermal detector is a possibility. Also, under certain circumstances, one can win additional accuracy by deliberately distorting the magnetic field so as to cancel the relativistic correction to ν_c'.

Mass comparisons at the 10^{-11} level and beyond will permit weighing molecular bonds and electronic binding energies. Measuring nuclei levels involved in gamma-ray emission will give a value for the gamma-ray energies in a.m.u. This information, combined with a precise determination of γ-ray wavelength, would yield a new value for $N_A h$[JOH84]. $N_A h$, in turn, can be combined with a precise value for the electron mass, in amu, and with the Rydberg, to determine an independent value for α^2.

We'd like to thank Deborah Kuchnir for technical assistance. This work was supported by the National Science Foundation (through grant PHY86-05893 and a Graduate Fellowship to E.A.C.), and by the Joint Services Electronics Program grant #DAAL03-89-C-0001. G.P.L. thanks the donors of the Petroleum Research Fund. We are very grateful to R. Van Dyck for extensive helpful discussions.

Table 1

Fitting Scheme:	linear	quadratic	cubic
run #1	84 (9)	80(4)	74(6)
run #2	74 (9)	75(8)	75(12)
run #3	72(3)	76(3)	77(3)
average	73(3)	77(2)	76(3)

Combined value: 0.9995988876(4)

Table 1: Determination of $M(CO^+)/M(N_2^+)$. The values listed in the table are the measured mass ratio $M(CO^+)/M(N_2^+)$ - .9995988800, as fit to the data from three different data runs, using three different polynomial forms for the time dependence of the magnetic field. The quoted error reflects the spread in the different fitting schemes, ± .2 ppb, and the typical "error" determined by assuming a given scheme, ± .3 ppb.

Table 2: Error. The first column lists the major amplitude-dependent corrections to ν_c' and ν_z. The second column gives the effect of the corrections on ν_c, to lowest order in the orbit radii. During the ν_c' measurement, $a_c = 0.024(2)$ cm, $a_z = .005$ cm r.m.s., and $a_m \lesssim .003$ cm. During the ν_z measurement, $a_c \lesssim .002$, $a_z = .120(7)$, and $a_m \lesssim .003$ cm. The errors indicated are due to thermal motion or imperfect cooling. Because we measure a mass doublet, the value of the mean correction is not particularly important. Fluctuations (fourth column) put a limit on the accuracy attainable with a *single* pulse-and-phase measurement. The fifth column is an upper limit to the systematic dependence on ion species, for which we assume the driving and cooling pulses are constant to 1%. B_2 and C_4, higher-order components of the magnetic and electric fields [BRG86], were compensated to $|C_4| \lesssim 5 \times 10^{-5}$ and $B_2 = 1.2(2) \times 10^{-6}\,\mathrm{cm}^{-2}$.

Figure 1: Steps in the axial signals as one ion after another is expelled from the trap. The ions were driven to 20% of the trap size.

Figure 2: For each plotted point, the following experiment is performed: the (initially cold) ion is pulsed into a cyclotron orbit of known initial phase, then allowed to evolve "in the dark" for the indicated amount of time. Then a π-pulse is applied, bringing the ion's cyclotron action and phase into the axial mode. As the ion's axial motion rings down, its phase is detected. The appropriate multiple of 360 degrees is added, and a line is fit to the points. The slope of the line is the offset from the frequency generator to the trap cyclotron frequency.

Figure 3: The data from run #3. The solid points are $\nu_c(N_2^+)$; the open points are $\nu_c(CO^+)$. A total of three ions were loaded, in order $N_2^+ - CO^+ - N_2^+$. The solid lines are a fit to the two frequencies assuming a field drift that is linear in time. The dotted line fit assumes a quadratic field drift. The indicated value for $\nu_c(CO^+) - \nu_c(N_2^+)$ results from the latter assumption, and corresponds to $M(CO^+)/M(N_2^+) = 0.9995988876(3)$.

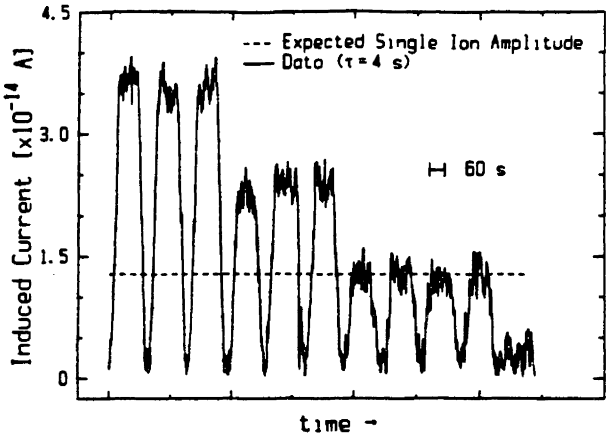

FIG. 1. Steps in the axial signals as one ion after another is expelled from the trap. The ions were driven to 20% of the trap size.

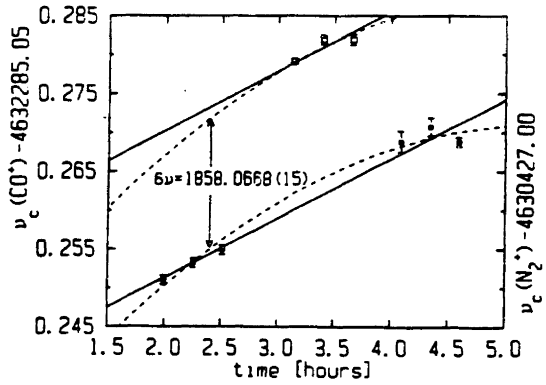

FIG. 3. The data from run 3 are shown. The solid squares are $\nu_c(N_2^+)$; the open squares are $\nu_c(CO^+)$. A total of three ions were loaded, in the order N_2^+-CO^+-N_2^+. The solid lines are a fit to the two frequencies assuming a field drift that is linear in time. The dotted-line fit assumes a quadratic field drift. The indicated value for $\nu_c(CO^+)-\nu_c(N_2^+)$ results from the latter assumption, and corresponds to $M(CO^+)/M(N_2^+)=0.999\,598\,8876(3)$.

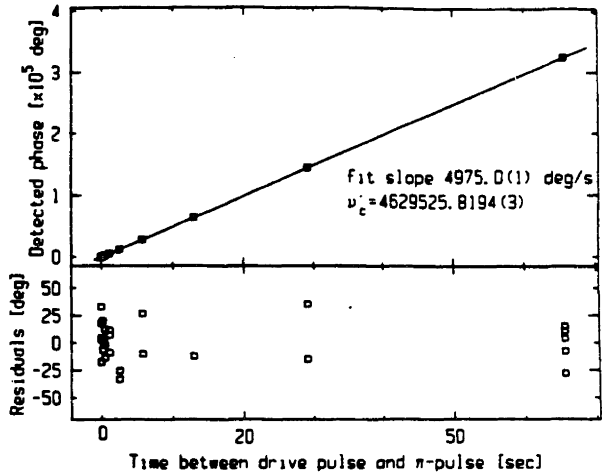

FIG. 2. For each plotted point, the following experiment is performed: The (initially cold) ion is pulsed into a cyclotron orbit of known initial phase, and then allowed to evolve "in the dark" for the indicated amount of time. Then a π pulse is applied, bringing the ion's cyclotron action and phase into the axial mode. As the ion's axial motion rings down, its phase is detected. The appropriate multiple of 360° is added, and a line is fitted to the points. The slope of the line is the offset from the frequency generator to the trap cyclotron frequency.

TABLE I. Determination of $M(CO^+)/M(N_2^+)$. The values listed in the table are the measured mass ratio $M(CO^+)/M(N_2^+)-0.999\,598\,8800$, as fitted to the data from three different data runs, using three different polynomial forms for the time dependence of the magnetic field. The quoted error reflects the spread in the different fitting schemes, ± 0.2 ppb, and the typical "error" determined by assuming a given scheme, ± 0.3 ppb. Combined value: 0.999 598 8876(4).

	Fitting scheme		
Run	Linear	Quadratic	Cubic
1	84(9)	80(4)	74(6)
2	74(9)	75(8)	75(12)
3	72(3)	76(3)	77(3)
Average	73(3)	77(2)	76(3)

TABLE II. Error. The first column lists the major amplitude-dependent corrections to ν_c' and ν_z. The second column gives the effect of the corrections on ν_c, to lowest order in the orbit radii. During the ν_c' measurement, $a_c=0.024(2)$ cm, $a_z=0.005$ cm rms, and $a_m \lesssim 0.003$ cm. During the ν_z measurement, $a_c \lesssim 0.002$, cm, $a_z=0.120(7)$ cm, and $a_m \lesssim 0.003$ cm. The errors indicated are due to thermal motion or imperfect cooling. Because we measure a mass doublet, the value of the mean correction is not particularly important. Fluctuations (fourth column) put a limit on the accuracy attainable with a *single* pulse-and-phase measurement. The fifth column is an upper limit to the systematic dependence on ion species, for which we assume the driving and cooling pulses are constant to 1%. B_2 and C_4, higher-order components of the magnetic and electric fields (Ref. 9), were compensated to $|C_4| \lesssim 5\times10^{-5}$ and $B_2=1.2(2)\times10^{-6}$ cm^{-2}.

Correction (mode affected)	Form of $\Delta\nu_c/\nu_c$	Mean value of $\Delta\nu_c/\nu_c$	rms thermal error	Upper limit of systematic variation with ion species
Relativity (ν_c')	$-\frac{1}{2}(\omega_c^2/c^2)a_c^2$	-2×10^{-10}	4×10^{-11}	5×10^{-12}
Electrostatic (ν_c')	$\frac{1}{4}(C_4/d^2)(\omega_m/\omega_c)(-\frac{1}{2}a_c^2+a_z^2-a_m^2)$	2×10^{-11}	4×10^{-12}	5×10^{-13}
Electrostatic (ν_z)	$\frac{1}{4}(C_4/d^2)(\omega_m/\omega_c)(-a_c^2+\frac{1}{2}a_z^2-a_m^2)$	5×10^{-10}	9×10^{-11}	1×10^{-11}
Magnetic (ν_c')	$(B_2/2)(-a_c^2+a_z^2-a_m^2)$	-3.5×10^{-10}	6×10^{-11}	7×10^{-12}
Magnetic (ν_z)	$(B_2/2)a_c^2$	3×10^{-12}	3×10^{-12}	1×10^{-13}

Chapter 5 Simultaneous Two-Ion Cyclotron Resonance

5A Basic Two Ion Theory

Mass comparisons using sequential resonance experiments on single ions require a magnetic field stability comparable to the desired accuracy of comparison. Take for example the ammonia mass doublet ($^{15}NH_3^+$ and $^{14}NDH_2^+$) whose masses differ by about five parts in 10^4. To be of use in fundamental constant work [JOH84], the mass ratio must be determined to nearly a part in 10^{12}. A sequential measurement (load one ion; measure; dump; load the other ion; measure; etc) must determine each ion's cyclotron frequency to microhertz out of megahertz. During each measurement, and while the ions are being exchanged, the magnetic field has to be constant to a parts in 10^{12}. Also draconian given current technology, is the requirement on electric field stability, parts in 10^9.

On the other hand, if the two ions are measured simultaneously, in the same trap, the requirements on field stability relax immensely. As we shall see in section 5C, below, the precision quantity is the instantaneous cyclotron frequency difference, which must be measured to 7 μHz out of 1.5 kHz. The magnetic field must be constant to only parts in 10^9, the electric field to a part in 10^5, both standards already achieved in our experiment [CWB89].

Even as simultaneous two-ion cyclotron resonance finesses the problem of temporal field drifts, however, it raises new issues. If the two ions are too close together in the trap, the coulombic coupling may perturb their cyclotron frequencies unacceptably. On the other hand, if the ions are well-spaced, any residual spatial inhomogeneity of the trapping fields may affect the two ions unequally. The first question to ask then, is what is the motion of two ions, relative to each other and relative to the trap electrodes, under the combined influence of the trapping fields and of the ion-ion coulombic repulsion?

The motion of two ions in a Penning trap is a three-body problem and can not in general be solved exactly. However, in the regime of experimental interest we can make several useful approximations. If the initial ion-ion separation ρ_s is large enough to keep the ion-ion coupling weak, we can carry over from the single ion solution the idea of independent cyclotron and axial motions for each ion. Ion interaction will perturb the frequencies of these four modes, to be sure (as discussed below), but we will not have to think of the axial or cyclotron motions as collective modes of the two ions.

The magnetron motion, however, is another story. The unperturbed magnetron frequencies of a mass doublet are so nearly degenerate that even a small perturbation will strongly couple the magnetron modes. We will use conservation principles to establish that the distance between the two ions -- an important quantity that sets the scale of ion-ion perturbations -- is an

approximate constant of the motion. Further, we will show that the geometry of the locked magnetron motion is such that, over time, the ions sample very similar fields.

Conserved Quantities

Regardless of the number of ions in the trap, the conserved quantities are the total energy and the z-component of the total canonical angular momentum [WBI85]. As a first pass at the problem, let us imagine that the axial and the cyclotron radii of both ions are zero, and write the energy and canonical angular momentum as follows:

$$E = \frac{-eV_t}{4d^2}(\rho_1^2+\rho_2^2) + \frac{e^2}{\rho_s} + \frac{1}{2}m_1\left(\dot{\vec{\rho}}_1\right)^2 + \frac{1}{2}m_2\left(\dot{\vec{\rho}}_2\right)^2 \qquad (5A.1)$$

$$L_z = \frac{eB}{2c}(\rho_1^2+\rho_2^2) + m_1\vec{\rho}_1\times\dot{\vec{\rho}}_1 + m_2\vec{\rho}_2\times\dot{\vec{\rho}}_2 \qquad (5A.2)$$

where $\vec{\rho}_s = \vec{\rho}_1 - \vec{\rho}_2$ is the ion-ion separation (Fig. 5.1). We now rewrite the equations, explicitly separating out the effects of the ion-ion perturbation:

$$E = \rho_1^2\left(\frac{-eV_t}{4d^2} + \frac{m_1\omega_{m1}^2}{2}\right) + \rho_2^2\left(\frac{-eV_t}{4d^2} + \frac{m_2\omega_{m2}^2}{2}\right) + \frac{e^2}{\rho_s} + S_{KE} \qquad (5A.3)$$

$$L_z = \rho_1^2\left(\frac{eB}{2c} - m_1\omega_{m1}\right) + \rho_2^2\left(\frac{eB}{2c} - m_2\omega_{m2}\right) + S_L \qquad (5A.4)$$

where we have substituted for the ions' velocities the values of

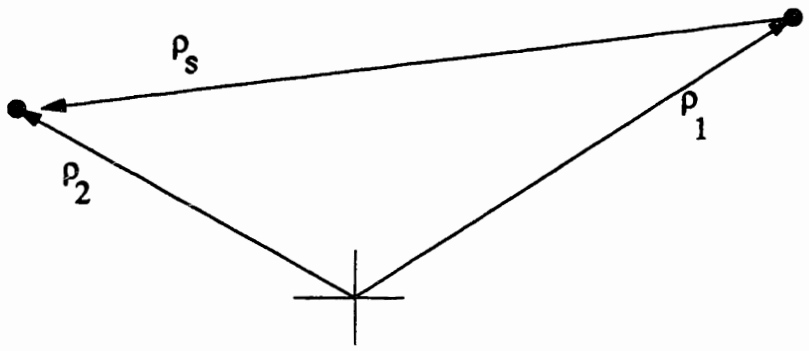

Fig. 5.1 The axis of the trap is perpendicular to the plane of the figure. When only the magnetron motions are considered, the angular momentum and energy of the system of two particles are well approximated by functions only of the distances $\rho_1 = |\vec{\rho}_1|$, $\rho_2 = |\vec{\rho}_2|$, and $\rho_s = |\vec{\rho}_s|$.

their unperturbed magnetron velocities: $\vec{\rho}_i = -\omega_{mi}\,\hat{z} \times \vec{\rho}_i$. The small errors associated with this substitution are accounted for in the terms S_{KE} and S_L (for Small bit of Kinetic Energy and of anguLar momentum, respectively). Here the ion-ion interaction is represented only by a potential term, e^2/ρ_s, and by the two small corrections S_{KE} and S_L. Define a mass splitting η such that $m_1 = m_o(1 + \eta)$ and $m_2 = m_o(1 - \eta)$. Here, and throughout the chapter, the subscripts 1 and 2 refer to properties of one ion or the other, and the subscript o refers to properties of a hypothetical ion whose mass is the average of the masses of the two ions. We now make two key approximations (whose validity we will check shortly): first, that $\omega_{m1}=\omega_{m2}=\omega_{mo}$, and second, that $S_{KE} = S_L = 0$, and rewrite the energy and angular momentum:

$$\frac{E}{m_o} - \frac{e^2}{m_o\rho_s} = (\rho_1^2 + \rho_2^2)\left(\frac{-\omega_{zo}^2}{4} + \frac{\omega_{mo}^2}{2}\right) + (\rho_1^2 - \rho_2^2)\left(\frac{\eta\,\omega_{mo}^2}{2}\right) \qquad (5A.5)$$

$$\frac{L_z}{m_o} = (\rho_1^2 + \rho_2^2)(\omega_{co}/2 - \omega_{mo}) + (\rho_1^2 - \rho_2^2)(-\eta\,\omega_{mo}) \qquad (5A.6)$$

ρ_1 and ρ_2 evolve over time, but conservation of energy and angular momentum put a strict limit on the amount ρ_s can change. In order to conserve L_z, changes in ρ_1^2 and in ρ_2^2 must be related. Eqn 5A.6 gives:

$$\delta(\rho_1^2 + \rho_2^2) = \frac{2\eta\,\omega_{mo}}{\omega_{co} - 2\omega_{mo}}\,\delta(\rho_1^2 - \rho_2^2) \qquad (5A.7)$$

We will simplify expressions using the inequality $\omega_c >> \omega_z >> \omega_m$. (In practise, the ratio is about 8000:160:1.5 for a mass 18 ion.) Combining Eqns. 5A.5 and 5A.7, we find that changes in the ion-ion potential energy are restricted:

$$\delta\left(\frac{e^2}{m_o \rho_s}\right) = \frac{\eta \omega_{mo}^2}{2} \delta(\rho_1^2 - \rho_2^2) \qquad (5A.8)$$

And what, typically, is the maximum expected change in $(\rho_1^2 - \rho_2^2)$? As we shall see in section 5B, below, ions are typically loaded into the trap with an initial separation $\rho_s = 2\rho_{com}$, where ρ_{com} is the length of the average position vector,

$$\vec{\rho}_{com} = (\vec{\rho}_1 + \vec{\rho}_2)/2. \qquad (5A.9)$$

Further, as we shall see in just a moment, both ρ_s and ρ_{com} are approximate constants of the motion. The maximum change in $(\rho_1^2 - \rho_2^2)$ we can expect then is about $2\rho_s^2$, which implies that the maximum possible change in ρ_s is

$$\frac{\delta \rho_s}{\rho_s} = \frac{\eta \omega_{mo}^2}{\kappa} \qquad (5A.9)$$

where we have defined the coupling constant,

$$\kappa = e^2/m_o \rho_s. \qquad (5A.11)$$

In the limit of degenerate masses, (η goes to 0), the ion-ion separation is a constant of the motion. ρ_s is nearly a constant of

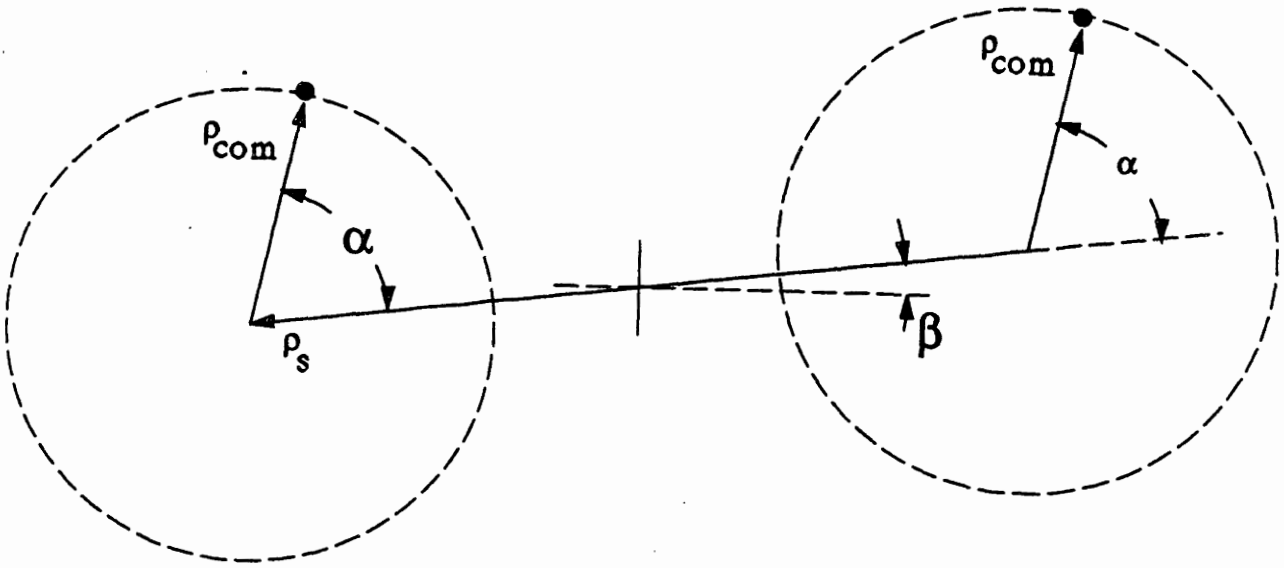

Fig. 5.2 Any initial positions of ion 1 and ion 2 can be described as superpositions of the common mode vector, $\vec{\rho}_{com}$, and the separation vector, $\vec{\rho}_s$. If the magnetic field lines come up out of the plane, both vectors rotate clockwise. In a frame rotating at ω_s, the ions trace out counterclockwise tandem circles centered on opposite sides of the origin. The angular frequency of the motion is $\omega_{com} - \omega_s$.

the motion as long as the mass splitting is small compared to the coupling, $\eta << \kappa/\omega_{mo}^2$.

We will look more carefully at the effects of nondegenerate masses on the orbits in section 5D, below, but for now keep $\eta = 0$, and make the purely geometrical observation that since ρ_s and $\rho_1^2 + \rho_2^2$ are both constant, so must† be ρ_{com}. The allowed ion motions thus decompose nicely into a common mode and a "stretch" mode (Fig. 5.2). The stretch mode is so called in analogy with tightly coupled harmonic oscillators, although of course in this case a vector pointing from one ion to the other does not stretch in length but merely rotates.

Let us recheck our earlier assumptions for self-consistency. First, how large are the supposedly small terms S_{KE} and S_L, and how much effect did our neglect of them have on the calculated length of the vectors, ρ_{com} and ρ_s? Because the ions are in a strong magnetic field, the electric field from each ion induces an E-cross-B drift in the other. These drifts are relatively small corrections to the unperturbed ion velocities, and (for the magnetron motion) the velocity terms are in turn relatively much smaller than the electric and magnetic potential contributions to the total angular momentum and total energy. The magnitude of the E-cross-B velocity is cE/B, or $ec/(B\rho_s^2)$. The largest change that this drift could cause in the angular momentum would be if the induced drift were perpendicular to the ion's position vector, and if that vector

---

†$\rho_s^2 = \rho_1^2 + \rho_2^2 - 2\vec{\rho}_1.\vec{\rho}_2$ = constant implies $\vec{\rho}_1.\vec{\rho}_2$ = constant.
Therefore $\rho_{com}^2 = \rho_1^2 + \rho_2^2 + 2\vec{\rho}_1.\vec{\rho}_2$ = constant.

were at maximum length. Given typical experimental initial conditions, $\rho_i \leq \rho_s$, so that the change in angular momentum must be less than $\delta S_L = m_o ce/(B\rho_s) = 2m_o\rho_s^2(\kappa/\omega_c)$. Similarly, the maximum change in the kinetic energy occurs when the drift velocity is adding to or subtracting from the ion's velocity when it is at its maximum, thus the maximum possible change in the kinetic energy is $\delta S_{KE} = m_o\rho_s^2(\omega_m/\omega_c)\kappa$. Reinserting the maximum values, δS_L and δS_{KE}, back into the the conservation equations (5A.5 and 5A.6) in which they were neglected, we can put an upper bound on the error associated with the approximation:

$$\frac{\delta(\rho_1^2 + \rho_2^2)}{\rho_s^2} = \frac{2\eta\omega_{mo}}{\omega_{co} - 2\omega_{mo}} \frac{\delta(\rho_1^2 - \rho_2^2)}{\rho_s^2} + O\left(\frac{\kappa}{\omega_{co}^2}\right) \qquad (5A.12)$$

$$\frac{\delta\rho_s}{\rho_s} = \frac{-\eta\omega_{mo}^2}{2\kappa} \frac{\delta(\rho_1^2 - \rho_2^2)}{\rho_s^2} + O\left(\frac{\omega_{zo}^2}{\omega_{co}^2}\right) \qquad (5A.13)$$

It is easy to verify that the errors in ρ_s and ρ_{com} associated with our other major approximation, that $\omega_{m1} = \omega_{m2} = \omega_{mo}$, are smaller still. The errors in the results obtained so far in this section are thus small as long as $\omega_{zo}^2 << \omega_{co}^2$, $\kappa << \omega_{co}^2$, and $\eta\omega_m^2 << \kappa$. These inequalities are all experimentally realizable. For instance, for the case of our ammonia example, with the reasonable initial value of ρ_s = 0.08 cm., we have $\kappa = 2 \times 10^7$, $\eta\omega_m^2/\kappa = 1 \times 10^{-3}$, $\kappa/\omega_{co}^2 = 1 \times 10^{-8}$, and $\omega_{zo}^2/\omega_{co}^2 = 5 \times 10^{-4}$.

Locked Motion

Having established the geometry of the modes (or approximated them, in the more realistic case of nondegenerate masses) by the use of conservation principles, we can confidently solve the equations of motion for the corresponding frequencies. The equations of motion for two particles moving in the mid-plane of a Penning trap are:

$$m_1\ddot{\vec{\rho}}_1 = \frac{eB}{c}\dot{\vec{\rho}}_1\times\hat{z} + \frac{eV_t}{2d^2}\vec{\rho}_1 + \frac{e^2(\vec{\rho}_1-\vec{\rho}_2)}{|\vec{\rho}_1-\vec{\rho}_2|^3} \qquad (5A.4)$$

$$m_2\ddot{\vec{\rho}}_2 = \frac{eB}{c}\dot{\vec{\rho}}_2\times\hat{z} + \frac{eV_t}{2d^2}\vec{\rho}_2 - \frac{e^2(\vec{\rho}_1-\vec{\rho}_2)}{|\vec{\rho}_1-\vec{\rho}_2|^3} \qquad (5A.15)$$

These equations are linear except for the cubic in the denominator of the interaction term. We use the results of our conservation principle argument, that $|\vec{\rho}_1-\vec{\rho}_2| = \rho_s$ is an approximate constant, to eliminate the nonlinear term. Dividing though by m_o, we get the equations

$$(1+\eta)\ddot{\vec{\rho}}_1 = \omega_{co}\dot{\vec{\rho}}_1\times\hat{z} + \frac{\omega_{zo}^2}{2}\vec{\rho}_1 + \kappa(\vec{\rho}_1-\vec{\rho}_2)$$
$$(1-\eta)\ddot{\vec{\rho}}_2 = \omega_{co}\dot{\vec{\rho}}_2\times\hat{z} + \frac{\omega_{zo}^2}{2}\vec{\rho}_2 - \kappa(\vec{\rho}_1-\vec{\rho}_2) \qquad (5A.16)$$

These coupled linear equations are exactly solvable. We get that the two normal mode frequencies are

$$\omega_{com} = \omega_{mo} + O\{(\eta^2\omega_{mo}^4)/(2\kappa\omega_{co})\}$$
$$\omega_s = \omega_{mo} + 2\kappa/\omega_{co} + O\{(\eta^2\omega_{mo}^4)/(2\kappa\omega_{co})\} \qquad (5A.17)$$

The normal mode motions correspond to clockwise motion of the vectors shown in Fig. 5.2. in the limit of $\eta\omega_m^2/\kappa << 1$. (The small corrections tc the geometry of the modes for nondegenerate mass are described in section 5C.) Viewed in a frame rotating at ω_s, the ions appear to drift counterclockwise in tandem, sketching out twin circles centered on either side of the trap center (Fig. 5.2). The ions take turns moving nearer to and further from trap center, with a period of motion $t_e = 2\pi/(\omega_s - \omega_{com}) = \pi\omega_{co}/\kappa$.

From the point of view of the precision mass spectroscopist, this tandem motion is very welcome. If its period is short compared to time between pulses of a separated oscillatory fields (S.O.F.) resonance measurement, the ions' orbits will average away, albeit incompletely, the effects of field inhomogeneities which are functions of distance from trap center. Better yet would be if ρ_{com} were cooled as much as possible while ρ_s remained relatively large (Fig. 5.3). In such a configuration the two ions would follow each other around and around the center of the trap, sampling almost exactly the same fields. We discuss schemes for accomplishing this specific cooling in section 5C below.

Axial and Cyclotron Motion

Now that we understand the basic principles of locked magnetron motion, we relax the requirement that the axial and cyclotron radii vanish. $\vec{\rho}_s$ and $\vec{\rho}_{com}$ no longer refer to the instantaneous ion positions, but rather to the guiding centers of each ion's axial-cyclotron motion. We require that the cyclotron

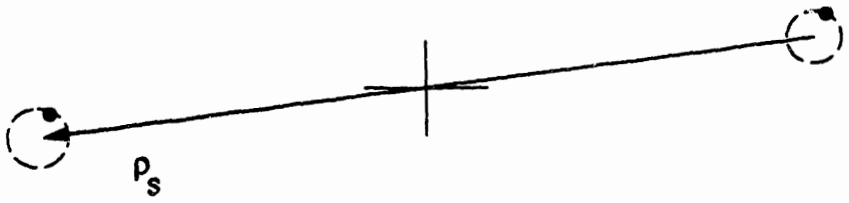

Fig. 5.3 If the center-of-mass motion is cooled, the ions are "parked" in orbits on either side of the origin. This configuration ensures that, as the ions move around the trap center, they sample very nearly identical fields. This minimizes the risk that inhomogeneities in the trapping fields will affect the measured frequency mass ratio.

radii, ρ_{c1} and ρ_{c2}, be small enough to avoid the possibility of a hard collision, that is, that $\rho_{c1} + \rho_{c2} < \rho_s$. The ion-ion potential averaged over the cyclotron and axial motion is no longer simply e^2/ρ_s, but is now a function of the cyclotron and axial radii as well as ρ_s. However, as long as the inter-ion potential (the quantity which appears in parentheses on the left-hand side of Eqn 5A.8) is a monotonic function of ρ_s, the result that ρ_s and ρ_{com} are constants of the motion remains valid. In the absence of hard collisions, the large separation between the mode frequencies ensures that energy and momentum will not be transferred from axial and cyclotron modes to the magnetron motion.

If the axial displacements z_1 and z_2 are small compared to ρ_s, then we can expand the axial component of the ion-ion repulsive force, keeping only the dipole term which is linear in $z_1 - z_2$.

$$F_{z1} = e^2 (z_1 - z_2) / ((z_1 - z_2)^2 + \rho_s^2)^{3/2}$$

$$F_{z1} = -F_{z2} \approx m_0 \kappa (z_1 - z_2), \qquad \text{for } |z_1 - z_2| \ll \rho_s \qquad (5A.18)$$

Using the dipole form for the coupling, and assuming weak coupling, that is $\kappa \ll |\eta\, \omega_z^2|$, it is easy to solve for the perturbed axial frequencies:

$$\omega'_{z1} - \omega_{z1} = \frac{-\kappa}{2\omega_{zo}} - \frac{\kappa}{2\omega_{zo}}\left(\frac{\kappa}{2\eta\omega_{zo}^2}\right) + \ldots \qquad (5.A.19)$$

$$\omega'_{z2} - \omega_{z2} = \frac{-\kappa}{2\omega_{zo}} + \frac{\kappa}{2\omega_{zo}}\left(\frac{\kappa}{2\eta\omega_{zo}^2}\right) + \ldots \qquad (5A.20)$$

The primed variables here refer to the frequencies shifted by the ion-ion perturbation. As long as the coupling is weak, $\kappa/(\eta\ \omega_z^2) << 1$, the perturbations are very nearly symmetric, that is, the the axial difference frequency, $(\omega'_{z1}-\omega'_{z2})$, is not significantly shifted.

In experimentally realizable situations the approximation $(z_1 - z_2) << \rho_s$ may not be valid. To obtain adequate signal/noise in the axial motion detector, the ions may well have to be driven to axial motion with peak amplitudes $a_{z1}, a_{z2} > \rho_s$. In this case, the coupling is nonlinear and κ is replaced with an effective coupling κ', which depends on the amplitudes a_{z1} and a_{z2}, and which is always less than κ, except when the amplitudes vanish. As the axial motions damp, κ' increases and the frequencies shift. The signals detected after exciting the axial motion will thus be "chirped". However, if the axial amplitudes remain equal to each other as the ions damp, the perturbation remains symmetric, and the frequency difference $\omega_{z1}' - \omega_{z2}'$ will be only slightly perturbed.

We have established a general picture of two ion dynamics in an experimentally interesting regime, with magnetron modes of the ions tightly locked into coordinated motion, and with the axial modes perturbed in frequency but still independent. We now turn temporarily from the two ion dynamics discussion to describe some preliminary experiments we have performed with two ions. Ion-ion perturbation of the cyclotron frequencies, and other topics in two ion motion will be covered in section 5C below.

Section 5B: Preliminary Two Ion Experiments

We describe in this section our preliminary experimental work on two-ion trapping.† The work demonstrates techniques for loading a single ion of each species into the trap, and confirms that, with appropriate initial inter-ion spacing, the axial motion of the two ions is qualitatively as predicted. We have worked with the doublet N_2^+/CO^+, whose masses differ by about 5 parts in 10^4. The apparatus, described in references [WLB88] and [CWB89], is a Penning trap at 4.2K, in an 8.5 Tesla magnetic field. When the ions are tuned to be resonant with our axial motion detector, the axial frequencies of the two ion species differ by 33 Hz out of about 160 kHz.

A pair of ions is loaded as follows: from a room temperature gas-handling manifold, we admit a small pulse of N_2 gas, which drifts down into the cryogenic portion of the apparatus and through a hole in the upper endcap into the trap volume, where it encounters a beam of electrons injected from below the trap. The average number of ions produced by electron collisions is proportional to the product of the electron current and the number of molecules injected. This product has been previously calibrated [KUC89] to produce, on the average, 1/2 ion with every gas pulse admitted. After each pulse of gas, we test for ions by driving the lower endcap and looking for the signal from the axially excited ion.

† A more detailed account of these experiments appears in D. Kuchnir's thesis [KUC89].

Occasionally, more than one ion is trapped, in which case we dump the trap and start again. It rarely takes more than a few attempts to catch a single N_2^+ ion.

Because the ionizing electron beam is thin and very nearly coaxial with the trap, ions are initially created near the axis of the trap, which is to say, created with a small magnetron radius. The moment the second ion is created, ion-ion separation ρ_s will be a constant of the motion. Thus if we wish the two ion motion to have a particular ρ_s, we must control how far the initially created N_2^+ ion is from the site of the CO ionization. Before loading the CO^+ ion, we drive the magnetron motion of the newly trapped single N_2^+ ion to about .6 mm, using a short resonant pulse at the magnetron frequency. Then we proceed as with N_2 to trap a single CO^+ ion. At the moment the CO^+ ion is created (at trap center), the N_2 ion is .6 mm from trap center. Thus initial ρ_s is .6 mm, and initial ρ_{com} is .3 mm.

If we load the second ion without preparing the first in a large magnetron orbit, the ions will be created with $\rho_{com} \sim \rho_s < 0.02$ cm. The axial signal detected under these conditions is very irreproducible. Sometimes a component of the axial signal appears at the average of the two unperturbed frequencies, and sometimes (especially when the ions are driven hard) we see individual signals at close to the unperturbed frequencies. With the radial separation so small, the approximations of section 5A, above, are invalid, and it is hard to predict what sort of motion should occur. It is possible that, as the axial motion damps, the ions come to an equilibrium

stacked vertically along the axis. In any case this sort of configuration is not appropriate for precision metrology and the remainder of the measurements described in this section were performed on ions radially spaced by about 0.6 mm.

The ions can not only be loaded one at a time, they can be unloaded individually as well. This is accomplished by resonantly driving only one of the ions into a large axial orbit, and then "dipping" the trap, i.e. adjusting the lower endcap voltage so as to draw the equilibrium position of the ions near the surface of the lower endcap. The ion with the large axial motion then collides with the wall, is neutralized and leaves the trap, leaving only the undriven ion trapped.

Truly simultaneous resonance measurements on the two ions requires the ability to detect both ions simultaneously. Unfortunately, the ions' axial frequency splitting, 33 Hz, is much larger than the effective bandwidth of our detector. The ions may be detected sequentially by alternately tuning the trap voltage so that first one, then the other ion comes in resonance with the detector, but we use a trick to bring components of both signals within the bandwidth of the detector simultaneously. Adding a small a.c. term to the trapping voltage modulates the frequency of the axial motion, generating sidebands spaced by the modulation frequency ν_{mod}. The d.c. trapping voltage V_t and ν_{mod} can be adjusted to bring the first upper sideband of N_2^+ and the first lower sideband of CO^+ both within the bandwidth of the detector.

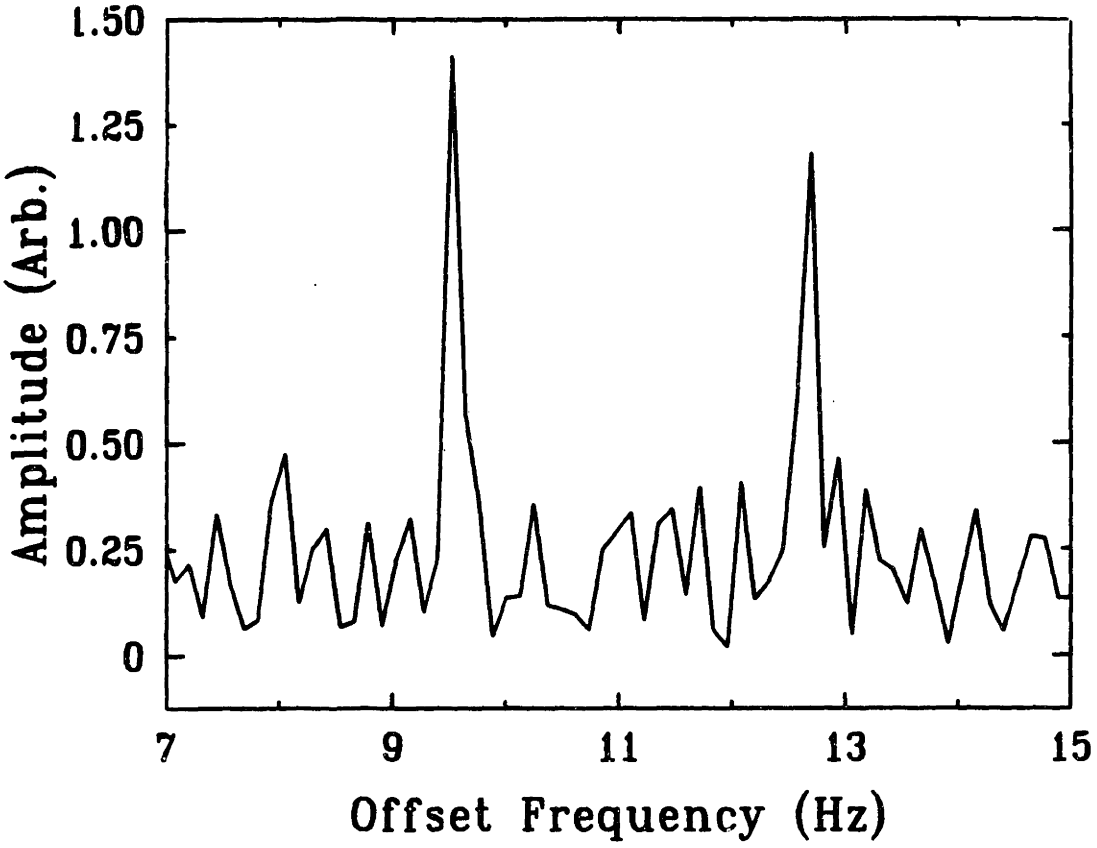

Fig. 5.4 The fourier transform of the signal detected after the axial motions of simultaneously trapped single CO^+ and N_2^+ ions are excited. The trapping voltage is modulated at 15 Hz, giving rise to sidebands on the axial frequencies of the ions. Although the axial frequency splitting of the ions is 33 Hz, the first upper sideband of the nitrogen ion and the first lower sideband of the carbon monoxide ion are separated by only 3 Hz and fall within the bandwidth of the axial motion detector. A calibration peak at 11 Hz has been removed from the data.

When the axial motions of both ions are excited with a short pulse, the signals from the ions are simultaneously detectable. [Fig. 5.4]

The amplitude of an ion's sidebands relative to the overall amplitude of its motion depends on strength of the modulation $\beta = (1/2)(V_{mod}/V_{trap})((\omega_z/2\pi\nu_{mod})$, where V_{mod} is the peak modulation voltage. The amplitude of the nth sideband is proportional to $J_n(\beta)$, where J_n is the nth order Bessel's function. Since damping of the axial motion is due to interaction with the detector, damping time is a function of the strength of the sideband that is in resonance with the detector (assuming that the ν_{mod} is large enough to ensure that only one sideband at a time interacts appreciably with the detector.) When the nth sideband is tuned to the detector the damping time is increased by a factor of $(J_n)^{-2}$ relative to the damping time for an unmodulated ion.

When both species of ion are in the trap, the observed axial frequencies differ from single-ion, unperturbed values. The qualitative nature of the shifts, a decrease of roughly 1 Hz for small excitations, with the shift becoming less pronounced for larger axial orbits, agrees with the model described in section 5A, above. A more quantitative comparison can not be made with these data because at the time the data were recorded there was an uncertainty in the overall calibration of orbit sizes and moreover the trapping voltage was drifting in time.

Even without good calibrations, however, there are several essential observations to be made:

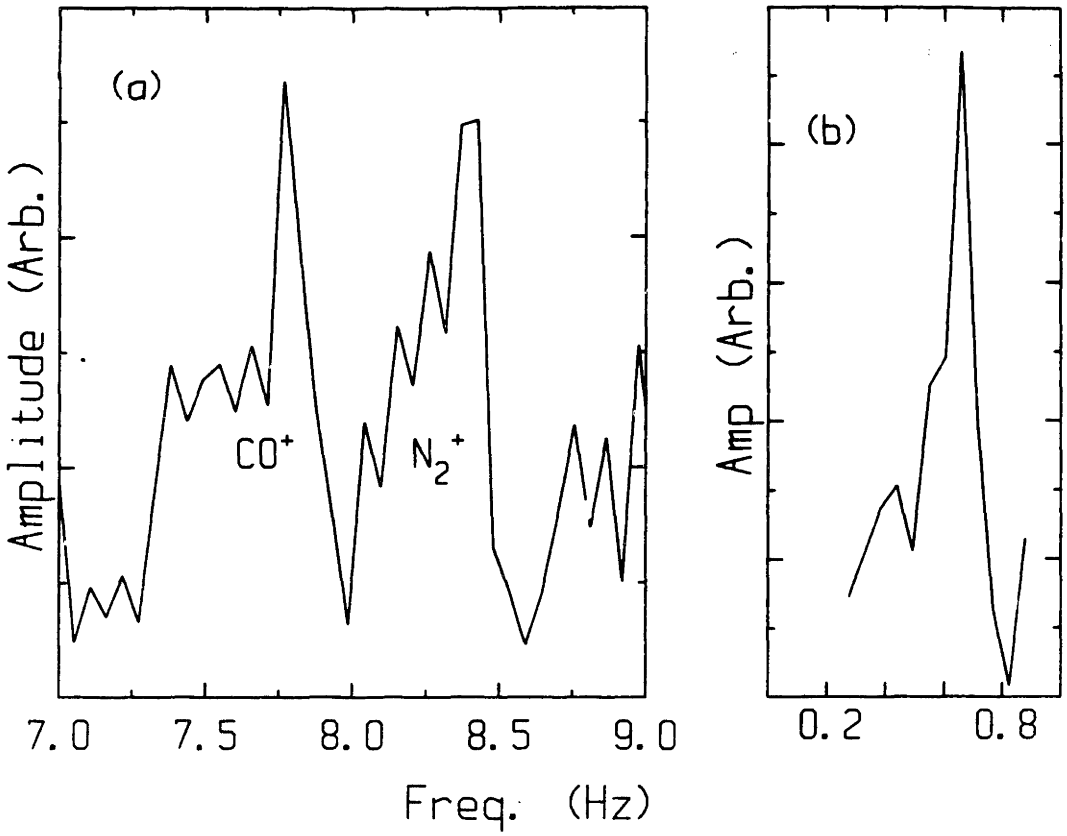

Fig. 5.5 The nonlinearity of the ion-ion interaction makes the axial frequency perturbation amplitude-dependent. As the ions damp their frequencies may shift over several of the fourier transform bin widths (a). In (b), we have convolved the signal shown in (a) to extract a signal at the difference frequency. The sharpness of the feature in (b) is evidence that the difference frequency remains quite constant as the ions damp.

First, the ion-ion perturbation is roughly constant in time. Over a period of 90 minutes, the axial frequency shifts changed by less that 35%. (Temporal drifts in the trapping voltage prevented a more stringent limit.) Since the perturbations scale as ρ_s^{-3}, these data suggest that ρ_s varied by at most 10%.

Second, the perturbations, even though manifestly amplitude-dependent, were quite symmetric. In (Fig. 5.5) the ions have been pulsed to axial orbits larger than the radial separation. As the ions' axial motion damps, the effective coupling becomes stronger and the frequencies of both ions shift downward. This "chirp" in frequency is on the order of several fourier transform bin widths, and the transformed peaks look correspondingly messy. But since the shifts are symmetric, that is to say, if at any given moment the CO^+ and the N_2^+ ion are each shifted the same amount from their unperturbed values, then the difference in their frequencies should remain constant, even as the individual frequencies shift. As described in the caption of [Fig 5.6], we numerically extract from the data the difference frequency, which is manifestly much more stable than either of the individual motions. The same numerical routine, incidentally, can extract a difference *phase* from the two chirped signals, which suggests a two-ion generalization of the phase-sensitive technique for measuring single ion cyclotron frequencies described in references [CWB89 and CWB90].

Of course, determining the axial frequency splitting of a mass doublet is itself a mass measurement. Corrections due to magnetic field tilt and electrostatic anharmonicities are small and moreover

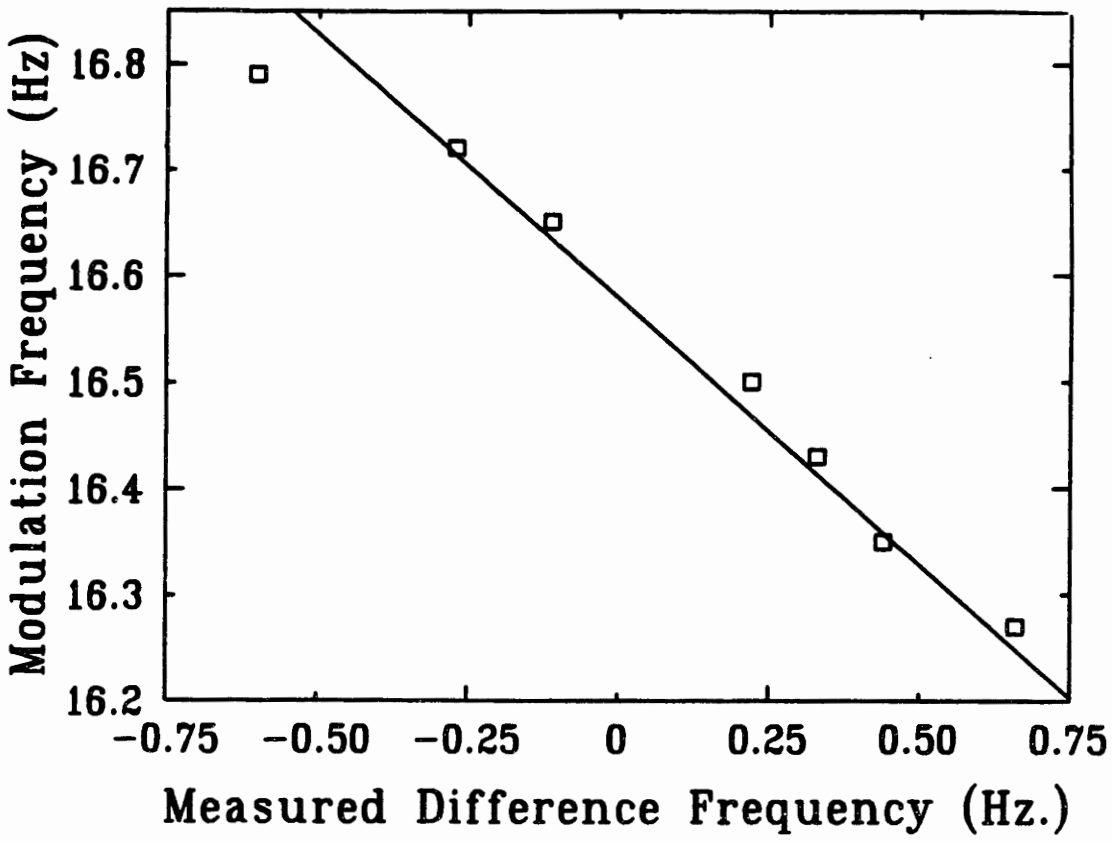

Fig. 5.6 The difference frequency between the two observed signals, δ_{vz}, is measured for a variety of modulation frequencies, ν_{mod}. Since we observe the first lower sideband of CO^+ and the first upper sideband of N_2^+, the difference between the frequencies of the actual axial motions is equal to $2\nu_{mod}+\delta_{vz}$. The combined result: $\nu_{z1}' - \nu_{z2}' = 33.14(3)$

should be identical for the two ions. Most important, temporal drifts in the trapping fields should not affect the measured mass ratio. Our measurement (Fig. 5.6) of $\omega_{z1}/\omega_{z2}=0.99979953(16)$ corresponds to a mass ratio

$M(CO^+)/M(N_2^+) = (\omega_{z1}/\omega_{z2})^2 = 0.9995991(3)$

in agreement with published values. Though an accuracy of 3 parts in 10^7 is not spectacular, attaining such an accuracy by comparing the *axial* mode frequencies illustrates the basic two-ion idea. Had we measured the axial frequency of a single CO^+ ion, dumped it out, loaded a single N_2^+ ion (a 30 minute procedure), and measured *its* frequency, we should have been lucky to measure the mass ratio to even five times worse accuracy, given typical drifts in the axial frequency.

5C More two-ion theory

Implication of the Brown and Gabrielse invariance theorem for two-ion measurements

Brown and Gabrielse have shown [BRG82] that for a certain class of trapping field imperfections (i.e., the quadrupole electric field not axially symmetric or magnetic field tilted with respect to the axis of the electric field) an invariance theorem relates the frequencies of motion in the trap to the free space cyclotron frequency $\omega_c^2 = (\omega_c')^2 + \omega_z^2 + \omega_m^2$, where ω_c', ω_z, and ω_m are the measured frequencies. The equality is true to all orders for a range of trap imperfections, and provides a convenient prescription for combining the measured trap frequencies to recover the cyclotron frequency of the ion in a purely magnetic field. For two ions we write:

$$\omega_{c1}^2 = (\omega_{c1}')^2 + \omega_{z1}^2 + \omega_{m1}^2$$
$$\omega_{c2}^2 = (\omega_{c2}')^2 + \omega_{z2}^2 + \omega_{m2}^2 \qquad (5C.1)$$

where for our the purposes of this section ω_{ci}', ω_{zi}, and ω_{mi} refer to the frequencies of each ion as measured in the imperfect trap but as unperturbed by ion-ion interaction. We want to examine which of these six trap frequencies need be measured, to what accuracy, and how they should be combined in order to determine, to a part in 10^{12}, the ratio

$$R = (m_1/m_2) = (1+\eta)/(1-\eta) = \omega_{c2}/\omega_{c1}. \qquad (5C.2)$$

Brown and Gabrielse [BRG82] show that

$$\omega_{z1}^2 \approx \frac{eV_t}{m_1 d^2}\left[1 - \frac{3}{2}\sin^2\theta\left(1 + \frac{1}{3}\cos\phi\right)\right] \qquad (5C.3)$$

where ε specifies the out-of-roundness of the electric field and θ and ϕ the tilt angle of the magnetic field. For a particle of mass m_2 in the same fields,

$$\omega_{z2}^2 \approx R\omega_{z1}^2 \qquad (5C.4)$$

How good is the approximation? For a typical mass doublet with mass less than 30 amu, and for reasonable trap parameters, the four quantities $(\omega_{zo}/\omega_{co})^2$, η, $\sin^2\theta$, and ε are each less than 10^{-3}, so we ignore terms quartic in any combination of these four quantities. The error in eqn (5C.4), for example, is on the order of $\eta(\omega_{zo}/\omega_{co})^2 \sin^2\theta < 10^{-9}$, which contributes an error of order $\eta(\omega_{zo}/\omega_{co})^4 \sin^2\theta < 10^{-12}$ to the error in our final determination of R (eqn 5C.6, below). Consistent with an overall error of less than 10^{-12} we may also approximate

$$\omega_{m2}^2 \approx \omega_{m1}^2 \qquad (5C.5)$$

Using the approximations (5C.4 and 5C.5), we subtract Eqn(5C.1a) from eqn(5C.1b), and solve for R:

$$R = \frac{\omega_{z1}^2}{2\omega_{c1}^2} + \left(1 - \frac{\omega_{z1}^2}{2\omega_{c1}^2}\right)\left(1 + \frac{[2\omega_{z1}^2 + (\Delta\omega_c')](\Delta\omega_c')}{(\omega_{c1}^2 - \omega_{z1}^2/2)}\right)^{1/2} + O\left((\omega_{zo}/\omega_{zo})^4 \eta \sin^2\theta + \ldots\right)$$

(5C.6)

and with no loss in accuracy at the part in 10^{12} level, we can replace ω_{c1}^2 with measured values:

$$\omega_{c1}^2 = (\omega_{c1}')^2 + \omega_{z1}^2 + (\omega_{z1}^2/2\omega_{c1}') \qquad (5C.7)$$

Thus to measure the mass ratio to a part in 10^{12}, it is sufficient to measure only three quantities, ω_{c1}', ω_{z1} and $\Delta\omega_c' = \omega_{c1}' - \omega_{c2}'$. The first two quantities may be measured to relatively low accuracy. Compared to the accuracy ultimately desired for R, the requisite precision for ω_{c1}' is lower by a factor of 2η, and for ω_{z1}, by a factor of $2\eta\ (\omega_{zo}/\omega_{co})^2$. At the level of parts in 10^9 for the cyclotron frequency and parts in 10^6 for the axial frequency, drifts in electric and magnetic fields are much less important, so in practice one can measure ω_{c1}' and ω_{z1} before putting the second ion in the trap, thereby ensuring that ion-ion interactions will not be a problem. $\Delta\omega_c'$, the only quantity which must be measured to very high precision, is extremely sensitive to drifts in the field, and thus must be measured with two ions in the trap.

To conclude this section, two points must be emphasized, and two questions raised: First, the treatment in this section ignores ion-ion perturbation. What error does ion-ion perturbation cause

in the measurement of $\Delta\omega_c$'? Second, the invariance theorem assumes there is no spatial variation of the magnetic field and no nonquadrupole components of the electric field. What is the effect of these field imperfections? These questions are addressed in the next two sections.

Ion-Ion perturbation of the cyclotron frequency

As a first pass at the important question of ion-ion perturbation of the cyclotron difference frequency, we solve a set of linear differential equations approximating the actual situation. Imagine the following idealized situation: The guiding centers of the cyclotron orbit of each ion are stationary, separated by ρ_s. In this picture, there is no trap electric field, no time-averaged net force between the two ions, and the magnetic field is not B_0 but B_0'. The idea here is not to represent the trap realistically but simply to provide the simplest possible mathematical framework that still preserves the two-dimensionality of the ion-ion cyclotron coupling. If the cyclotron radius is small compared to ρ_s, we can approximate the interaction force as a linear function of ion displacement:

$$\mathbf{F}_1 = \frac{e^2(\mathbf{r}_1 - \mathbf{r}_2 + \rho_s)}{|\mathbf{r}_1 - \mathbf{r}_2 + \rho_s|^3} - \frac{e^2\rho_s}{\rho_s^3} \approx m\kappa(x_1 - x_2)\,\hat{\mathbf{x}} - 2m\kappa(y_1 - y_2) \qquad (5C.8)$$

and $\mathbf{F}_2 = -\mathbf{F}_1$.

When we include the Lorenz force, we get a system of four linear differential equations for the motion of the two ions in two dimensions. Guessing solutions:

$x_1 = \mathrm{Re}(A_{x1} e^{i\omega t})$, $x_2 = \mathrm{Re}(A_{x2} e^{i\omega t})$,

$y_1 = \mathrm{Re}(A_{y1} e^{i\omega t})$, and $y_2 = \mathrm{Re}(A_{y2} e^{i\omega t})$, (5C.9)

and solving the characteristic equation for ω we get

$$\omega_1' = \omega_o/(1+\eta) + \kappa/(2\omega_o) + \kappa^2/(8\eta\omega_o^3)$$

$$\omega_2' = \omega_o/(1+\eta) + \kappa/(2\omega_o) - \kappa^2/(8\eta\omega_o^3) \qquad 5C.10$$

The answer is reassuring. For a reasonable value of κ, the error in the all-important $\omega_1 - \omega_2$ can be very small --- in our example of the two ammonia molecules, for $\rho_s = 0.07$ cm, $\kappa = 2 \times 10^7$ and $\delta(\omega_1-\omega_2)/\omega_o = 2 \times 10^{-13}$.

But we must be careful. Although the perturbation in the difference frequency is small, the perturbation in either frequency alone is considerable. In the example cited in the paragraph above, $\delta\omega/\omega = 5 \times 10^{-9}$. Thus if we aspire to parts in 10^{-12} accuracy, we rely on the perturbation being strictly symmetric, i.e. that the perturbation on one ion due to the other is the same as the perturbation of the other ion due to the one --- to better than a part in 10^3! As we have seen, this is true in the case of linear coupling, but what if the cyclotron radii are large enough to be a non-negligible fraction of the ion separation? For coupling beyond the linear approximation, the size of the frequency perturbation

will depend on the cyclotron radii, and if the cyclotron radii of the two ions were not exactly the same, we can readily imagine that the ion-ion perturbations would *not* be symmetric.

This troublesome question of nonlinearity in the coupling may have to be addressed experimentally -- by measuring the difference frequency as a function of a deliberately caused asymmetry in cyclotron radii. In addition, we are pursuing the issue both numerically and analytically, and will report these results soon. [CKB90]

The Magnetron Motion when the Ion Masses are not Equal

We shall learn in this section that when the ion masses are not exactly the same, the average magnetron radii are not the same for the two ions. In the presence of residual field imperfections, the difference in the average magnetron radii means a systematic error in measuring the difference in the cyclotron frequency.

We have seen in section 5A that during locked two-ion magnetron motion the distance from the center of the trap to a given ion oscillates slowly with a period determined by the difference in frequencies of the two normal modes, $2\pi/(\omega_{com} - \omega_s)$. In the limit that the two ion masses are equal, the ion motion has an important property. Averaged over one period of the slow oscillation, the average distance to the center of the trap, and all its moments, are the same for each ion. $\langle\rho_1^2\rangle = \langle\rho_2^2\rangle$, $\langle\rho_1^4\rangle = \langle\rho_2^4\rangle$, and so on. Since perturbations to the cyclotron frequency due to residual field imperfections are functions of the distance to the

center of the trap, to the extent this averaging process is imperfect we must expect systematic errors.

For ions of approximately equal mass, the conservation of energy and angular momentum severely constrain the range of possible paired ion motion. (Eqn. 5A.8 and 5A.10) The configuration shown in Fig. 5.7, a modification of the degenerate mass orbit, satisfies the conservation laws to first order in $\eta\omega_{mo}^2/\kappa$. The ions trace out twin circles on either side of the origin, and both circles themselves orbit the origin. As in the degenerate case, the centers of the circles are colinear with the origin but the distances from each circle's center to the origin, g_1 and g_2, differ from each other, and the radii of the circles, f_1 and f_2, are unequal as well.

$$(g_1 - g_2)/(g_1 + g_2) = \eta\omega_{mo}^2/2\kappa$$
$$(f_1 - f_2)/(f_1 + f_2) = -\eta\omega_{mo}^2/2\kappa \qquad 5C.11$$

As the mass difference η vanishes, we recover the original mass degenerate configuration shown in Fig 5.2, and for this reason we use analogous nomenclature for the radii: ρ_{com} refers to $(f_1 + f_2)/2$ and ρ_s to (g_1+g_2). Similarly the frequency ω_s corresponds to $-\dot{\beta}$ and ω_{com} to $\dot{\alpha} - \dot{\beta}$.

We want to calculate the time-averaged moments of the radii:

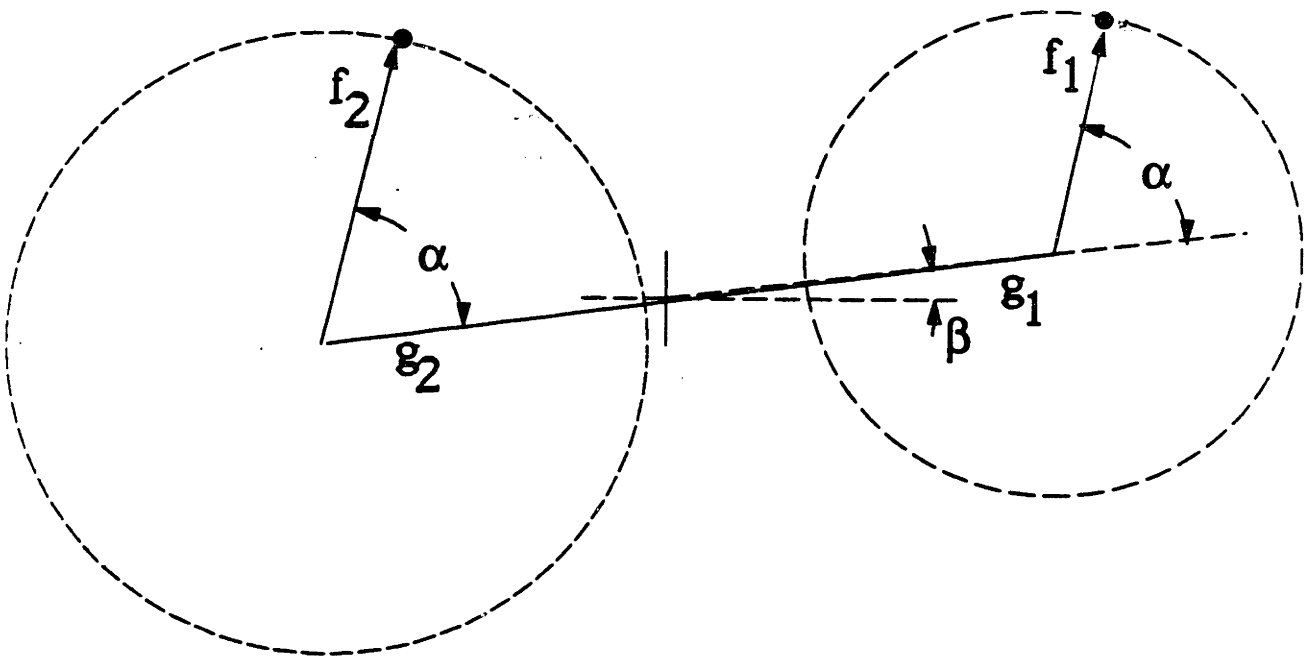

Fig. 5.7 Conservation laws dictate the allowed orbits for two trapped ions of unequal mass. To first order in $\eta\omega_{mo}^2/\kappa$, the pictured orbits conserve angular momentum and energy. By analogy with the degenerate mass limit, Fig. 5.2, $\dot{\beta}$ is $-\omega_s$ and $\dot{\alpha}$ is $-(\omega_s - \omega_{com})$. In a frame that rotates with $\dot{\beta}$, the ions move in tandem counterclockwise around their respective epicycles with angular frequency $\dot{\alpha} = [\, 2\kappa/\omega_{co} \,]$.

$$\langle \rho_i^n \rangle = \frac{\oint dt\ \rho_i^n}{\oint dt} = \frac{\int_0^{2\pi} d\alpha\ (1/\dot{\alpha})\rho_i^n}{\int_0^{2\pi} d\alpha\ (1/\dot{\alpha})} \qquad (5C.12)$$

The instantaneous frequency difference between the two modes $\dot{\alpha}$, determines the rate at which the two ions take turns moving closer and further from the center of the trap, and is itself basically a consequence of the ExB drift induced by the interaction electric field. A simple estimate based the separation between the ions, as determined from fig. 5.7, and from the resulting ExB velocity, gives the form of $\dot{\alpha}$:

$$\frac{\delta\dot{\alpha}}{\dot{\alpha}} = 3\,\frac{\rho_{com}}{\rho_s}\,\frac{\eta\omega_{mo}^2}{\kappa}\cos\alpha$$

Now we can evaluate the integral 5C.12 for n=2:

$$2\,\langle \rho_1^2 - \rho_2^2 \rangle / \langle \rho_1^2 + \rho_2^2 \rangle = \left(\frac{2\omega_{mo}^2\eta}{\kappa}\right)\left(1 + O(\rho_{com}/\rho_s)\right) \qquad (5C.13)$$

Whether or not ρ_{com} has been cooled to be much smaller than ρ_s, the important result, as we shall see in section 5D, is that the relative difference in the mean square radii scales as $1/\kappa$, that is, scales as the mean separation between the two ions cubed.

Cooling ρ_{com}

Using a variant on the sideband magnetron cooling technique it will be possible to cool or heat independently the two normal mode magnetron radii. The basic idea is to adjust the axial frequency modulation rate ν_{mod} so that the axial sidebands of the two ions overlap as nearly as possible. (See Section 5B) We then apply a sideband cooling drive coupling the magnetron motion and the axial motion. The coupling drive should be weak and somewhat off-resonance. In the limit that the coupling drive detuning is much larger than the frequency difference between the two axial sidebands, and in the limit that the "avoided crossing" frequency shift (See section 3B) is smaller than that frequency difference, the locked common mode magnetron motion maps directly into a small common mode axial motion, and the stretch magnetron mode maps into a stretch axial motion. Only the common mode motion couples net image current into the endcaps, and thus only the common mode damps. (Or heats, depending on the sign of the coupling drive -- see [BRG86])

An alternate configuration, with the sideband frequencies well separated and the detuning drive coupling as close as possible to the average of the two sideband frequencies, results in the stretch magnetron motion coupling to a common mode axial motion, and vice versa, so that only the stretch magnetron mode damps or heats.

The details of these calculations, which are somewhat lengthy, are unfortunately not ready for presentation as this thesis comes due, but are being written up for publication. [CKB90]

5D Two-ion Economy of Errors

In section 5C, when we applied the Brown and Gabrielse invariance theorem to two ion measurements we learned that part per trillion mass comparison requires three frequency measurements: two of single ion frequencies and one very high precision measurements of the two-ion cyclotron difference frequency. Errors affecting single-ion measurement are discussed in section 3B, so in this section we cover only the various sources of error which affect the crucial two-ion trap cyclotron difference frequency measurement.

Sources of error in measuring $\Delta\omega_c' = \omega_{c1}' - \omega_{c2}'$ fall roughly into three categories. The first category consists of errors having to do with the locked magnetron motion and ion-ion perturbation. The magnitudes of these errors scale as high powers of ρ_s and of $1/\rho_s$, respectively. In the second category are errors associated with the the cyclotron motion, and in particular with the cyclotron radii of the two ions being of unequal length during the measurement. Into the third category we lump everything else, a hodge-podge of effects, most of them being much smaller than those in the first two categories, but some requiring careful attention. We discuss the three categories in the order mentioned.

Errors Associated with the Magnetron Motion

Assuming that we have cooled ρ_{com}, the scale of several of the largest sources of error is determined by ρ_s, the distance that

the magnetron locking maintains between the guiding centers of the cyclotron motions. As we have seen in section 5C, the ion-ion perturbation of $\Delta\omega_c'$ scales as $\kappa^2 \sim 1/\rho_s^6$, at least in the linear limit. On the other hand, errors in each ion's cyclotron frequency caused by imperfections in the trapping fields scale as the second or higher power of the distance from the ion to the center of the trap, $\rho_s/2$. In section 5C we saw that differences in the average distance from the center of the trap scale as $1/\kappa$, so errors in the difference frequency $\Delta\omega_c'$ scale as $\rho_s^2/\kappa \sim \rho_s^5$.

If we measure the difference frequency several times, varying ρ_s, we can trace out the curve of measured $\Delta\omega_c'$ vs ρ_s. The high power law dependence on ρ_s and $1/\rho_s$ should be very distinctive. (Fig. 5.8) The total error in $\Delta\omega_c'$ will be minimized by using a value measured along the flat section of the curve. Experimentally, an estimate of the residual error can be obtained by checking just how flat the curve is in the optimum region. Obviously, as we make the trapping fields more perfect we can operate at a larger values of ρ_s and reduce errors both from ion-ion interaction and from field gradients.

Let us look at a concrete example. Recall from Eqn. 3.9 that the trap cyclotron frequency has a quadratic dependence of the magnetron radius, determined by the residual values of the field flaws B_2 and C_4. With ρ_{com} cooled, each ion will have a magnetron radius of about $\rho_s/2$. The cyclotron frequency of each ion will then be perturbed as follows:

$$\delta\omega_{ci}'/\omega_{co} = [\ -B_2/2\ -(3/2)(\omega_{zo}^2/\omega_{co}^2)C_4/d^2]\ [\rho_s^2/4] \qquad (5D.1)$$

As far as this goes, it is not a problem. Identical shifts for the two ions will not affect $\Delta\omega_c'$. But recall that as a consequence of the two ions' having unequal masses, they will not have identical average radii, and thus the shifts will be slightly different for the two ions. Using equation 5C.2, we determine the perturbation to the difference frequency from field flaws:

$$[\delta\Delta\omega_c'/\omega_c]_{field} = [-B_2/2-(3/2)(\omega_{zo}^2/\omega_{co}^2)C_4/d^2]\ [m_o\omega_{mo}^2\eta\rho_s^5/(2e^2)] \qquad (5D.2)$$

And from equation 5C.13, we see that the ion-ion perturbation contributes a perturbation

$$[\delta\Delta\omega_c'/\omega_c]_{ion\text{-}ion} = \kappa^2/(4\eta\omega_{co}^4) = e^4/(4\eta m_o^2\omega_{co}^4\rho_s^6) \qquad (5D.3)$$

The total perturbation to $\Delta\omega_c'$ associated with the magnetron motion is just the sum of the field and the ion-ion terms. Roughly speaking, the total error will be at a minimum (and the curve of measured $\Delta\omega_c'$ vs ρ_s will be at its most flat) when the two terms contribute equal errors. Using this criterion, we calculate the optimum ρ_s

$$[\rho_s]_{optimum} = \{e^6[(2\eta^2 m_o^3\omega_{co}^4\omega_{mo}^2)(-B_2/2-(3/2)(\omega_{zo}^2/\omega_{co}^2)C_4/d^2)]^{-1}\}^{1/11} \qquad (5D.4)$$

and the corresponding total error is

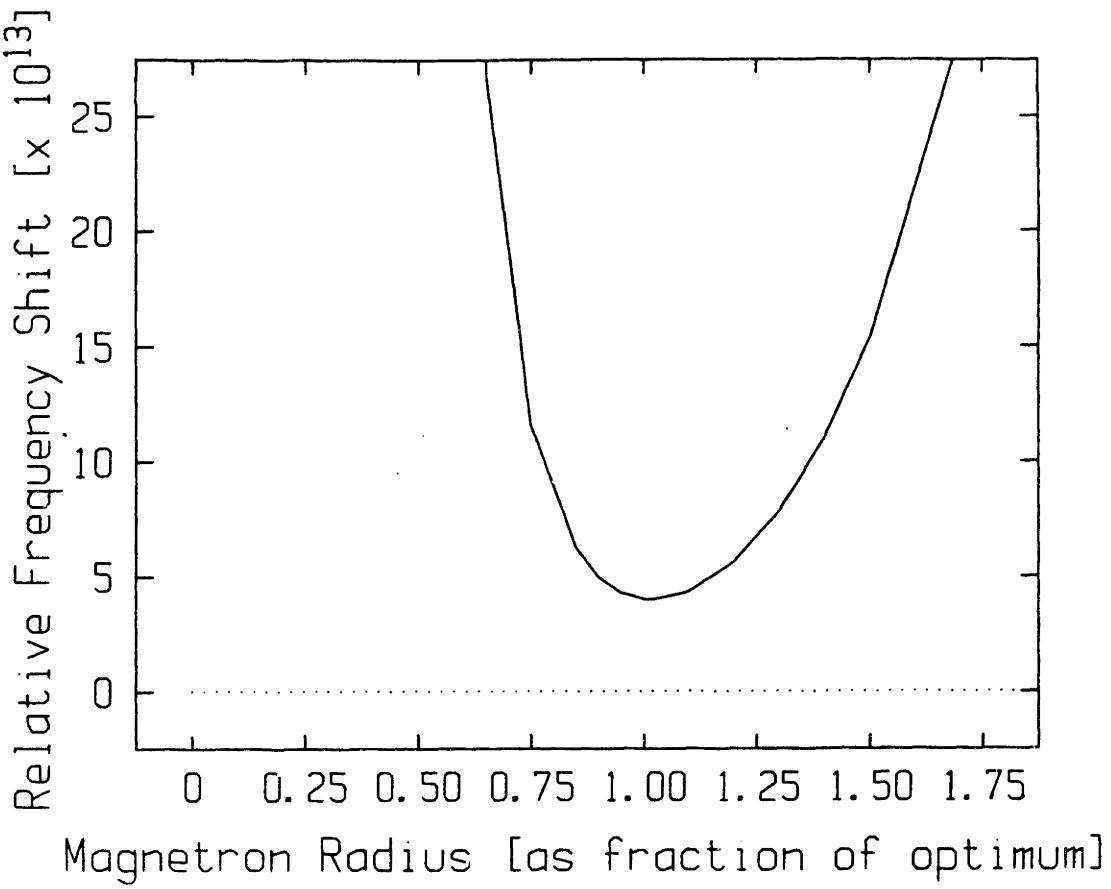

Fig. 5.8 Error in the measured value of $\omega_{c1} - \omega_{c2}$ as a function of ρ_s. Errors from ion-ion perturbation scale as ρ_s^{-6}, and errors from trapping field flaws scale as ρ_s^{5}. Over the region where the curve is relatively flat, the total error from field flaws and ion-ion perturbation is minimized.

$$[\delta\Delta\omega_c'/\omega_c]_{total}$$
$$=2\{2^{-16}e^8\eta m_o^{-4}\omega_{co}^{-20}\omega_{mo}^{12}\}^{1/11}$$
$$\{B_2/2(3/2)(\omega_{zo}^2/\omega_{co}^2)C_4/d^2\}^{6/11} \qquad (5D.5)$$

Let us numerically evaluate these errors for our isomeric ammonia doublet. We should have no difficulty shimming out field flaws until $|B_2| < 1 \times 10^{-7}/cm^2$ and $|C_4| < 2 \times 10^{-5}$. We then find that the optimum separation will be around $\rho_s = 0.065$ cm. Assuming the common mode magnetron motion is cooled, two ions separated by .065 cm will each be 0.03 cm from trap center. The cyclotron frequency of each ion will be shifted by field flaws less than 1 part in 10^{10}, and by ion-ion perturbations about 7 parts in 10^9. The effects combined cause an error in the measured value of $\Delta\omega_c'/\omega_c$ of about 5×10^{-13}. There is a range of possible values of ρ_s, from .081 cm. to .052 cm., for which the total error associated with the magnetron motion will be less than about 2×10^{-12}.

Errors associated with the cyclotron radii

Both field imperfections and special relativity can give the cyclotron frequency a dep ndence on the cyclotron radius ρ_c. Assuming that the dominant effects from the electric and magnetic field flaws are from, respectively, the B_2 and the C_4 components, the leading frequency corrections for the i_{th} ion are (from equation 3.9)

$$\delta\omega_{ci}'/\omega_{co} = \{\, 3(\omega_{zo}^2/\omega_{co}^2)C_4/d^2 - B/2 + \omega_{co}^2/(2c^2) \,\}\, \rho_{ci}^2 \qquad (5D.6)$$

In a well-tuned trap, the relativistic term, $\omega_{co}^2/(2c^2)$, will be larger than the field flaw terms. Depending on the performance of the detector used, signal-to-noise considerations will set some lower limit on the size to which the cyclotron radius is driven during a resonance measurement, and thus determine a minimum relativistic frequency shift in ω_{ci}'. This shift should be the same for each ion, but only to the extent that the two ions are excited to identical cyclotron radii. In designing the experiment, care must be taken to ensure that the electronics which generate and deliver the rf pulses used to drive the cyclotron motion produce the same amplitude pulse at both frequencies, lest there be a serious systematic error introduced into the measurement of the difference frequency. Also troublesome is the possibility of thermal errors. Whatever technique is used to cool the cyclotron motions between measurements is bound to leave some residual thermal cyclotron motion in each ion. When the next measurement is performed, this residual motion will add randomly to the driven response, causing random and in general unequal fluctuations in the cyclotron radii. The measured difference frequency will exhibit thermal fluctuations about some average. Although the average will not be systematically shifted from its correct value, the fluctuations may be large enough to require an impractical number of measurements to average away to parts in 10^{-12}.

For example, in our experiments the cyclotron motion is cooled by exchanging its action with the resistively cooled axial motion with pi-pulses. [CWB90] The cyclotron cooling limit with

this technique is $T_c=(\omega_c/\omega_z)\,T_z$, where T_z is the effective temperature of resistance the axial motion sees -- for our axial detector, T_z = 15K. For our ammonia doublet, the cyclotron cooling limit would thus be 650K, corresponding to a root mean square cyclotron radius for each ion $(<\rho_{ci}^2>)^{1/2}$ = 0.0014 cm. With our existing detector sensitivity, we are required to excite the ions to ρ_{ci} = 0.019 cm to get the requisite signal-to-noise to measure the difference frequency. The average relativistic shift for each ion would then be 4 parts in 10^{10}. If the electronics reliably delivered drive pulses which were balanced to .4%, the systematic error in the difference frequency would be 3 parts in 10^{12}. But thermal fluctuations would be on the order of a 6 parts in 10^{11} per measurement. Since a single S.O.F. measurement with parts in 10^{11} resolution could take 10^3 seconds, averaging the thermal fluctuations to parts in 10^{12} could take many days of data collection. Clearly, efforts to improve detector sensitivity and cyclotron cooling methods will pay off.

Another way of reducing ρ_{ci}-related errors has already been alluded to in Chapter 3B. If B_2 were deliberately adjusted, not to the minimum attainable value, but rather as close as possible to ω_{co}^2/c^2, (i.e., about 2 x 10^{-6}) the effect of special relativity and of the field gradient would cancel out, and ω_{ci}' could be made independent of ρ_{ci}. Of course, the price one pays is an increased dependence on magnetron radius. Referring to equation 5D.5, above, we see that a B_2 of 2 x 10^{-6} during an ammonia doublet measurement gives a systematic error of perhaps 2 x10^{-12}.

It is also possible to adjust C_4 and B_2 such that the cyclotron frequency depends neither on cyclotron radius nor on magnetron radius. The drawback here is that the rather large required value of C_4 causes unacceptably large "chirp" in the axial ring-down motion, which will make it impossible to do the phase-sensitive frequency measurements we plan.

Other perturbations at a part in 10^{12}

At a part in 10^{12} resolution, a whole host of little effects start to become significant. For instance:

Dipole-Dipole interaction of the cyclotron motion with its image charge in the electrodes: Van Dyck et al [VMF90] have shown that, especially in small traps, this effect can be significant. For a larger trap with characteristic size d = 0.55 cm, this effect is on the order of two parts in 10^{11}, but as with the other corrections we have discussed, should be the same for both ions to better than a part in 10^{12}.

Axial dependence of trapping fields: Because we don't have to measure the axial frequency during a precision cyclotron measurement, the axial displacement can be very small -- just the thermal value. The long-period S.O.F. measurements will span many thermal equilibration periods, so that both ions will have many opportunities to reequilibrate with the effective resistor in the axial motion detector, which will thoroughly average out any initial differences in thermal axial displacement the two ions might have.

Conclusion

No section called "Other perturbations at a part in 10^{12}" can be considered complete at this time. No matter what one is trying to measure, attempting three orders of magnitude improvement in accuracy will bring one up against unforeseen sources of error.

I hope this thesis has explained how we managed to skirt the difficulties we encountered on our way here to part per billion mass comparisons. And I hope that I have been able to point out a route around at least the problems that have already appeared on the horizon, away off in the direction of parts per trillion

ARR87 W.D. Arnett and J.L. Rosner Phys. Rev. Lett. **58**, 1906 (1987).

BGL85 S.D. Boris, A.I Golutvin, L.P. Laptin et al, JETP Letters **42**, 130 (1985).

BRG82 L. Brown and G. Gabrielse, Phys Rev. A **25**, 2423 (1982).

BRG86 L. Brown and G. Gabrielse, Rev. Mod. Phys. **58**, 233 (1986).

COH84. C. Cohen-Tanoudji, lecture notes, College de France (1984).

CDL77 C. Cohen-Tannoudji, B. Diu, and F. Laloe, *Quantum Mechanics* (Wiley, New York, 1977).

CWB89 E. A. Cornell, R. M. Weisskoff, K.R. Boyce, R.W. Flanagan, Jr., G. P. Lafyatis, and D.E. Pritchard, Phys. Rev. Lett. **63**, 1674 (1989).

CWB90 E. A. Cornell, R. M. Weisskoff, K.R. Boyce and D.E. Pritchard, Phys Rev. A **41**, 312 (1990).

CWB90b E. A. Cornell, R. M. Weisskoff, K.R. Boyce, R.W. Flanagan, Jr., G. P. Lafyatis, and D.E. Pritchard, Phys. Rev. Lett. **64**, 2099 (1990).

DAT85 J. Dalibard and C. Cohen-Tannoudji, J. Opt. Soc. Am. B **2**, 1707 (1985).

DEH67 H. G. Dehmelt, Adv. At. Mol. Phys. **3**, 53 (1967).

FLA87 R. M. Flanagan, Jr., Ph.D. thesis, MIT 1987 (unpublished).

GAB83 G. Gabrielse, Phys Rev. A **27** 2277 (1983).

GAT88 G. Gabrielse and J. Tan, J. Appl. Phys. **63**, 5143 (1988).

GAB90 G. Gabrielse, Phys. Rev. Lett. **64** 2098 (1990).

HAC83 I. Hacking, *Representing and Intervening* (Cambridge, Cambridge, 1983) p. 236.

JOH84 W.H. Johnson, in *Precision Measurements and Fundamental Constants II,* edited by B. N. Taylor and W.D. phillips, NBS Special Publication No. 617 (U.S. GPO, Washington, D.C. 1984), p. 335.

KUC89 D.L. Kuchnir, undergraduate thesis, MIT, 1989 (unpublished).

MOO87 F.L. Moore (private communication).

MOO89 F.L. Moore (private communication).

MOO89 F.L. Moore, Ph.D. thesis, University of Washington, 1989 (unpublished).

PBI85 J. D. Prestage, J.J. Bollinger, W.M. Itano, and D.J. Wineland, Phys,. Rev. Lett. **54**, 2387 (1985).

RAM56 N. Ramsey, *Molecular Beams* (Clarendon, Oxford, 1956).

VMF85 R. S. Van Dyck, Jr., F. L. Moore, D. L. Farnham, and P. B. Schwinberg, Int. J. Mass Spectosc. Ion Processes **66**,327 (1985).

VMF86 R. S. Van Dyck, Jr., F. L. Moore, D. L. Farnham, and P. B. Schwinberg, Rev. Sci. Instr. **57**, 593 (1986).

VMF88 R. S. Van Dyck, Jr., F. L. Moore, D. L. Farnham, and P. B. Schwinberg, in *Proceedings of Frequency Standards and Metrology*, edited by A. DeMarch (Springer-Verlag, Berlin, 1988), p.349.

VMF90 R. S. Van Dyck, Jr., F. L. Moore, D. L. Farnham, and P. B. Schwinberg, Submitted to Physical Review (1990).

VSD78 R. S. Van Dyck, Jr., P.B. Schwinberg, and H. Dehmelt, in *New Frontiers of High-Energy Physics*, edited by B. Korsunoglu, A. Perlmutter, and L. Scott (Plenum, New York, 1978), p. 159.

VSD87 R. S. Van Dyck, Jr., P. B. Schwinberg, and H. G. Dehmelt, Phys Rev. Lett. **59**, 26 (1987).

WAA85 A.H. Wapstra and G. Audi, Nucl. Phys. **A432**, 1 (1985). See also same authors, same volume, p. 55, p. 140 and p.185.

WBI83 D. J. Wineland, J.J. Bollinger, and Wayne M. Itano, Phys. Rev. Lett. **50**, 628 (1983).

WBI85 D. J. Wineland, J.J. Bollinger, andWayne M. Itano, and J.D. Prestage, J. Opt. Soc. Am. B **2**, 1721 (1985).

WEI88 R. M. Weisskoff, Ph.D. thesis, M.I.T., 1988 (unpublished).

WID75 D. J. Wineland and H.G. Dehmelt, Int J. Mass Spectrosc. Ion Proc. **16** 338 (1974);**19**, 251 (1975).

WLB88 R. M. Weisskoff, G. P. Lafyatis, K. R. Boyce, E.A. Cornell, R. W. Flanagan, Jr., and D. E. Pritchard, J. Appl. Phys. **63**, 4599 (1988).

Aknowledgements

It is a pleasure to have the opportunity to aknowledge considerable assistance from my M.I.T. colleagues, without whom this work could never have been completed:

My advisor, Dave Pritchard, introduced me to mass spectroscopy and provided five years of thoughtful guidance, for which I am extremely grateful. Kevin Boyce's wide-ranging competence turned vague ideas into experimental reality time and again. Robert Weisskoff and Greg Lafyatis saw the experiment through its most intransigent stage and left behind a working apparatus, of all things. Bob Flanagan was responsible for the cryogenic and magnetic foundations of the experiment. Debbie Kuchnir's efforts on the two-ion project were superb.

Having Kris Helmerson around the lab made life easier for everybody. David Keith always had time to discuss a crazy idea, and George Welsh always had time to cure ailing software. I would also like to thank friends from the Pritchard and Kleppner group for many favors large and small: Chris Ekstrom, Barbara Hughey, Michael Ioffe, Chun-ho Iu, Mike Kash, Juan Latasa, Alex Martin, Peter Martin, Vasant Natarajan, Bruce Oldaker, Scott Paine, Eric Raab, Brian Stewart, Rick Stoner, Ke-Xun Sun, and Min Xiao.

Conversations with ion trappers around the country helped enormously. In particular, I wish to aknowledge Jerry Gabrielse, Fred Moore, Bob van Dyck and Dave Wineland.

I thank Alexi Assmus for help preparing this manuscript and for a critical reading of Chapter 5.